FABIAN YESID SOLER ROMERO

COMPOUND FLOODING ON AN ESTUARINE ENVIRONMENT: CASE STUDY OF TAGUS ESTUARY

UNIVERSIDADE DO ALGARVE

Faculdade de Ciências e Tecnologia

2025

FABIAN YESID SOLER ROMERO

COMPOUND FLOODING ON AN ESTUARINE ENVIRONMENT: CASE STUDY OF TAGUS ESTUARY

Master's in Coastal Hazards, Risks, Climate Change Impacts and Adaptation

Performed under the supervision of:
Luis Pedro Almeida &
Juan L. Garzon Hervas

UNIVERSIDADE DO ALGARVE

Faculdade de Ciências e Tecnologia

2025

Declaração de autoria de trabalho

Declaration of Authorship of work

COMPOUND FLOODING ON AN ESTUARINE ENVIRONMENT:
CASE STUDY OF TAGUS ESTUARY

Declaro ser o autor deste trabalho, que é original e inédito. Autores e trabalhos consultados estão devidamente citados no texto e constam da listagem de referências incluída.

I declare to be the author of this work, which is original and unpublished. Authors and works consulted are duly cited in the text and are included in the list of references.

Fabian Yesid Soler Romero
Faro, 15 July 2025

COPYRIGHT

ACKNOWLEDGEMENT

This master's thesis marks the culmination of an invaluable two-year chapter in my life. This journey was made possible by many people and institutions who supported me along the way, and to whom I owe deep gratitude.

First, I would like to thank my supervisor, Luis Pedro Almeida, for his consistent guidance and solid support throughout this thesis. His mentorship, constructive feedback, and insightful discussions have been fundamental to my learning and growth as for the culmination of this study. I also extend my sincere thanks to Cintia and all my colleagues at Colab+Atlantic who contributed to this work in various ways. A special thanks goes to my co-advisor, Juan Garzón, for his detailed review of my work and for offering valuable insights that significantly improved the quality of this study.

I would also like to express my appreciation to the program coordinators, Álvaro Semedo, Óscar Ferreira, and Javier López, for their exceptional teaching and dedicated guidance throughout the master's program. I am grateful to the University of the Algarve, IHE Delft and University of Cantabria, as well as to all the professors involved in the program, for their engaging courses, fieldwork, seminars and workshops. These experiences have provided me with invaluable knowledge and practical skills.

My deepest gratitude goes to my parents, Cecilia and Julio, whose example taught me that discipline and hard work lead to meaningful achievements. This accomplishment is as much theirs as it is mine. I am also thankful to my brother, Alexander; my sister, Andrea; and my niece, Sofía, for their constant encouragement and emotional support during times of uncertainty and self-doubt. To my girlfriend, Caterina, thank you for bringing immense joy into my life and for standing by me through the difficult moments. Your unwavering support and radiant smile helped me stay focused and motivated throughout this journey. I am grateful to God for granting me the courage, strength, and resilience to face the challenges of this life-changing Erasmus experience, and for allowing me to enjoy countless wonderful moments over the past two years.

Finally, I would like to thank all my COASTLEES friends for the laughter, trips, adventures, and unforgettable memories. I proudly say that I have great Erasmus friends from many different parts of the world. A heartfelt thanks as well to my friends in Colombia, who remained a constant source of support while being far from home.

De nuevo y para todos los mencionados, Muchas Gracias!

Note: My co-advisor Juan L. Garzon has been funded by the FCT through the project with reference CEECINST/00146/2018/CP1493/CT0012, through the Associate Laboratory ARNET under the project LA/P/0069/2020 and CIMA through the grant UIDP/00350/2020 (https://doi.org/10.54499/UIDP/00350/2020)

ABSTRACT

The combined occurrence of coastal, fluvial and/or pluvial flood drivers can lead to compound flood events, which can trigger devastating social, economic, and ecological impacts, particularly in low-lying zones, including estuarine environments. A great number of these areas, which are home to significant populations worldwide, are increasingly at risk, as the intensity, phasing and frequency of such drivers are projected to change. These flood-induced impacts arise from the potential increase in inundation magnitude due to the non-linear interactions between various flood drivers, where their combined effects can exceed the simple sum of their individual contributions. Understanding their joint impacts and accurately estimating compound flood magnitudes is therefore essential for effective coastal management and disaster risk reduction.

In this study, a numerical modeling framework was applied to analyze the interaction between different flood drivers (storm surge, peak river discharge, extreme rainfall and astronomical tides) in the Tagus Estuary. The first phase involved a coupled hydrodynamic model (MOHID), implemented to simulate tidal, wave, and current circulation within the estuary using oceanic and riverine boundary conditions. Based on these results, a flood model (SFINCS) was applied to simulate flooding processes along the northern and southern margins of the estuary under various scenarios.

The flood model was validated using a storm event that occurred in the study area in December 2022. Subsequently, joint probability and extreme value analysis for 100-year return period values were estimated for the flood drivers and used to define multiple modeling scenarios along with different Sea Level Rise projections. These scenarios were designed to examine the flood driver's interaction, focusing on the flood magnitudes in the context of compound flooding. This study demonstrated that compound events resulting from the interaction of pluvial/fluvial and coastal drivers can increase flood extent and depth by three to four times compared to events driven solely by coastal forces, such as a storm surge coinciding with spring tides in the estuary. Furthermore, the analysis revealed that rainfall is the primary cause of flooding in the Tagus Estuary.

Keywords: Compound coastal flooding, Tagus Estuary, Storm Surge, extreme precipitation, SFINCS

RESUMO

As regiões estuarinas figuram entre os ambientes costeiros mais vulneráveis às consequências das alterações climáticas e da crescente urbanização. A ocorrência simultânea ou sucessiva de múltiplos fatores de inundação, como chuvas intensas, descargas fluviais elevadas, marés astronômicas e tempestades costeiras, pode levar a eventos de inundações compostas, cujo impacto é frequentemente mais severo do que a atuação isolada de cada forçante. Este tipo de evento é particularmente crítico em estuários densamente urbanizados e com baixa altitude, como é o caso do Estuário do Tejo. Apesar da relevância crescente desse tema, os estudos em território português que abordam a interação entre forçantes atmosféricos, fluviais e oceânicos de forma conjunta ainda são escassos.

Diante desse contexto, o presente trabalho tem como principal objetivo investigar a influência relativa de diferentes forçantes, precipitação extrema, descarga fluvial, marés, tempestades e elevação do nível médio do mar, na geração de inundações na região do Estuário do Tejo. Para isso, foi implementada uma abordagem integrada de modelação numérica, dividida em duas componentes: a simulação da circulação hidrodinâmica e a modelação da propagação da inundação sobre a superfície terrestre. A estrutura metodológica adotada permitiu avaliar o impacto atual e futuro das inundações compostas com base em diferentes cenários de forçamento, validados a partir de um evento extremo recente ocorrido em dezembro de 2022, que afetou significativamente a região de Lisboa.

A primeira etapa consistiu na modelação da circulação hidrodinâmica através da utilização de um modelo tridimensional (MOHID) que representa a dinâmica das massas de água estuarinas e costeiras. Esse modelo foi configurado para representar condições históricas do evento de validação, processando dados de maré, vento, pressão atmosférica, temperatura da água e descarga fluvial. Foram utilizadas condições de contorno baseadas em modelos climáticos e oceanográficos regionais, com resolução espacial e temporal adequada para a área em estudo. O modelo foi acoplado a um módulo de ondas para representar a interação entre marés e agitação marítima, permitindo obter resultados mais realistas sobre os níveis d'água nas zonas costeiras e de transição para o ambiente terrestre.

Os dados resultantes dessa modelação hidrodinâmica foram exportados e serviram como entradas para a segunda componente da modelação, voltada para a simulação das inundações sobre o território. Para isso, utilizou-se um modelo de inundação baseado em grelha regular e de elevada eficiência computacional (SFINCS), executado através de uma estrutura em Python voltada para

estudos hidrológicos. O domínio do modelo abrangeu uma área superior a 980 km², com resolução espacial de 10 metros, sendo executado em modo subgrid, o que permitiu maior detalhe na representação da propagação da água, mantendo baixos custos de simulação. A configuração incluiu dados topográficos e batimétricos, bem como informações sobre rugosidade superficial e infiltração, a partir de dados raster e vetoriais.

A validação do modelo foi realizada com base na comparação entre os resultados simulados e evidências observacionais do evento extremo de dezembro de 2022. Para isso, foram utilizadas imagens de satélite com detecção automática de áreas alagadas, além de vídeos e fotografias georreferenciadas obtidas em redes sociais e veículos de comunicação. A correspondência espacial observada entre os dados modelados e os registros reais indicou uma boa performance do modelo em áreas como Alcântara, Algés e Loures, refletindo sua capacidade de representar eventos reais com boa precisão.

Posteriormente, foram definidos onze cenários distintos de simulação, englobando três tipos principais de forçamento: (i) eventos extremos de precipitação e descarga fluvial; (ii) eventos costeiros compostos por maré astronômica, tempestade e elevação do nível do mar; e (iii) eventos compostos que integram simultaneamente os dois tipos anteriores. A definição dos cenários considerou diferentes níveis de severidade com base em análise de probabilidade conjunta de precipitação e maré, bem como projeções de elevação do nível do mar para os horizontes temporais de meados e final do século XXI. Além disso, foram incorporados dados de uso e ocupação do solo para melhor contextualização espacial dos impactos.

Os resultados dos cenários permitiram identificar que a coocorrência de precipitação extrema, descarga fluvial e forçamentos oceânicos amplifica significativamente a magnitude das inundações no Estuário do Tejo quando comparada a eventos desencadeados apenas por forçamentos oceânicos. Em simulações utilizando projeções idênticas de elevação do nível do mar (SLR), os cenários compostos resultaram em extensões de inundação até 3 a 4 vezes maiores do que aquelas provenientes de eventos exclusivamente oceânicos em áreas de baixa altitude.

Adicionalmente, observou-se que o cenário exclusivamente pluvial/fluvial foi responsável pela maior área de inundação. Esse achado ressalta a predominância dos forçantes continentais no comportamento hidrodinâmico da região do estuário, especialmente em períodos de precipitação extrema.

Análises complementares permitiram identificar as áreas mais vulneráveis, com destaque para zonas com altitudes inferiores a 10 metros em relação ao nível médio do mar. A sobreposição entre as áreas inundadas e os diferentes tipos de uso e cobertura do solo revelou que as zonas agrícolas e naturais são as mais afetadas em termos absolutos. No entanto, as áreas urbanas, apesar de menos extensas, concentram maior densidade populacional e infraestrutura crítica, como estradas, hospitais e redes de transporte público, tornando-as prioritárias em termos de planejamento urbano e resposta a emergências.

Foi também realizada uma análise comparativa entre os resultados do modelo e mapas oficiais de risco de inundação, evidenciando boa concordância espacial, principalmente na zona norte do estuário. Esse cruzamento reforça a confiabilidade do modelo implementado e destaca seu potencial como ferramenta de apoio à gestão do risco em áreas urbanas e industriais. A capacidade de gerar cenários com elevado nível de detalhe permite ainda que o modelo seja utilizado como base para a formulação de políticas públicas de adaptação às alterações climáticas.

Como conclusões principais, o trabalho confirma que: a inclusão da subida do nível do mar amplia significativamente a área e intensidade da inundação, indicando tendência de agravamento futuro; as inundações compostas representam uma ameaça real e crescente que exige ações coordenadas de monitoramento, planejamento urbano e proteção civil; a precipitação extrema e a descarga fluvial são os principais determinantes da inundação na região estudada, especialmente em cenários atuais; e a combinação entre modelos hidrodinâmicos e de inundação permite simulações robustas e com elevado nível de detalhe, úteis para aplicação prática por autoridades locais. Este estudo representa uma contribuição relevante para o entendimento dos riscos de inundação composta no Estuário do Tejo, oferecendo um referencial técnico e metodológico que pode apoiar planos de adaptação às alterações climáticas e estratégias locais de mitigação de desastres.

Palavras-chave: Inundações compostas costeiras, Estuário do Tejo, maré de tempestade, precipitação extrema, SFINCS

TABLE OF CONTENTS

LIST OF FIGURES

LIST OF TABLES

LIST OF EQUATIONS

LIST OF ACRONYMS

APA	Agência Portuguesa do Ambiente
CMEMS	Copernicus Marine Environment Monitoring Service
COS	Carta de Uso e Ocupação do Solo
CRS	Coordinate Reference System
DEM	Digital Elevation Model
DGT	Direção-Geral do Território
EVA	Extreme Value Analysis
GEE	Google Earth Engine
GIS	Geographic Information System
IPMA	Instituto Português do Mar e da Atmosfera
MhAST	Multivariate Hazard Assessment Statistical Tool
LiDAR	Light Detection and Ranging
QGIS	Quantum Geographic Information System
SAR	Synthetic Aperture Radar
SFINCS	Super Fast Inundation of Coasts
SLR	Sea Level Rise
SNIRH	Sistema Nacional de Informação de Recursos Hídricos

I. Introduction

1.1 Background

Over 600 million people worldwide live in low-lying coastal regions (Muis et al., 2016), and studies estimate that approximately 80% of casualties resulting from flooding occur within 100 kilometres of the coastline (Pan Hu et al., 2018). These areas are fundamental to the global economy, providing essential goods and services such as fisheries, tourism and trade infrastructure (e.g. ports and harbours), as well as ecosystem services such as coastal protection (Luisetti et al., 2014). For example, it is estimated that these regions contribute around USD 2.5 trillion to the global economy each year (Hoegh-Guldberg et al., 2015). However, many coastal zones, including certain estuaries with low-lying topography, are particularly vulnerable to flooding (Booi et al., 2022). In this context, coastal flooding poses severe risks, including loss of life, infrastructure damage, environmental degradation, health challenges, and significant economic losses with potentially devastating consequences for both human and ecological systems (Santos et al., 2017).

Estuaries are key coastal environments that provide essential ecosystem services, such as fisheries and shellfish production, coastal protection, biodiversity support, and cultural benefits like recreation and education, which are vital for human well-being, economic activities, and ecosystems health (Barbier et al., 2011). However, certain estuaries are highly vulnerable due to the impacts of urbanization and human settlements, which threaten their ecological balance and ecosystem services (Booi et al., 2022). Estuarine areas are particularly exposed to various stressors that can cause flooding, including high river discharge, increased meteorological tides, storm surges and intense localised rainfall (Ward et al., 2018). Each of these factors can pose a significant flood hazard in isolation (Leonard et al., 2014). Furthermore, when multiple hazard drivers interact, they can produce disproportionately severe impacts, even if the individual drivers are not extreme (Zscheischler et al., 2020). This interaction between multiple flood drivers is known as compound flooding, whereby the occurrence of coastal, pluvial (rain-related) or fluvial (river-related) events can exacerbate the adverse effects of flooding (Green et al., 2025). The combined effects of a compound flood event can potentially change the magnitude of the flood hazard both in space and time, along with the associated impacts and risks (Orton et al., 2018).

Zscheischler et al. (2020) classified compound climate events into four main types: Preconditioned events, where antecedent conditions worsen subsequent flooding; Multivariate events, where two or more hazards occur simultaneously in the same area, leading to flooding; Temporal compound events, where multiple hazards occur in succession in the same area, intensifying impacts; and Spatially compounding events, where impacts across different locations combine to affect broader regions. Specifically, in estuarine environments, different compound processes corresponding to these categories may arise from interactions between fluvial discharge, storm surges, high tides, and intense rainfall (Green et al., 2025). These factors can act together to increase the severity of flooding beyond what would be expected from each factor alone (Ward et al., 2018). Furthermore, sea-level rise, which is projected to reach up to 0.67 m or more by 2100 along the Portuguese coast (Lopes et al., 2022), is likely to exacerbate the impacts of compound flooding, thereby increasing the exposure of low-lying estuarine zones (Sun et al., 2024).

1.2 Problem Statement

Traditionally, most flood risk assessments have been focused on a single hazard or driver, or have considered multiple hazards, accounting for their potential simultaneous occurrence, within a probabilistic framework (Harrison et al., 2021). In regions like estuaries and deltas, the complexity of flood mechanisms involving tides, storm surges, and waves can be further intensified by river flows and precipitation (Green et al., 2025). For instance, heavy rainfall during storms can lead to high river discharge, which might contribute to coastal flooding. Furthermore, storm surge can block river outflow, which can trigger compound flooding (Olbert et al., 2017). These interactions are often non-linear, meaning their combined effects can exceed the simple sum of their individual contributions (Zscheischler et al., 2020).

Due to the challenges posed by climate change, there is an urgent need for robust methodologies that can accurately account for the complex interaction between pluvial, fluvial and coastal drivers while evaluating flood hazards in regions already prone to flooding (Bermudez et al., 2021). Particularly, in estuarine and delta environments, the correct application of numerical models that can resolve different hydrodynamic processes that converge there, and their potential co-occurrence or close succession, is essential for an adequate hazard magnitude estimation (Eilander et al., 2023).

In the Tagus Estuary, a densely populated and economically significant area, the interaction and combined occurrence of flood drivers remains insufficiently understood, especially under future climate change scenarios (Lopes et al., 2022). There is an urgent need for studies that use an integrated approach to analyze compound flood events in this estuarine system (Rilo et al., 2022). These studies are necessary to support more accurate flood hazard assessments and inform effective climate adaptation strategies.

1.3 Research Objectives

This study aimed to analyse the interaction between pluvial, fluvial and coastal flood drivers in the Tagus Estuary, identifying the key processes that cause coastal flooding in this region. To conduct this analysis, a modeling framework was applied to simulate the estuary's hydrodynamic circulation (MOHID) and the flooding (SFINCS) conditions along its northern and southern margins.

The specific objectives of this study are as follows:

1. To validate the numerical modeling framework for simulating hydrodynamic circulation within the Tagus Estuary and flood conditions along its margins based on a past flood event.
2. Define and run different modelling scenarios involving combinations of pluvial, fluvial and coastal flood drivers during extreme (100-year return period) events under both present-day and future conditions accounting for projected sea level rise.
3. Quantify flooding characteristics, such as flood extension and depth, for each modelling scenario and dominant physical processes.
4. Identify the areas most prone to flooding along the margins of the Tagus Estuary under the modelled compound coastal flood scenarios.

II. State of the Art

The study of compound coastal flooding has evolved significantly over the decades, progressing from early observations to more developed numerical modelling techniques. This section outlines the chronological development of research into compound coastal flooding alongside the evolving definitions and typology of compound climate events.

2.1 Early Observations and Foundations

The initial mention of compound-like flood phenomena can be traced back to studies in the 1960s and 1970s. These included the work of Rossiter (1961), who described multi-hazard events, such as storm surges coinciding with high tides. Hewitt and Burton (1971) then described compound meteorological events as the interaction of several elements acting together above their respective damage thresholds.

Early works such as those by Ho and Myers (1975) and Prandle and Wolf (1978) analysed the joint probabilities of coastal flood drivers, focusing primarily on tidal-surge dynamics. These studies emerged from the field of coastal engineering, investigating the potential for flood conditions to be exacerbated by extreme sea levels due to the combined occurrence of coastal hydrodynamic processes. Subsequently, Mantz and Wakeling (1979) applied joint probability analysis to examine the interaction between rainfall and tidal surge in triggering flooding in Norfolk, UK. From that point onwards, research in this field evolved to establish the interplay between river flow and coastal drivers. For example, Loganathan et al. (1987) conducted a study to estimate the joint probability of the combined occurrence of extreme tides and river discharge in Chesapeake Bay, Virginia, USA. The authors discovered a statistical correlation between high tides and high river flow.

2.2 Methodological Expansion

During the 1990s, analytical methods for investigating compound flood phenomena evolved. Studies such as those by Tawn (1992) and Coles and Tawn (1994) explored potential extreme sea levels using a joint probability approach and statistical methods for multivariate extremes, focusing on structural design and the risk of failure. Subsequently, Dixon and Tawn (1994) established the statistical basis by applying joint probability analysis to hydrological extremes. Then, Jones (1998) emphasised the value of the structure function (joint probability approach) for analysing the interaction of flood drivers, introducing a more optimised approach for estimating extreme water levels from tidal peaks and river levels.

During the early 2000s, joint probability and statistical methods evolved from exploratory studies to a more structured approach to analysing compound flooding. For example, Svensson and Jones (2002) analysed the correlation between storm surges and extreme river discharge in several British estuaries using a probabilistic approach. They concluded that the simultaneous occurrence of extreme river flow and sea surge posed a potential risk along the east coast of Britain. In the same year, McIennes et al. (2002) developed a coastal ocean model (GCOM2D) capable of numerically simulating the hydrodynamics of tides, storm surges and riverine runoff on the Gold Coast Broadwater on the east coast of Australia. Subsequently, Hawkes and Svensson (2003) adopted a more intricate probabilistic approach, considering significant wave height, sea level, storm surge, tide, river flow, precipitation, and wind-sea in numerous coastal regions across England, Wales, and Scotland.

2.3 Numerical Modeling Development

In the late 2000s, advancements in numerical methods shifted the analysis of compound flooding away from a probabilistic approach towards a numerical modelling approach based on physical processes. Studies such as that of Stamey et al. (2007) examined the interaction between storm surges, tides and river discharge from tropical storms by applying a numerical tool based on the ELCIRC hydrodynamic model. In the same year, White (2007) developed a new methodology combining numerical modelling techniques (one-dimensional hydraulic modelling) with statistical analysis (joint probability) to define the relationship between river flow, tides, and storm surges in a case study of Lewes in East Sussex, UK. Following this trend, Lin et al. (2010) applied a numerical modelling framework comprising the Weather Research and Forecasting (WRF) model and the two-dimensional (2D) depth-averaged hydrodynamic Advanced Circulation (ADCIRC) model to simulate extreme rainfall, winds, and storm surges. The authors validated this numerical tool by simulating Hurricane Isabel and its landfall on Chesapeake Bay in the USA.

During the 2010s, more sophisticated numerical modelling techniques emerged for investigating compound flooding phenomena. In the USA in particular, a significant amount of research was carried out to explore compound flooding generated by tropical storms in more depth. Consequently, ADCIRC software (usually coupled with SWAN) became widely used for modelling hurricane-related compound flooding, taking into account coastal and fluvial drivers.

Studies such as those by Tromble et al. (2010), Dietrich et al. (2010), Blanton et al. (2012), and Kerr et al. (2013) analysed hurricanes and tropical storms such as Katrina, Isabel, Alberto, Gustav, Irene, Earl and Ike.

Similarly, some researchers have applied HEC-RAS and SWAT numerical models to simulate compound flooding, for example Mashriqui et al. (2014) modelled Hurricane Isabel and Lian et al. (2013) modelled compound flooding after Typhoon Longwang in China. Additionally, Bevacqua et al. (2019) pioneered the analysis of compound flooding in the context of sea level rise (SLR), examining the interaction between fluvial and pluvial drivers using a copula-based joint probability approach under projected SLR scenarios. During this period, DELF3D was also widely used in compound flooding studies, as demonstrated by the work of Klerk et al. (2015), Petroliagkis et al. (2016), Kumbier et al. (2018), Herdman et al. (2018) and Lee et al. (2019).

In the context of the Tagus Estuary, De Pablo et al. (2019) developed a numerical modeling approach using the MOHID Water Modeling System to simulate estuarine hydrodynamics. While not specifically focused on compound flooding, this study is highly relevant because it provides a validated framework for understanding the estuary's physical behavior under different forcing conditions. The authors assessed the influence of meteorological factors, such as wind and atmospheric pressure, as well as river discharge, on water levels and circulation patterns. The model's results were rigorously validated against in situ observations, demonstrating high accuracy in reproducing tidal propagation and hydrodynamic variability. This work established MOHID as a reliable tool for simulating the Tagus Estuary's complex dynamics, providing a valuable baseline for future research.

2.4 Conceptual Refinement and Typology

Alongside numerical advancements, the conceptual framework of compound events was explored. The term 'compound event' was officially defined for the first time in the IPCC Special Report on Extremes (SREX) in 2012, where it referred to two or more extreme, climate-related events occurring either simultaneously or in succession. This definition also encompasses the combination of extreme events with underlying conditions that amplify the magnitude of the impacts, as well as combinations of non-extreme events that can trigger an extreme event or a combined impact (Seneviratne et al., 2012).

Leonard et al. (2014) emphasised two key characteristics for defining compound events: the involvement of multiple variables or events that give rise to the impact and statistical dependence among the drivers. Building on this, Zscheischler et al. (2018) conducted a more comprehensive analysis, defining compound weather and climate events as the combination of multiple drivers or hazards contributing to societal or environmental risk. The authors emphasised the importance of interactions among drivers, processes, and phenomena across spatial and temporal scales. Subsequently, Zscheischler et al. (2020) proposed categorising climate-related compound events into the following types:

- Preconditioned: where a hazard results in an amplified impact due to a preceding condition.
- Multivariate: where the co-occurrence of multiple climate drivers and/or hazards in the same geographic region causes an impact.
- Temporal compounding (sequential): where the sequence of hazards affecting a given region leads to or intensifies an impact compared to a single hazard.
- Spatially compounding where spatially co-occurring hazards collectively cause an impact.

2.5 Recent growth and global trends

Since 2020, more advanced numerical and statistical methods have been used to investigate compound flooding. For example, Ganguli et al. (2020) used a Copula-Markov chain Monte Carlo simulation in conjunction with a DELFT-3D model to simulate the projected changes in storm surges and river discharge, and to evaluate future compound hazards in northwestern Europe based on sea level rise projections (RCP 8.5). Similarly, Wu et al. (2021) estimated the probability of compound floods in the estuarine portion of the Swan River in Western Australia by applying numerical (MIKE21) and statistical (joint probability method (JPM), frequency analysis, and peak over threshold (POT)) approaches, with different return periods used for the simulations.

Nowadays, most numerical models (such as DELFT3D and HEC-RAS) require significant computational capacity to numerically solve fluvial, pluvial, and coastal processes numerically. To address this issue, Leijnse et al. (2021) developed SFINCS (Super-Fast Inundation of CoastS),

which is a computationally efficient, reduced-physics solver that solves simplified mass and momentum equations while accounting for key flood drivers, such as storm surges, precipitation and upstream river discharges. Nevertheless, in order to provide accurate boundary conditions and capture the influence of large-scale atmospheric and oceanic processes, SFINCS must be coupled with other regional models, such as hydrodynamic or meteorological models, which supply essential inputs such as water levels, river flows, and rainfall patterns.

In subsequent years, numerical modelling became the predominant approach among researchers for addressing compound flooding. For example, Muñoz et al. (2022) investigated the combined occurrence of fluvial, pluvial, and coastal drivers during Hurricanes Harvey and Sandy by combining Delft3D-FM with joint probability methods, copulas, and the Peak Over Threshold (POT) approach. Subsequently, Nederhoff et al. (2024) developed a robust and computationally efficient tool (PS-CoSMoS) for resolving compound coastal flooding in complex estuarine environments. This tool couples the cross-shore profile model (XBeach) and the overland flooding model (SFINCS) and has been validated through its application to the Puget Sound region of Washington State (USA) and the greater Salish Sea. Other studies have started to analyse climate change adaptation measures based on compound flood modelling, as in the case of Kupfer et al. (2025). In this study, the authors used a DELFT3D model to simulate compound floods in the Baltic Sea, considering different scenarios involving storm surge barriers and other measures.

2.6 Comprehensive Review and Definitions

While numerical and statistical models have been developed to address compound coastal flooding, some authors have focused on advancing the field's conceptual framework by conducting systematic reviews of existing literature. Two comprehensive reviews stand out in this regard: Sun et al. (2024) and Green et al. (2025). Both studies synthesise findings from a wide range of case studies and modelling approaches related to compound coastal flooding. While their definitions emphasise the interactions between coastal, fluvial, and pluvial processes, they differ slightly in focus. Both comprehensive reviews highlight that, despite growing scientific interest, significant research gaps remain. The authors argue that the integration of coastal, fluvial, and pluvial drivers is limited, largely due to insufficient observational data. Furthermore, the two reviews conclude that numerical and statistical methods also lack consistent frameworks, making comparisons across studies difficult.

Sun et al. (2024) define compound coastal flooding as resulting from the interplay of multiple hazard-inducing factors driven by meteorological, hydrological, and hydrodynamic processes. They classify these drivers into three main categories: (1) oceanic processes, such as storm surges; (2) riverine discharges resulting from upstream precipitation; and (3) localised precipitation. This definition emphasises the physical origins of these processes and their combined potential to trigger flooding. Figure 1 provides an overview of these processes.

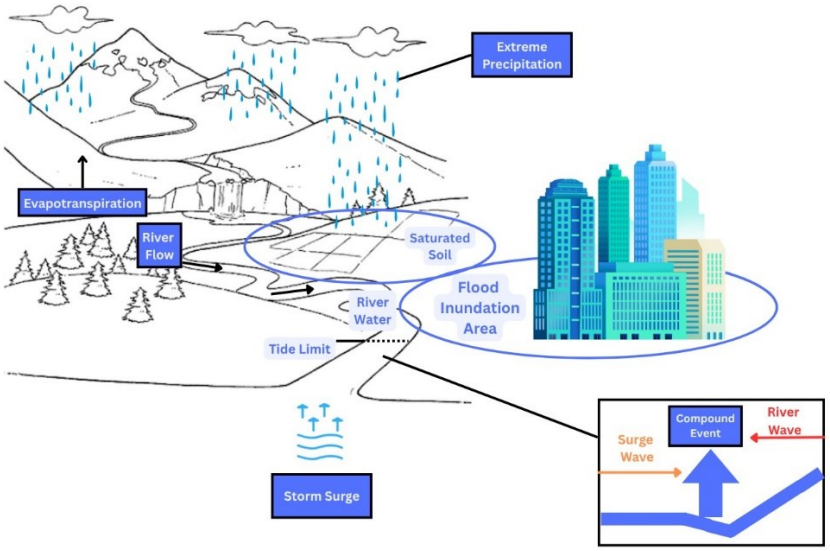

Figure 1. Compound coastal Flooding scheme. Adapted from Sun et al. (2024)

A clear example of compound coastal flooding is when a storm causes extreme precipitation and a storm surge. This occurred during the severe flood event in Ravenna, Italy, in February 2015, which was classified as a spatial compound event (Zscheischler et al., 2020). In this instance, a low-pressure system produced heavy rainfall across several catchments, accompanied by a storm surge. Together, these triggered a compound flood event (Bevacqua et al., 2017). This process is illustrated in Figure 2.

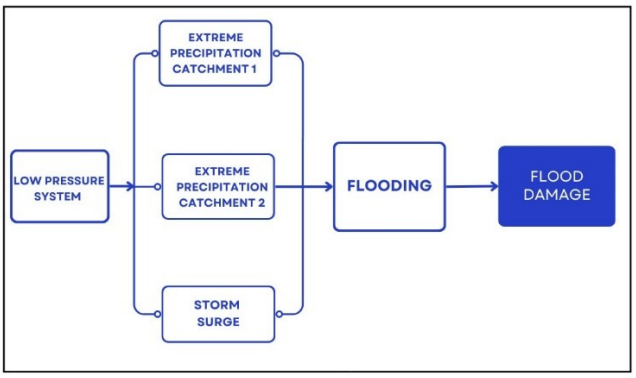

Figure 2. Compound flood event in Ravenna, Italy in 2015 - compound process scheme. Adapted from Zscheischler et al. (2020)

III. Study Area

The Tagus Estuary, located on the western coast of Portugal, is the largest estuarine environment on the Iberian Peninsula. Its outer section is directly exposed to the Atlantic Ocean, where wave action plays a dominant role (Rusu et al., 2011). In contrast, the inner estuary is more sheltered and influenced primarily by tidal and fluvial dynamics (Fortunato et al., 2017). The Tagus and Sorraia rivers are the primary sources of freshwater flowing into the estuary. Their discharges are regulated by upstream reservoirs and dam infrastructure (Rilo et al., 2022). Figure 3 provides an overview of these features.

The estuary borders 18 municipalities that collectively comprise the Lisbon Metropolitan Area, a highly urbanized and densely populated region affected by natural hydrometeorological processes and intense human activity (Rilo et al., 2015). The high degree of urban development along the estuary's margins increases its vulnerability to flooding (Tavares et al., 2015).

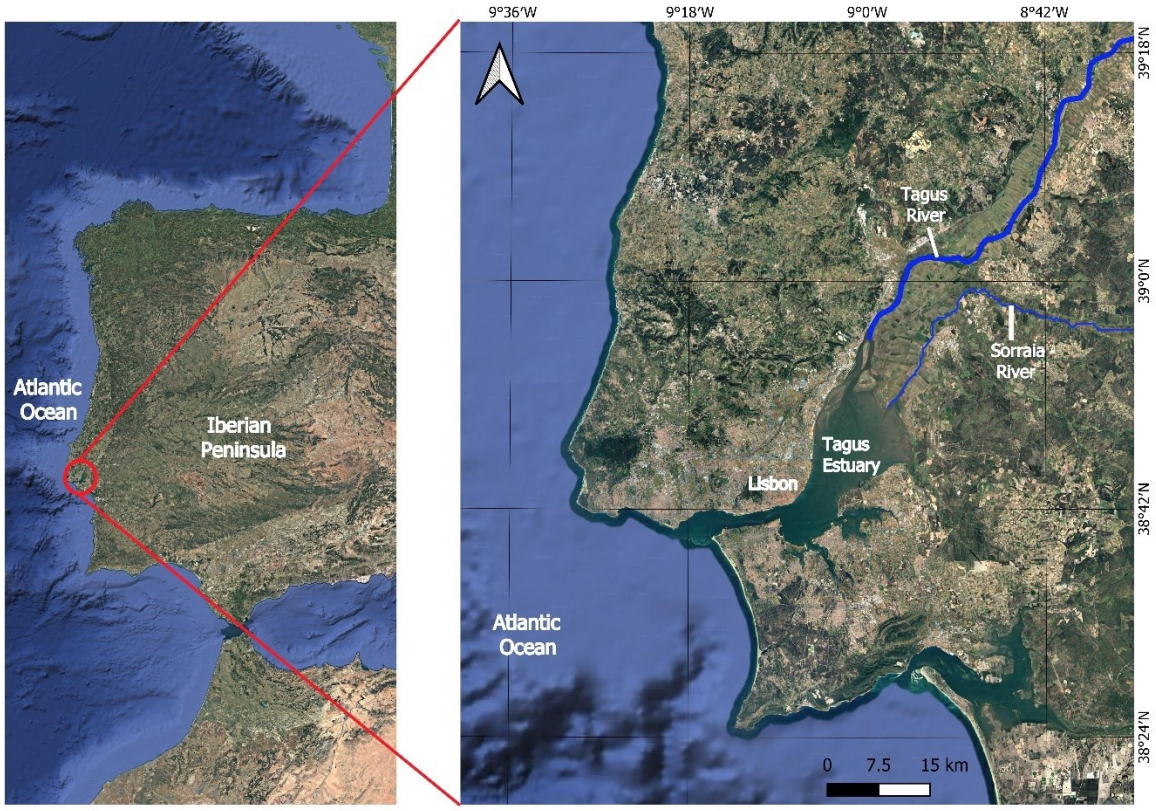

Figure 3. Study area. Source basemap: Google Satellite (QGIS)

3.1 Morphology

The Tagus estuary encompasses three main areas that are interconnected and interact dynamically: the mouth of the Tagus River, the inner estuarine zone, and the inlet channel located in the nearby coastal area covering a surface area of about 320 km² (Guerreiro et al., 2015). The estuary features a complex geomorphology, characterized by a long, narrow inlet channel (referred to as the Tagus corridor) that links the Atlantic Ocean to a shallower interior area containing tidal flats and salt marshes, known as the Mar da Palha (Ribeiro et al., 2022), as illustrated in Figure 4.

The Tagus corridor measures 12 km in length, 2 km in width, and reaches a maximum depth of 40 m meanwhile the central section of the Tagus estuary is the biggest one, covering about 15 km in width, 30 km in length and featuring an average depth of approximately 7 m (Fortunato et al., 2017). The mouth of the Tagus River is located at the northern part of the estuary. It marks the transition between the fluvial system and the estuarine waters and is a key site for supplying freshwater and fluvial sediments to the estuary (Vaz et al., 2019). The morphology of the Tagus estuary contributes to tidal range amplification due to resonance effects, which in turn influence water levels (Guerreiro et al., 2015).

Intertidal zones make up about 40% of the estuarine area and are particularly prominent near areas such as Pancas, Montijo, and Seixal, located at the southern margin of the estuary (De Pablo et al., 2019). By contrast, the Caparica area is located south of the estuarine inlet facing direct exposure to the Atlantic Ocean. The municipality of Loures is located just inland of the northern estuarine margin and is part of the Lisbon metropolitan area. Particularly its riverfront area, lies adjacent to the Mar da Palha mudflats and floodplains (Santos et al., 2024) as shown in Figure 4.

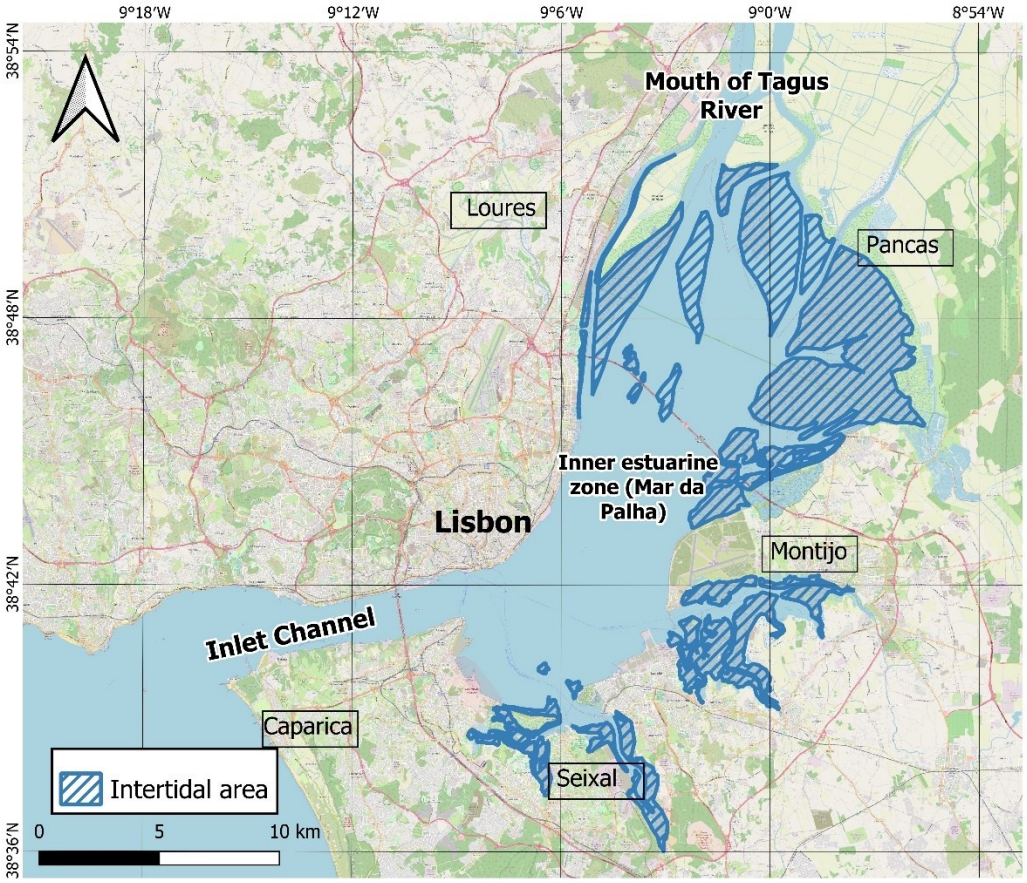

Figure 4. Main morphologic areas of the Tagus estuary. Shapefile source: Direção-Geral do Território (2022). Source basemap: OpenStreetMap (QGIS)

3.2 Hydrodynamics

The Iberian Atlantic coast tides are semi-diurnal and storm surges increase from south to north (Rilo et al., 2022). The hydrodynamics of the Tagus estuary are primarily influenced by its intricate bathymetry, the tidal flow within the estuary and the freshwater discharge from the Tagus River (De Pablo et al., 2019). The Tagus estuary is characterized as a semidiurnal, mesotidal system that is typically well mixed, with an average tidal amplitude of 2.4 m at the river mouth and the tidal range fluctuates between 0.9 m during neap tides and 4.1 m during spring tides (Fortunato et al., 2017). Ocean waves do not penetrate significantly in the inner part of the estuary (Guerreiro et al., 2015).

Observations from the Almourol hydrological station (located approximately 80 km upstream the estuary) between 2006 and 2019 indicate that the Tagus River discharge rates ranging from 0 to 9,874 m^3/s, with an annual average of 263 m^3/s (Vargas et al., 2008). According to Portela (1996), the mean annual discharge of the Sorraia River is equivalent to around 8.5% of the Tagus River's flow.

The estuary's extensive tidal flats contribute to its strongly ebb dominated nature while tidal forces are the primary drivers of estuarine circulation. Other factors, including river flow, weather patterns, and interactions with the estuary's morphology and bathymetry also play significant roles (De Pablo et al., 2019).

3.3 Regional Climate Patterns

Portugal has a Mediterranean climate, which is characterized by cool, wet winters and hot, dry summers. This climate is largely shaped by Portugal's geographical location between the Atlantic Ocean and the Mediterranean Sea (Mora and Veira, 2020). While most precipitation occurs during the winter months, rainfall patterns exhibit significant interannual variability in both time and space. This variability is influenced by several factors, including the country’s latitude, atmospheric circulation patterns, topography, and the interaction between oceanic and continental systems (Rilo et al., 2022). Trigo and DaCamara (2000) further highlight the role of the North Atlantic Oscillation (NAO), noting that its negative phase is typically associated with wetter than average winters.

IV. Methodology

This study employed a combination of numerical modeling, satellite remote sensing, Extreme value and Joint Probability Analysis and GIS-based data processing to simulate and evaluate compound flooding in the Tagus Estuary. The methodology comprised the acquisition and preprocessing of multi-source datasets, including climatological, hydrological, and oceanographic data from national Portuguese monitoring entities and open-access portals. These data sets were processed and used to define the boundary conditions for the numerical flood model (SFINCS). Boundary water levels were obtained from the hydrodynamic circulation model (MOHID) to solve the circulation inside the estuary, while precipitation inputs were derived from observational records. The model was then validated using the December 2022 flood event in the Tagus Estuary covering the Lisbon metropolitan area. Following validation, a multivariate statistical and extreme value analysis were conducted to assess the joint probability of drivers contributing to compound flooding. Based on that, a series of synthetic flood scenarios were simulated to evaluate flood extent and depth under varying forcing combinations. Finally, the results of each scenario were analyzed by GIS tools. This workflow is outlined in Figure 5.

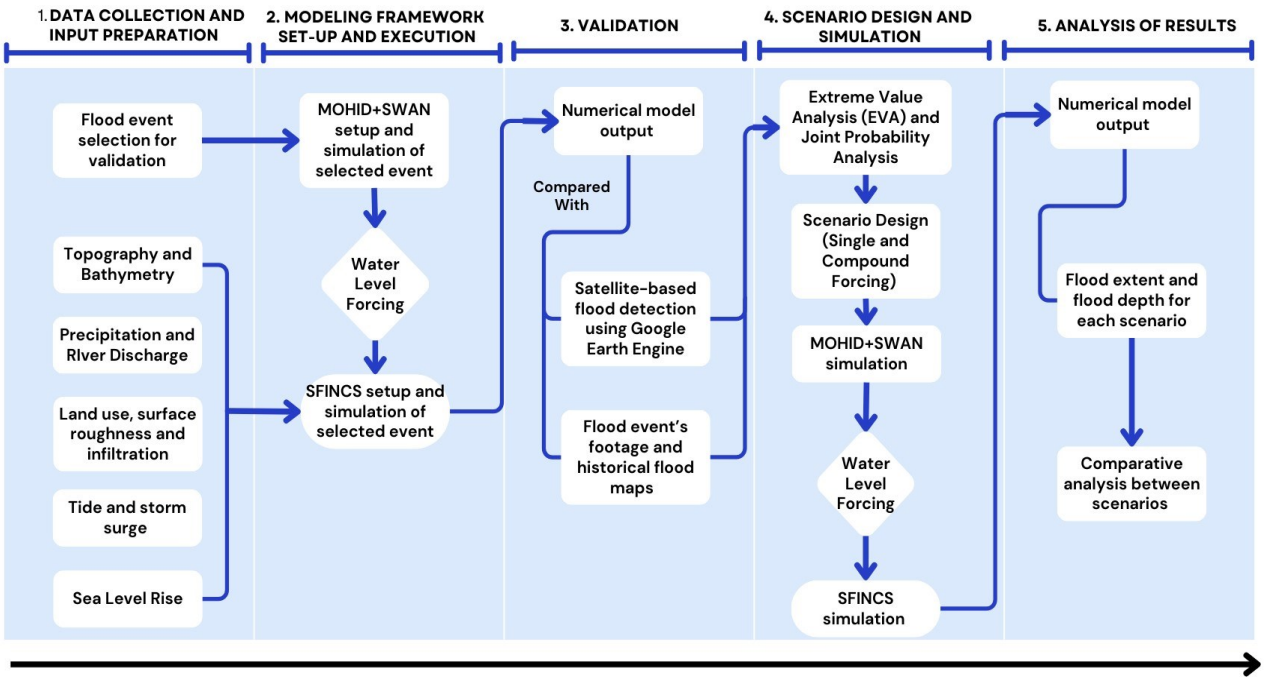

Figure 5. Methodological Framework of the Study

4.1 Data Collection and input preparation

4.1.1 Topography and Bathymetry

The bathymetry raster file corresponding to the Tagus estuary was downloaded from the Portuguese Hydrographic Institute (Instituto Hidrográfico, 2025) website. It has a spatial resolution of 25 x 25 meters and covers the entire spatial domain of the model. The deepest areas of the estuary are in the inlet channel, reaching a maximum depth of 49.19 meters. In the inner estuarine zone, depths reach up to 12 meters, as shown in Figure 6.

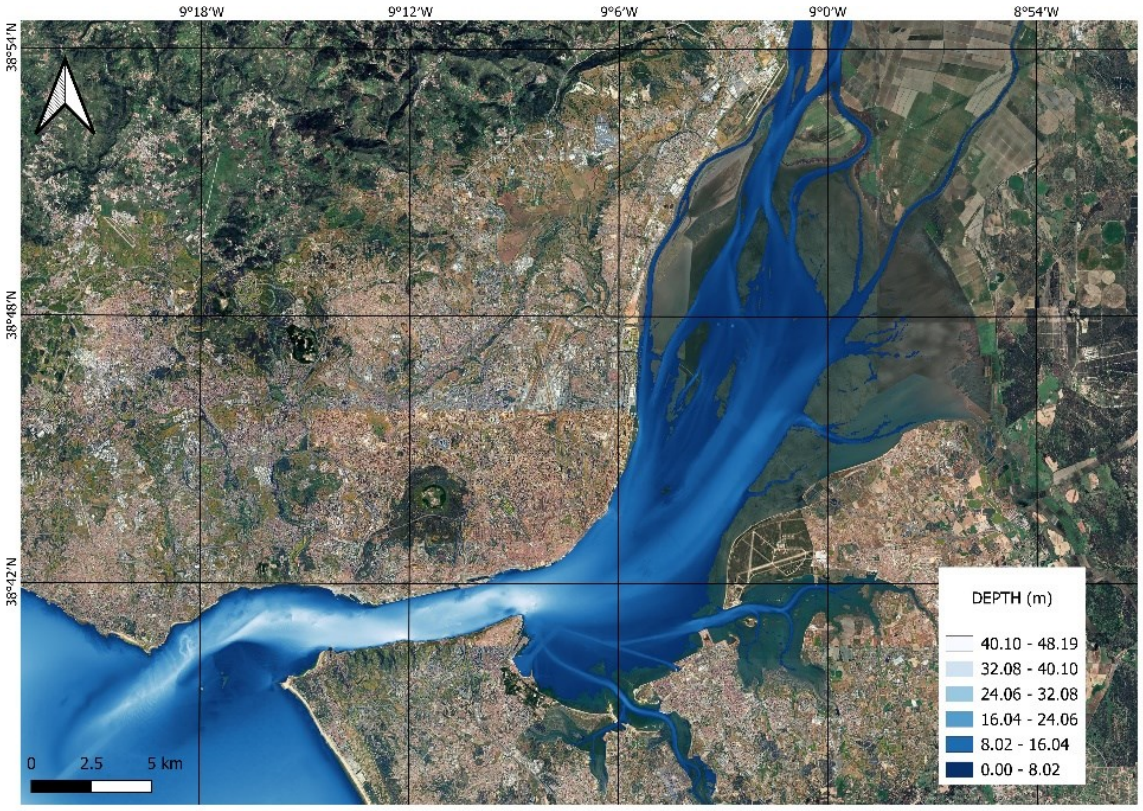

Figure 6. Bathymetry of the study area. Data Source: Instituto Hidrográfico (2025). Source basemap: Google Satellite (QGIS)

The data collection process to obtain the digital elevation model (DEM) of the study area was carried out with the aim of achieving the highest spatial resolution possible. Three elevation models covering the modeling domain were collected: (1) a LiDAR-based elevation model with a spatial resolution of 2 x 2 meters, generated in 2015 and covering the northern margin of the estuary, obtained from the Direção-Geral do Território (n.d.) ; (2) a LiDAR-based elevation model with the same spatial resolution, generated in 2014 and covering the southern margin of the estuary, obtained from Direção-Geral do Território (n.d.) ; and (3) the ALOS AW3D30

elevation model with a spatial resolution of 25 x 25 meters, downloaded from the Coastal monitoring and management group of the Faculty of Sciences of the University of Porto (CIIMAR, 2025). The three digital elevation models mentioned, as well as four verification profiles between the DEMs, are illustrated in Figure 7.

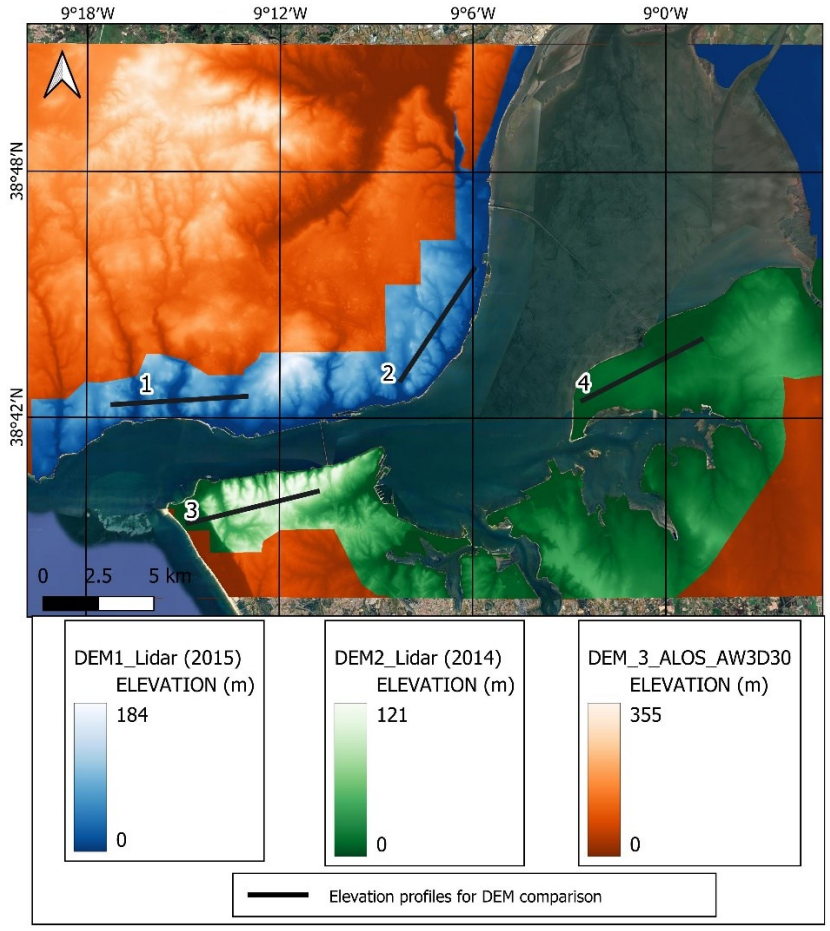

Figure 7. Digital Elevation Model (DEM) raster files employed in the study. Source DEMs: Direção-Geral do Território (n.d.) and CIIMAR (2025). Source basemap: Google Satellite (QGIS)

The three digital elevation models were subjected to a verification process regarding their spatial resolution by comparing the DEMs generated from LiDAR data with the ALOS AW3D30 DEM. The latter covers the entire continental area of Portugal, and therefore, the coverage areas of DEM 1 and DEM 2 are also included within DEM 3. Consequently, four verification profiles were generated to compare DEM 1 (Lidar – 2015) and DEM 2 (Lidar -2014) against DEM 3 (ALOS AW3D30). In general, the elevation differences between the LiDAR-based DEMs and the ALOS DEM for most of the overlapping areas do not exceed 2 meters. However, in some areas along the northern side of the estuary, slightly higher elevation differences are observed, as shown in Figure 8.

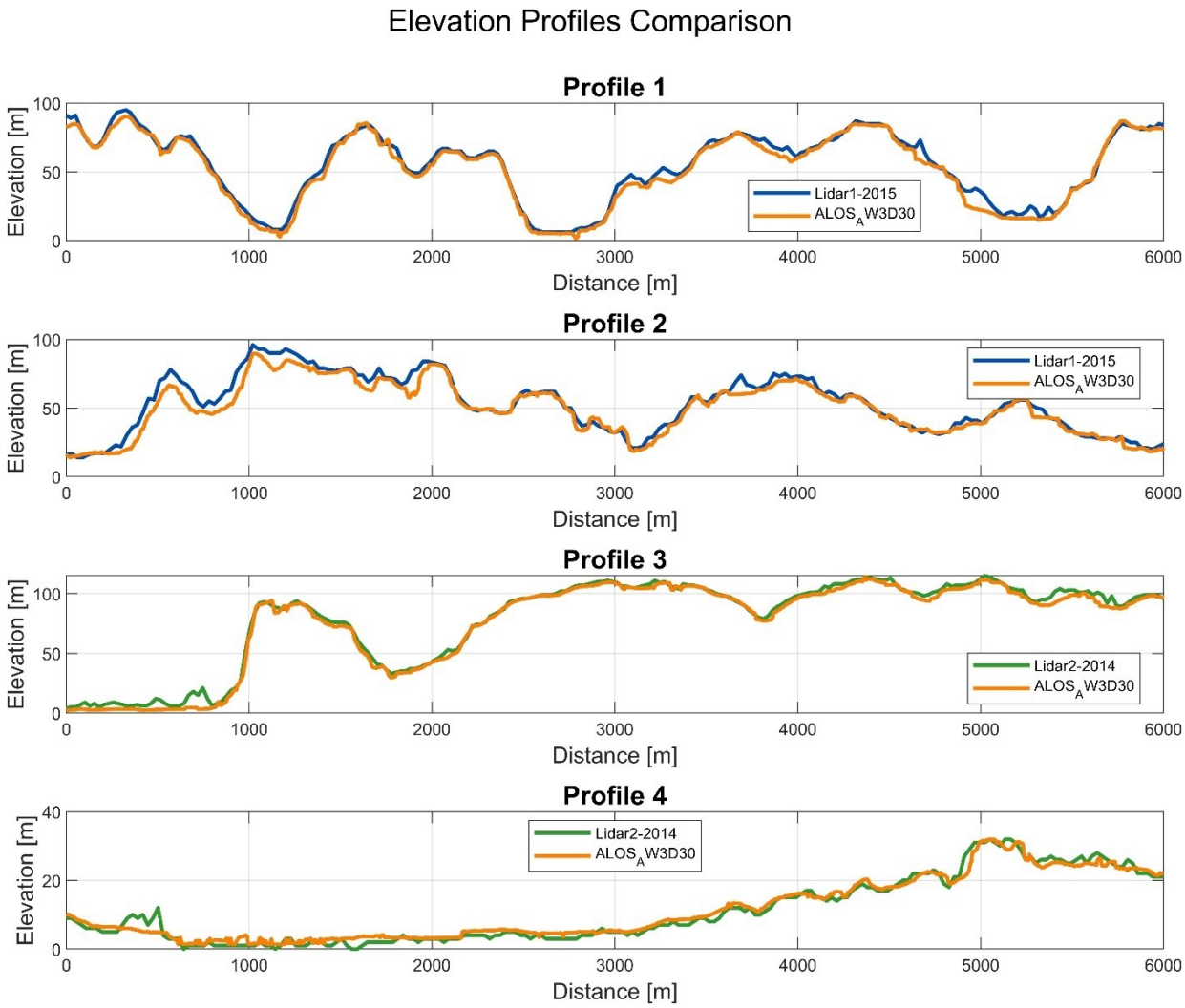

Figure 8. Lidar and regional DEM profiles comparison. Source DEMs: Direção-Geral do Território (n.d.) and CIIMAR (2025).

The final terrain elevation model used as input for the flood numerical model was the result of a geoprocessing operation (merge and resampling) performed in QGIS software, combining the three elevation datasets above mentioned to generate a final DEM for the spatial domain of this study. Based on that, the topography of the spatial domain of the model can be described as follows: The northern margin of the estuary exhibits a complex topography with a significant elevation gradient. Close to the estuary shoreline, elevations are generally low (0–59.2 meters). Moving inland, the elevation gradually increases reaching the highest peaks in the northwest sector of the spatial domain. These higher elevations, reaching up to approximately 355 meters, correspond to the hilly and mountainous terrain north of Lisbon. Numerous drainage channels and tributary valleys are also visible, contributing to the estuarine system.

The southern margin of the Tagus Estuary shows a generally flatter topography compared to the north. The immediate coastal area and large portions of the inland regions are dominated by low-lying terrains, mostly within the 0–59.2 meters elevation range. Some localized areas slightly inland rise to elevations between 59.2 and 118.4 meters, but the southern region lacks the steep elevation gradients seen to the north. This flatter terrain characterizes the extensive floodplains and agricultural areas. The final Digital Elevation Model (DEM) used as topographic input for the numerical flood model is presented in Figure 9.

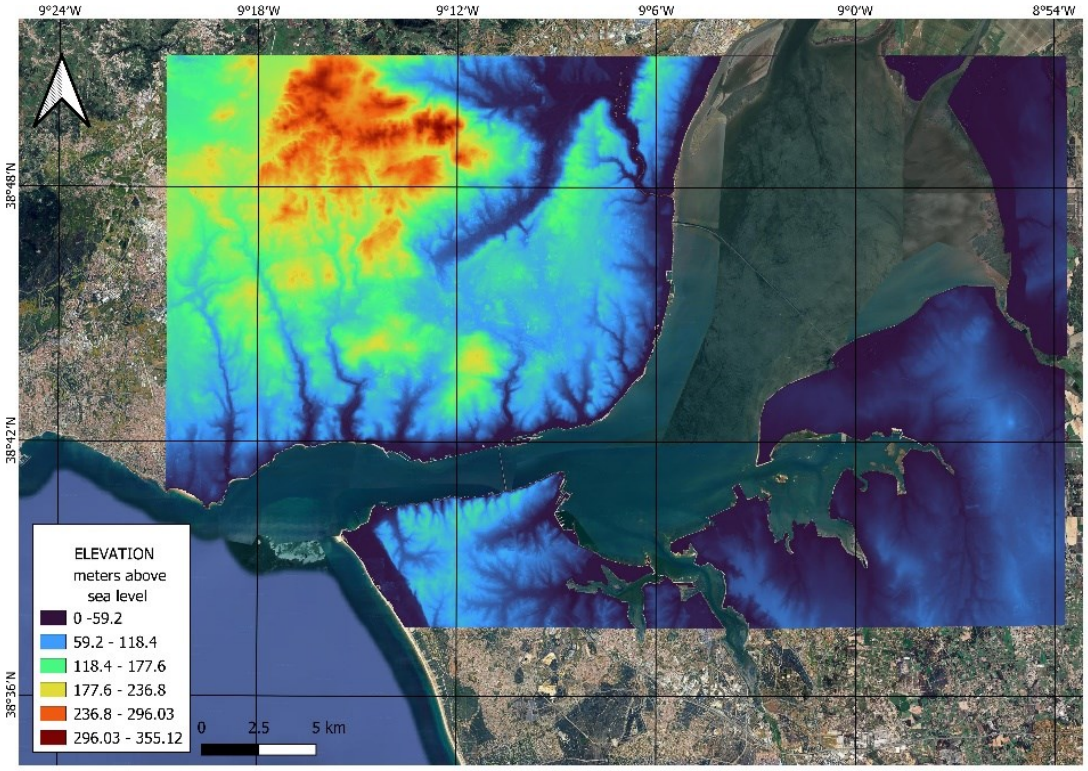

Figure 9. Final Digital Elevation Model (DEM) used as topographic input for the numerical flood model. Source DEMs: Direção-Geral do Território (n.d.) and CIIMAR (2025). Source basemap: Google Satellite (QGIS)

4.1.2 Precipitation, River and Dam Discharge

Data on local precipitation, river discharge and regulated flow releases from the nearest upstream dam to the estuary were collected. The precipitation data within the study area were requested from the Instituto Português do Mar e da Atmosfera (n.d.), which provided the historical time series from three active rain gauge stations located on the northern margin of the estuary. A description of these stations is presented in Table 1.

Name	Altitude (m)	Coordinates		Start date of measurements
		Latitude	Longitude	
Lisboa / Geofísico	77	38.719	-9.15	17/03/1999
Lisboa / Gago Coutinho	103.9	38.766	-9.128	25/06/1997
Lisboa / Tapada da Ajuda	70	38.71	-9.183	28/01/2010

Table 1. Rain Gauge stations used in the study. Source data: Instituto do Mar e da Atmosfera – Instituto Português do Mar e da Atmosfera (n.d.)

The river and dam discharge data were obtained from the website of the Sistema Nacional de Informação de Recursos Hídrico (SNIRH) – (Agência Portuguesa do Ambiente, n.d.). For river discharge (Tagus river), the hydrometric station with the most complete dataset and closest location to the estuary was the Almourol station (Lon. -8.359, Lat. 39.459), located approximately 80 km upstream from the estuary. Similarly, dam discharge data were obtained from the closest dam to the estuary, the Albufeira de Belver hydroelectric dam (Lon. -7.997, Lat. 39.480), located approximately 120 km upstream from the Tagus estuary. The locations of the different monitoring stations are shown in Figure 10.

It should be noted that SNIRH does not operate any monitoring stations for the Sorraia River within the area of influence of this study, which lies downstream of the Montargil Dam (constructed in 1958, located at Lon. -8.176167, Lat. 39.053). The river's discharge is regulated by this dam. However, in this study, the hydrodynamic circulation was simulated using MOHID, and this tributary was incorporated into the simulations as part of the operational circulation model, which resolves the hydrodynamics of this water body.

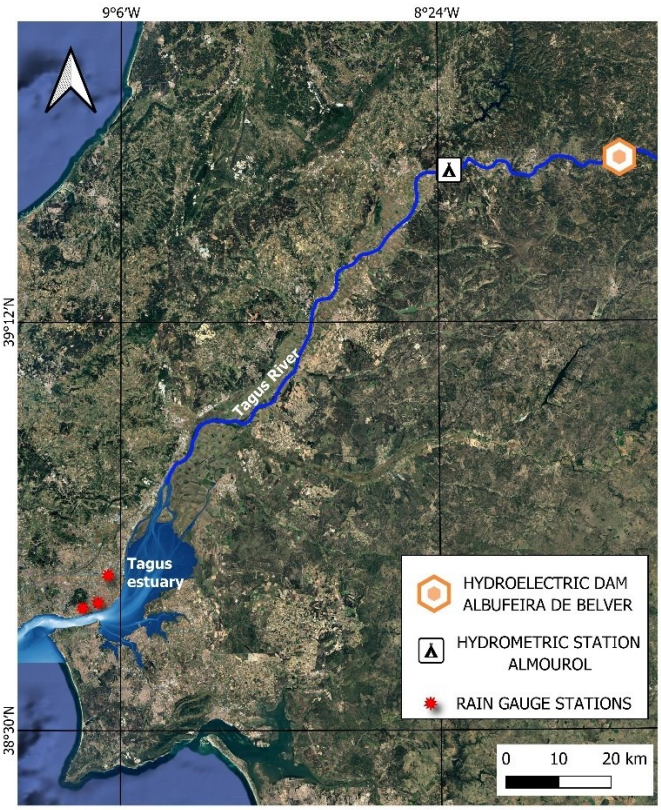

Figure 10. Map of hydrometric and rain gauge monitoring stations. Source basemap: Google Satellite (QGIS)

The temporal resolution of the precipitation dataset is 10 minutes. Due to the proximity of the rain gauges, average values were calculated for the overlapping periods of the three gauges, resulting in a final dataset covering the period from July 1997 to December 2024. Additionally, the maximum accumulated precipitation in this period occurred on December 13, 2022, as shown in Figure 11.

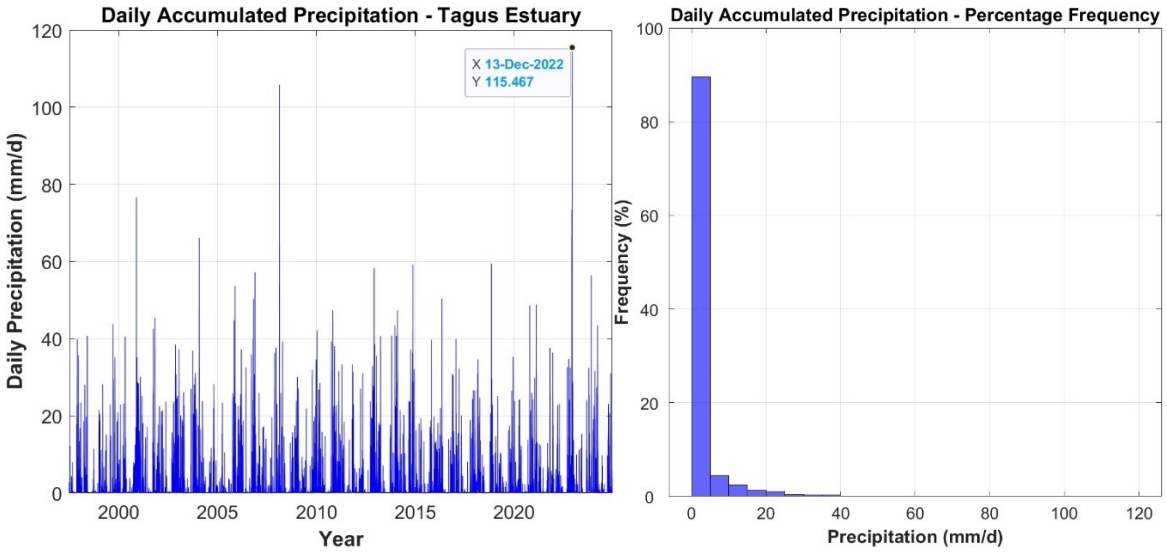

Figure 11. (a) left: Timeseries of daily accumulated precipitation in the Tagus Estuary; (b) right: Frequency distribution of daily precipitation data in the Tagus estuary. Source data: Instituto Português do Mar e da Atmosfera (n.d.)

The river discharge data of the Tagus River at the Almourol station have an hourly temporal resolution. Based on these data, daily average flow values were calculated for the entire dataset. The resulting daily average flow was 289.3 m³/s; however, several discharge peaks have been recorded over the five decades of monitoring, such as the one on December 14, 2022, as shown in Figure 12.

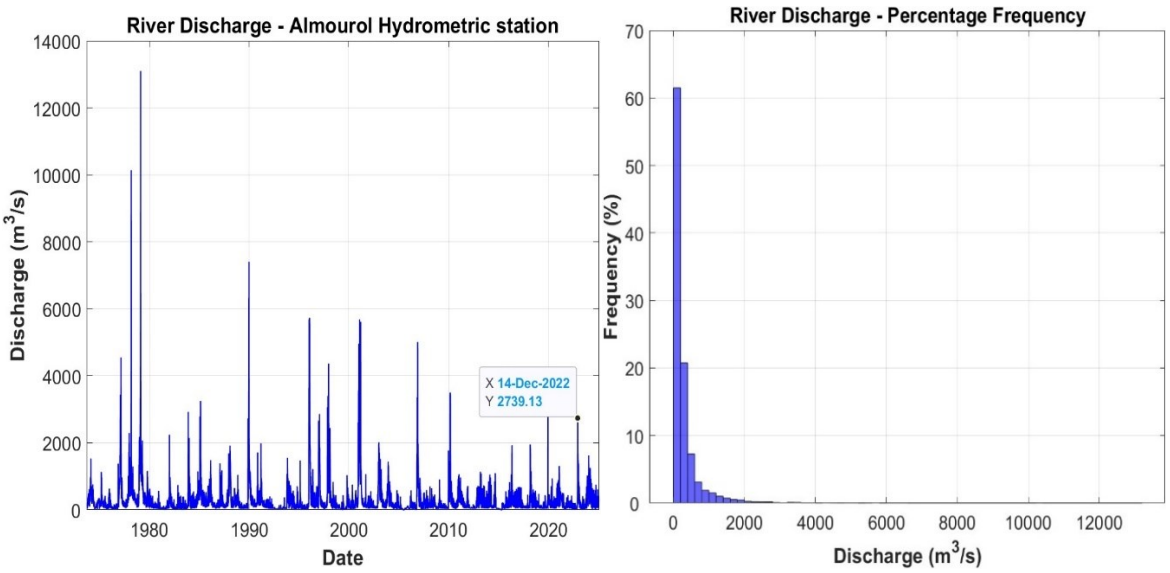

Figure 12. (a) left: Timeseries of daily average river discharge at Almourol Station; (b) right: Frequency distribution of daily average river discharge at Almourol Station. Source data: Agência Portuguesa do Ambiente (n.d.)

The dam discharge data monitored at the Albufeira de Belver hydroelectric (which was constructed in 1952) have a daily temporal resolution (daily average). During 87.84% of the monitored period, the dam discharge was 0 m³/s. It should be noticed that the dam discharge events have been associated with maximum precipitation events that triggered the need for such releases, such as the one occurred on December 13, 2022. These discharge events and their frequency are shown in Figure 13.

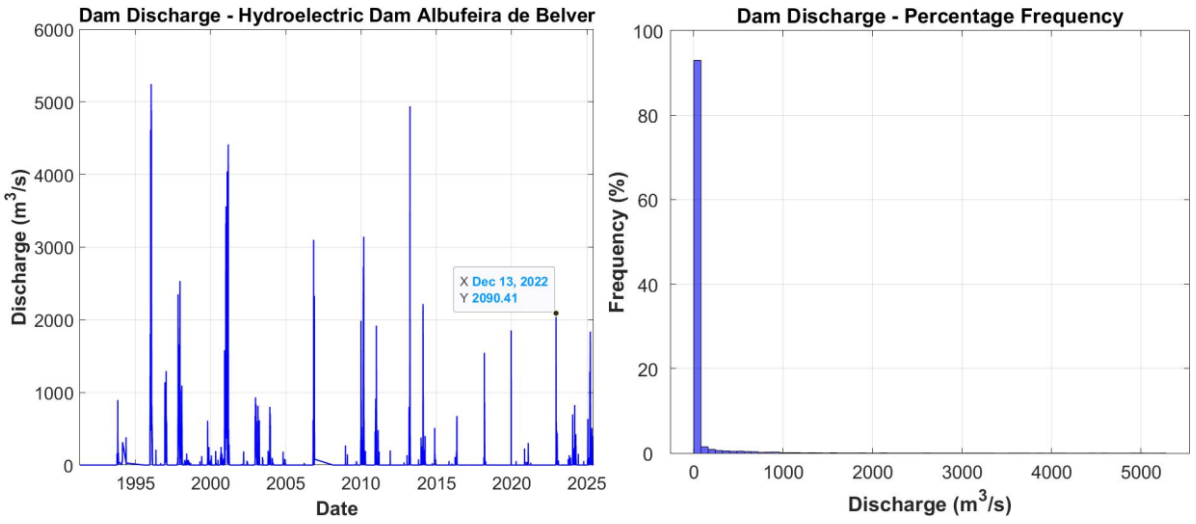

Figure 13. Timeseries of daily dam discharge at Albufeira de Belver station; (b) Frequency distribution of daily dam discharge at Albufeira de Belver station. Source data: Agência Portuguesa do Ambiente (n.d.)

Considering the Tagus river artificially regulated condition, which is mainly controlled by upstream dams (Rilo et al., 2022), as further evidenced in Figures 12 and 13 through the analysis of historical discharge data from the Belver hydroelectric dam and historical river discharge series at the Almourol hydrometric station, it can be observed that dam releases largely determine the river flow, especially during extreme weather events that lead to dam discharges due to potential reservoir filling, such as the one that took place on December 2022.

In this way, it was observed that during maximum precipitation events in the study area, the discharge of the Tagus River increased as well as the dam releases. For this reason, a statistical analysis of historical river discharge series was not carried out, given the artificial-driven nature of historical flow values in this river.

However, for the simulations of the different scenarios conducted in this study, the same storm shape from the December 2022 event was used, considering the observed increase in river discharge in response to maximum precipitation. Therefore, in this study, the single forcing is defined as pluvial/fluvial, taking into account the intrinsic relationship between these two variables.

4.1.3 Land Use, Rugosity and Infiltration

The land use dataset was obtained from the Direção-Geral do Território (2022). The Carta de Uso e Ocupação do Solo (COS) file, corresponding to the year 2022 was used in the study. The data consist of a raster file with a spatial resolution of 10 x 10 meters. Surface roughness values (Manning's roughness coefficient) were determined based on the land use categories derived from this land cover dataset. Infiltration values were obtained from the global raster GCN250 Global Curve Number Dataset (Jaafar and Ahmad, 2019), which contains curve number infiltration capacity by curve number method, with a spatial resolution of 210 x 210 m and a range of curve number from 53 to 85, where higher values (lower infiltration capacity) were found in urban areas. Regarding land cover, a large portion of the estuary margins is classified as artificial (urbanized) surfaces, which represent 33.08% of the total model domain area. Similarly, extensive agricultural areas are found predominantly along the southern margin of the estuary, accounting for 26.96%. In addition, large areas of coniferous, broadleaf, and herbaceous vegetation are present, as shown in Figure 14.

.

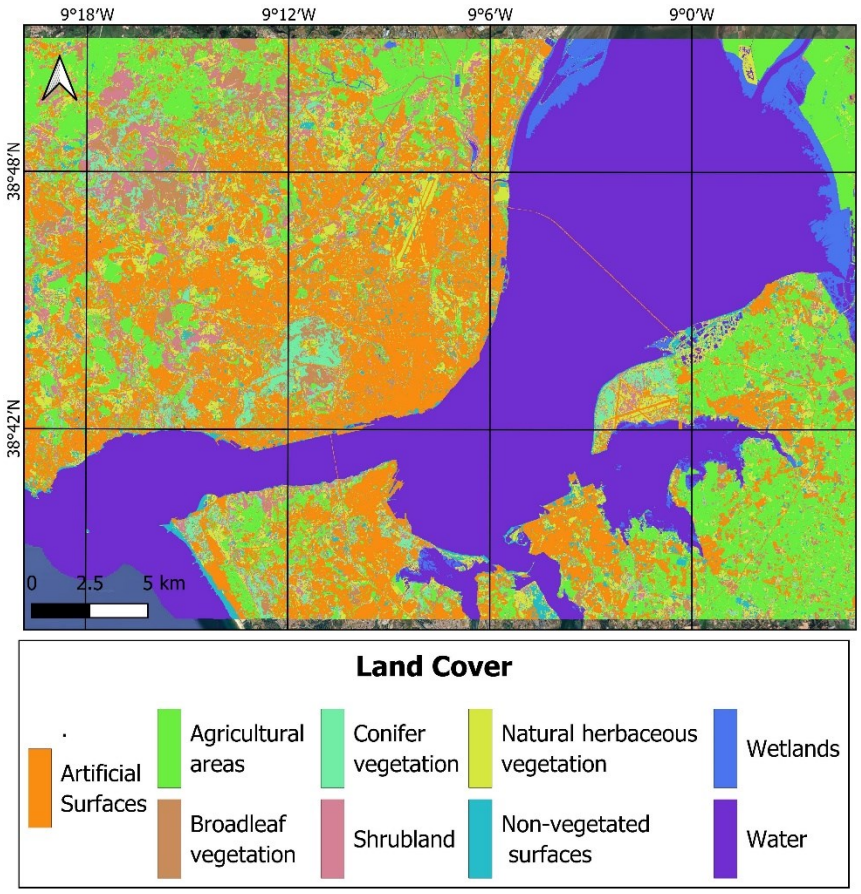

Figure 14. Land cover classification of the study area. Categories include artificial surfaces, agricultural zones, various vegetation types, wetlands, and water bodies.Data source: Direção-Geral do Território (2022)

The corresponding surface roughness values were assigned according to the different land cover categories classified by Direção-Geral do Território (2022) and based on a literature review of values commonly used in hydrodynamic modeling for these types of land covers. These roughness values were subsequently adjusted during the model calibration phase based on the observed flooded areas and water depths.

Specifically, Manning's coefficient values were assigned based on the findings of Papaioannou et al. (2018) and Emery et al. (2021). A Manning's coefficient of 0.05 s/m^(1/3) was assigned to urbanized areas, while agricultural areas (including autumn/winter and spring/summer annual crops, as well as other agricultural land) were assigned a value of 0.04 s/m^(1/3). Forested areas, such as Cork Oak and Holm Oak forests, Eucalyptus forests, and other broadleaf forests, were represented with a value of 0.12 s/m^(1/3). Coniferous forests, including Maritime pine, Stone pine, and other coniferous species, were assigned a coefficient of 0.10 s/m^(1/3). Shrubland areas were assigned a value of 0.09 s/m^(1/3), while natural herbaceous vegetation was represented with a coefficient of 0.04 s/m^(1/3). Bare land was assigned a lower value of 0.02 s/m^(1/3), reflecting minimal surface resistance. Wetlands were represented with a Manning's coefficient of 0.10 s/m^(1/3), while open water bodies were assigned a value of 0.03 s/m^(1/3).

4.1.4 Tide and Storm Surge

The tide data were obtained from the Faculty of Sciences of the University of Lisbon (FCUL) (Antunes, n.d.), which provides tide forecasts for Portugal's main ports. The data correspond to the Port of Lisbon (see Figure 15). These forecasts are based on harmonic analysis models developed at FCUL using data from 1999, 2006, 2007, 2009, 2010, and 2016. These forecasts have an average accuracy of 3 cm and 3 minutes, excluding the effects of meteorological surges. According to the 2022 tide dataset (see Figure 16) and observations by Fortunato et al. (2017), the tidal range fluctuates between 0.9 m during neap tides and 4.1 m during spring tides.

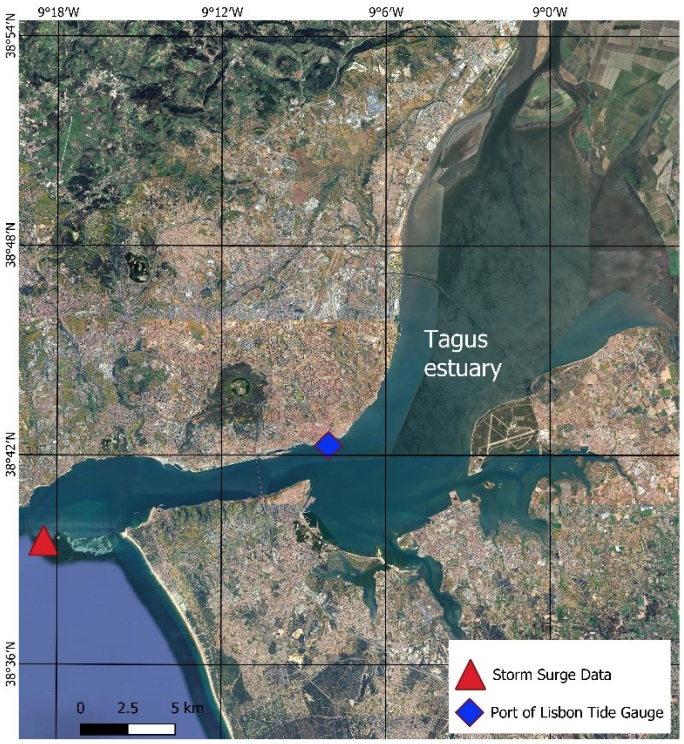

Figure 15. Storm Surge and Tides observation points. Data source Basemap: Google Satellite (QGIS)

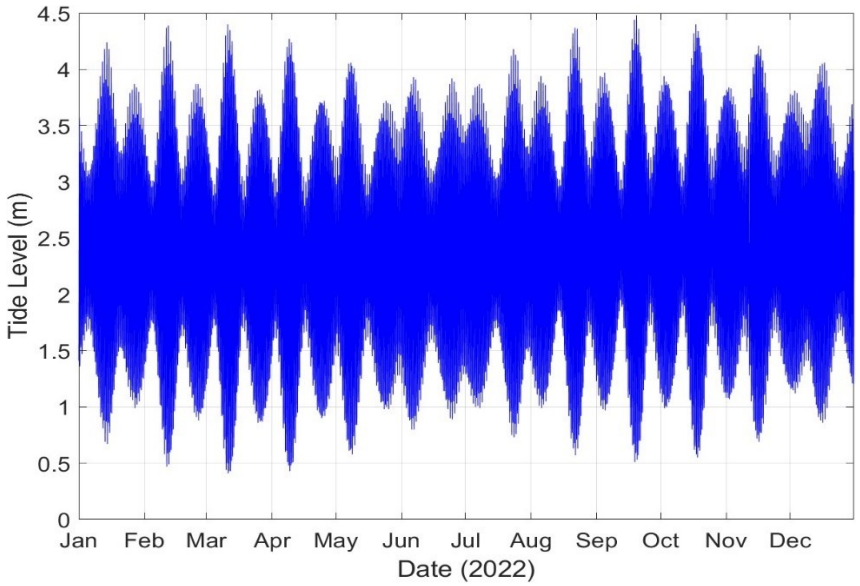

Figure 16. Tide level data of Port of Lisbon tide Gauge (2022). Data source: Antunes (n.d.); Chart Datum: +2.08 m

The storm surge data was obtained from the Copernicus Climate Change Service (2022), for a 25-year period reanalysis dataset at a location near the mouth of the estuary (see Figure 15). The dataset analyzed showed peak storm surge levels exceeding 0.6 meters under extreme conditions, as shown in Figure 17.

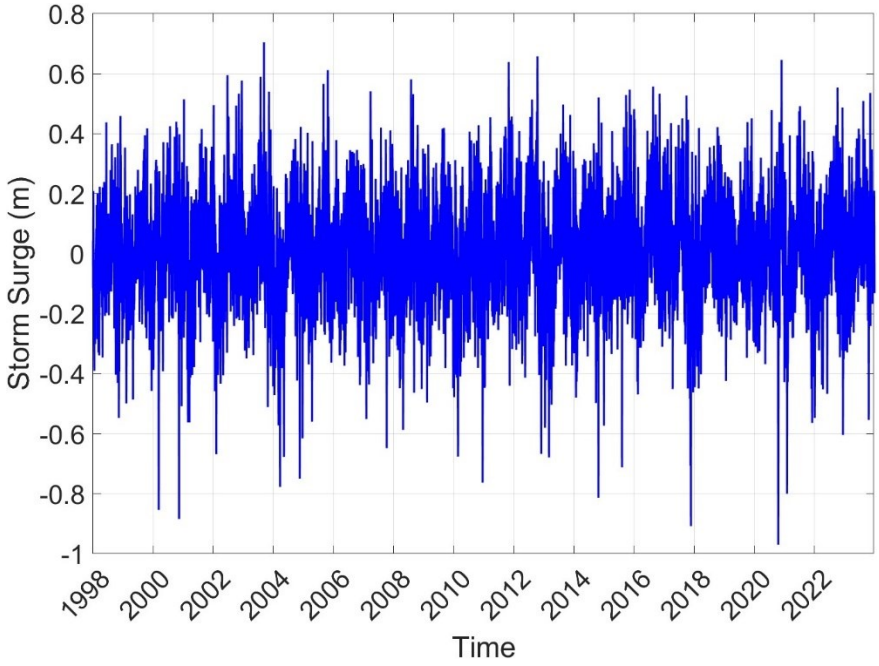

Figure 17. Storm surge data at the mouth of the estuary. Data source: Copernicus Climate Change Service (2022).

4.1.5 Sea Level Rise

The sea level rise (SLR) values used in this study are based on the projections provided by Lopes et al. (2022), who analysed historical extreme sea levels in Portuguese estuarine systems, including the Tagus Estuary, to evaluate future SLR scenarios. As a result of this analysis, the authors estimated SLR values along the Portuguese coast under different Shared Socioeconomic Pathways (SSPs) and time horizons. According to this study, for the SSP2-4.5 scenario, the projected SLR is 0.27 m for the period 2046–2065, increasing to 0.52 m by 2081–2100. Under the high-emission SSP5-8.5 scenario, the projections are 0.30 m for 2046–2065 and 0.67 m for 2081–2100. These projected values were applied in some of the flood scenarios analysed in the present study.

4.2 Validation event

The selected validation event was the flood that occurred in the study area in December 2022. During this month, two extreme precipitation occurrences were recorded: one on December 7, with a daily accumulated precipitation of approximately 70 mm, and another between December 12 and 13, with a maximum daily accumulated precipitation of approximately 110 mm, as well as an high storm surge event on December 7, reaching up to approximately 0.47 meters, as it is illustrated in Figure 18.

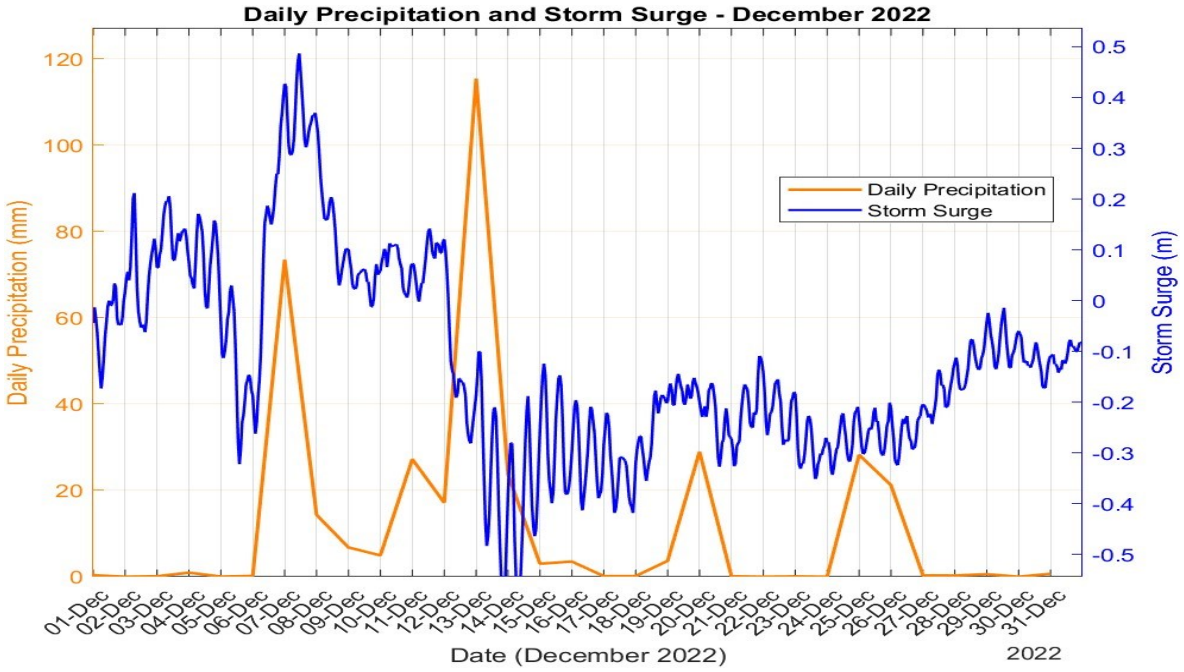

Figure 18. Storm surge and daily accumulated precipitation timeseries for December 2022 storm. Source data: Instituto Português do Mar e da Atmosfera (n.d.) and Copernicus Climate Change Service (2022)

The first significant precipitation event occurred around 7 December. During this event, there was no substantial increase in river discharge; however, a controlled release from the Albufeira de Belver Dam took place afterwards, although with a relatively modest flow. By contrast, the second precipitation event on 13 December led to a rapid surge in river discharge, peaking at almost 2,700 m^3/s. Dam discharge also increased, reaching slightly above 2,000 m^3/s. The concurrent rise in river and dam discharges during the second precipitation peak suggests that rainfall was the main cause of the increased river flow and reservoir releases. It is likely that the dam helped to reduce the increased river flow during the first event, but was less effective during the second event, possibly due to higher rainfall intensity or limited storage capacity. The relatively short time lag between the peaks in rainfall and discharge illustrates the basin and reservoir system's swift hydrological response to precipitation, as shown in Figure 19.

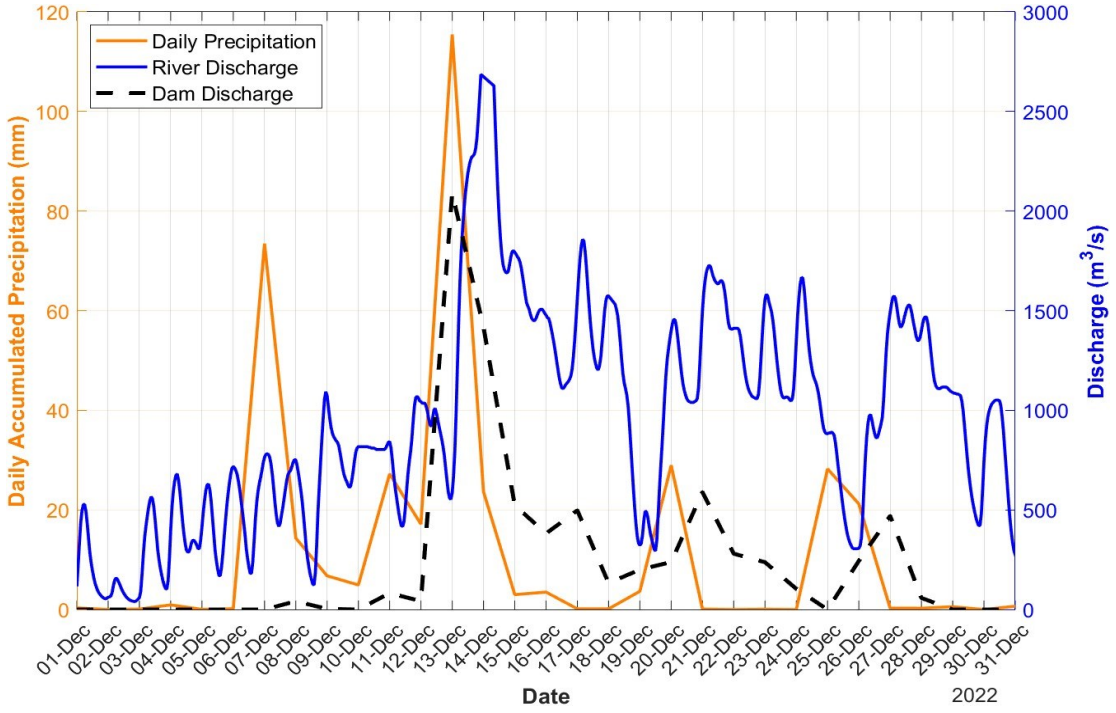

Figure 19. Daily accumulated precipitation, daily average river discharge and dam discharge timeseries for December 2022 storm. Data Source: Instituto Português do Mar e da Atmosfera (n.d.) and Agência Portuguesa do Ambiente (n.d.)

According to Ferreira et al. (2025), the precipitation recorded between December 12 and 13 was the highest extreme precipitation event ever recorded, at least throughout the monitoring period of the Dom Luís Observatory in Lisbon, which dates back to 1863. The authors argue that this event was driven by a combination of large-scale atmospheric conditions, including a negative phase of the North Atlantic Oscillation, a southerly jet stream position, and positive sea surface temperature anomalies over the North Atlantic. Additionally, the authors state that these factors contributed to the formation of multiple low-pressure systems that moved towards Western Europe. An atmospheric river (AR), first detected on 10 December, remained active for 72 hours due to high moisture transport and favourable uplift conditions. The AR made landfall in Portugal on 12 December, associated with a deep extratropical cyclone, resulting in record-breaking 24-hour precipitation.

Based on the analysis conducted, pre-conditioning conditions in terms of compound flooding were observed, as an initial precipitation peak potentially led to soil saturation, failure of urban drainage systems, as well as the filling of the Albufeira de Belver hydropower reservoir, resulting in high flow rates of the Tagus River. These factors were potentially decisive in the flooding process that caused extensive material damages.

This flood event caused considerable economic impacts in different areas of the Lisbon metropolitan area, as reported by local information sources such as news broadcasts, newspapers, and social media. Photographs and videos were collected concerning flooded areas within the study area during the selected flood event. The collection of footage from various information sources, such as social media and local newspapers (Expresso, 2022), resulted in the identification of three specific areas where there is clear evidence of flooding during the storm event. These areas are: (1) Algés (Lon. 38.69, Lat. -9.22), (2) Alcântara (Lon. 38.70, Lat. -9.17), and (3) Loures (Lon. 38.83, Lat. -9.16).

4.3 Satellite-Based Flood Detection using Google Earth Engine

Synthetic Aperture Radar (SAR) satellite data is widely used for large-scale flood mapping due to its ability to penetrate cloud cover and operate independently of sunlight. These capabilities enable consistent global coverage and effective application across diverse land cover types (Zhao et al., 2024). Therefore, to support the validation of the numerical flood model, Synthetic Aperture Radar (SAR) data from the Sentinel-1 were processed using Google Earth Engine (GEE). The aim of this task was to extract the flood extent associated with the December 2022 flood event in the Tagus Estuary. The workflow applied is described below.

First, the area of interest was defined to include the northern and southern margins of the Tagus Estuary, which are potentially affected by flooding. Sentinel-1 Ground Range Detected (GRD) imagery with a spatial resolution of 10 meters was acquired for both the pre- and post-event periods. Four images were used for the pre-event analysis: two acquired on November 26, 2022; one acquired on December 1, 2022; and one acquired on December 2, 2022. Five images were collected for the post-event analysis: two on December 8, 2022, and three on December 13 and 14, 2022. Then, filters for both ascending and descending orbits were applied to maximize spatial coverage and minimize potential temporal gaps. The analysis employed the vertical-horizontal (VH) polarization channel because it is more sensitive to flooded surfaces, especially in vegetated or urban areas (Mason et al., 2021).

Then, the Sentinel-1 images were framed in a mosaic and clipped to the study area. To reduce speckle noise inherent to SAR data, a Refined Lee filter was applied. This adaptive filter preserves edges while smoothing homogeneous areas, thus improving the reliability of backscatter differences used for flood detection (Yommy et al., 2015). After filtering, the images were converted back to the decibel (dB) scale for subsequent analysis. Flooded areas were identified using a change detection approach based on differences in backscatter intensity between the pre- and post-event images according to the method described by Liang et al. (2020). The inspector tool was used to identify the threshold that differentiates dry and water surfaces. Based on that, the detection criteria were defined as follows:

- Pixels with pre-flood VH backscatter > -22 dB (indicating dry or non-water surfaces).
- Pixels with post-flood VH backscatter < -22 dB (indicating water-covered surfaces, characterized by backscatter reduction due to specular reflection).

Permanent water bodies were identified separately as areas where both pre- and post-flood backscatter remained consistently below -22 dB, allowing the differentiation between dynamic flooding and permanent water surfaces. To minimize noise and eliminate small, isolated detections, a connected component analysis was performed. Only flood patches with at least 50 connected pixels were retained. Morphological operations (focal minimum and maximum filters) were applied to smooth the flood extent boundaries.

The final flood extent map was exported at 5-meter spatial resolution. This product was subsequently used as observational data to validate the flood extent simulated by the numerical hydrodynamic model. The SAR-derived flood extent provided valuable information on the spatial distribution and extent of inundation, particularly in urban areas such as Loures which was heavily affected during the event.

To assess the performance of the SFINCS numerical model in reproducing observed flood extents, a pixel-by-pixel comparison was conducted between the model output and SAR-based flood detection data. Both datasets were converted into binary raster files, where:

- **1** represents flooded areas;
- **0** represents non-flooded areas.

The comparison was carried out by overlaying the two raster datasets and classifying each pixel into one of the following categories:

- **True Positive (TP):** Pixels where both SFINCS and SAR detect flooding (SFINCS output = 1, SAR = 1).
- **False Positive (FP):** Pixels where SFINCS predicts flooding, but SAR does not (SFINCS output= 1, SAR = 0).
- **False Negative (FN):** Pixels where SAR detects flooding, but SFINCS does not (SFINCS output = 0, SAR = 1).

Precision, Recall, and F1-score are standard evaluation metrics commonly used to assess the performance of numerical models against SAR-based flood detection results (Fakhri and Gkanatsios, 2025). In this study, these metrics were applied to evaluate the accuracy of the SFINCS model. The corresponding equations are presented below.

$$Precision = \frac{TP}{TP + FP}$$

Equation 1. Precision performance metric

$$Recall = \frac{TP}{TP + FN}$$

Equation 2. Recall performance metric

$$F1 - score = \frac{2 * \text{ Precision } * \text{ Recall}}{Precision + Recall}$$

Equation 3. F1 - score performance metric

This method of computing standard performance metrics allows for a quantitative assessment of how well the SFINCS model captures the spatial extent of flooding compared to SAR observations.

4.4 Hydrodynamic Modeling with MOHID

4.4.1 Model Description: MOHID 3D Hydrodynamic Framework

The first component of the modelling framework applied in this study involved simulating the hydrodynamic circulation in the estuary using the MOHID circulation model, which is a three-dimensional finite volume framework designed to simulate flow dynamics in shallow water

systems (Martins et al., 2001). It operates by solving three-dimensional incompressible primitive equations, incorporating the assumptions of hydrostatic equilibrium and the Boussinesq approximation. The model's core calculations are based on the principles of momentum and mass conservation (equations 1 and 2).

$$\frac{\partial u_i}{\partial t} + \frac{\partial (u_i u_j)}{\partial x_j} = -\frac{1}{\rho_0}\frac{\partial p_{atm}}{\partial x_i} - g\frac{\rho(\eta)}{\rho_0}\frac{\partial \eta}{\partial x_i} - \frac{g}{\rho_0}\int_{x_3}^{\eta}\frac{\partial \rho'}{\partial x_i}\,dx_3 + \frac{\partial}{\partial x_j}\left(\upsilon\frac{\partial u_i}{\partial x_j}\right) - 2\varepsilon_{ijk}\Omega_j u_k,$$

Equation 4. Momentum equation for hydrodynamic modeling

$$\frac{\partial u_1}{\partial x_1} + \frac{\partial u_2}{\partial x_2} + \frac{\partial u_3}{\partial x_3} = 0,$$

Equation 5. Mass conservation equation for hydrodynamic modeling

where u_i are the velocity vector components in the horizontal Cartesian x_i directions (i=1,2), u_i are the velocity vector components in the three Cartesian directions x_j (j=1–3), υ is the turbulent viscosity and P_{atm} is the atmospheric pressure. ρ is the specific mass, ρ′ is its anomaly, ρ0 is the reference specific mass, ρ(η) represents the specific mass at the free surface, g is the acceleration of gravity, t is the time, Ω is the Earth's velocity of rotation and ε is the alternate tensor. The details of the model discretization are thoroughly explained in Martins et al. (2001).

4.4.2 Model Setup and Coupling Configuration

A coupled hydrodynamic model was applied, combining two components: the MOHID circulation model and the SWAN Nearshore Waves Model, in order to generate data on nearshore hydrodynamic conditions. The MOHID model focuses on simulating water level variations by processing meteorological data, bathymetry, water level, and marine boundary conditions, using as input Global Circulation Models such as CMEMS. Simultaneously, the SWAN model utilizes bathymetry, wind fields, boundary conditions, and roughness to predict wave conditions in the nearshore area. Together, these models provide a comprehensive understanding of water level and wave dynamics in the nearshore, delivering essential output data for the next stage in the modelling framework of this study (flood model).

It is worth mentioning that this circulation model is currently operational under the domain known as *LisOcean*, as part of an automated process that integrates data from global or regional climate models (such as CMEMS) to feed its database.

Within this framework, multiple hydrodynamic circulation simulations have been conducted in the study area, covering extended historical periods.

For this circulation model, a coupling was established between the MOHID Land and LisOcean domains with the objective of simulating river discharge conditions (Tagus and Sorraia Rivers) and oceanic conditions, which together determine the hydrodynamic circulation within the estuary. The simulation was performed in three dimensions using a regular and uniform grid. For the validation scenario, the simulation was run in non-stationary mode, covering the period from 2022/12/01 to 2022/12/18. The model required approximately five initial simulation days to allow for numerical stabilization before continuing the main computation.

Boundary conditions related to water level, currents, temperature, and atmospheric pressure were obtained from the regional circulation model CMEMS. All tidal components were derived from the FES circulation model, while meteorological parameters such as wind speed were extracted from the AROME model. Based on this, the simulation period began with the coupling to SWAN, in which the circulation model MOHID was executed iteratively to generate outputs that were fed into SWAN. This allowed for the hydrodynamic simulation of waves in the nearshore (using the JONSWAP frequency spectrum), which were then used to recalculate total water levels with MOHID. This approach enabled the estimation of the different processes contributing to total water level and generated outputs with a spatial resolution of approximately 270 meters.

From the hydrodynamic circulation results, a grid of water level time series was obtained for the entire simulation period. The results were exported in .hdf5 format and read and processed using MATLAB scripts for their subsequent preparation for the next modelling phase. The process described above was first executed for the validation scenario and then replicated for the different modelling scenarios.

4.5 Flood Modeling with SFINCS

4.5.1 Model Description: SFINCS Hydrodynamic Flood Model

The second component of the modelling framework applied in this study involved the application of the SFINCS model which incorporates advection in the momentum equation while accounting for processes like spatially varying friction, infiltration, and precipitation. The computational mesh of SFINCS consists of a rectangular, equidistant, staggered grid where bed levels, water

levels and water depths are defined in cell centers (Leijnse et al., 2021). The staggered SFINCS grid with bed level d and water level ζ in the cell centers (+) and water depth h and fluxes q in velocity points is outlined in Figure 20.

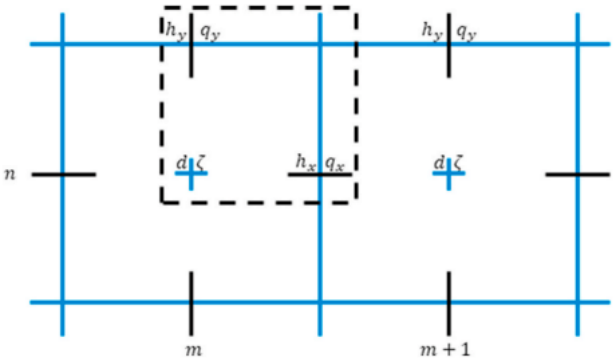

Figure 20. SFINCS grid scheme. Source: Leijnse et al., (2021)

Equation 6 shows the volumetric flow rate per unit width along the spatial domain. In this context, ${q_x}^t$ represents the flow rate at the preceding time step. The water depth ${h_x}^t$ at the cell interface is calculated as the average water depth between the two neighbouring cells, while Δz denotes the difference in water levels between these cells. The symbols g and n stand for the gravitational constant and the Manning friction coefficient, respectively.

$$q_x^{t+\Delta t} = \frac{q_x^t - g h_x^t \frac{\Delta z}{\Delta x} \Delta t}{\left(1 + g \Delta t n^2 q_x^t \Big/ {h_x^t}^{7/3}\right)}$$

Equation 6. Volumetric flow rate per unit in SFINCS. Source: Leijnse et al., (2021)

The momentum equation that is applied in SFINCS is presented in the equation 7. It is composed by two more terms: the wind drag term ${\tau_{w,x}}/{\rho_w}$ where ρw refers to water density and the advective term adv_x.

$$q_x^{t+\Delta t} = \frac{q_x^t - \left(g h_x^t \frac{\Delta z}{\Delta x} + adv_x - \frac{\tau_{w,x}}{\rho_w}\right) \Delta t}{\left(1 + g \Delta t n^2 q_x^t \Big/ {h_x^t}^{7/3}\right)}$$

Equation 7. Momentum equation applied in SFINCS. Source: Leijnse et al., (2021)

For coastal applications, SFINCS models are typically driven along the 2-meter depth contour. The model domain extends from the seaward boundary of the swash zone, where most waves have already broken, to the dry land up to a user-specified height contour. The model does not resolve the surf zone. Users must provide time-series data for the slowly varying (ζ0) and rapidly varying (ζ) water levels at the seaward edge of the swash zone.

These time-series can be derived from larger-scale circulation models and phase-resolving surf zone models, respectively. Alternatively, SFINCS can automatically generate time-series of rapidly varying water levels at each boundary point using a set of empirical relationships. These relationships estimate wave set-up and wave height at the swash zone boundary based on offshore wave conditions and the bed slope of the surf zone (Leijnse et al., 2021).

4.5.2 Model Setup and Simulation Configuration

The flood model setup in SFINCS was developed using the SFINCS Q4 v2.0.3 Cauberg release and executed through the Python package HydroMT, which is a framework for water-related modeling studies. Consequently, the model inputs and parameterization were configured using a Python script developed within this modeling framework. First, several libraries were imported, such as numpy, pandas, geopandas, and hydromt_sfincs, which contain the necessary functions for the proper configuration of the model. The model setup workflow is described below.

First, the data library and output folder were set, as well as the spatial reference system, which was defined as WGS84/UTM Zone 29N (CRS: 32629). A regular and uniform mesh with a spatial resolution of 10 x 10 m was configured. Next, the spatial domain of the model was defined by inputting a file in .GEOJSON format. This spatial domain covers an area of 985.35 km², resulting in a mesh configuration of 2,503 × 3,930 cells. Subsequently, the digital elevation model (2 x 2 m resolution) and bathymetry of the water body were loaded, both referenced to the MSL datum. Then, SFINCS was set to subgrid mode for this simulation, which allowed the model to compute flood dynamics on a coarser computational grid (10 × 10 m) while resolving topographic variations and inundation patterns at a finer resolution (5 × 5 m). This approach achieved computational efficiency. Afterwards, a mask file of active and inactive cells was defined, keeping as active those cells corresponding to the northern and southern margins of the estuary, where SFINCS solved the flood dynamics. For the validation scenario (December 2022 storm event), the model was executed for a period from December 5th, 2022 at 00:00 until December 16th at 23:00, in order to cover the two precipitation peaks that occurred during this period.

The files corresponding to surface roughness and infiltration (curve number) were loaded in raster format. Following this, the model was forced using the MOHID outputs, based on the water level grid resulting from the circulation model within the estuary. Since both the topography and bathymetry files were referenced to the MSL (Mean Sea Level) datum, the water level time series

was adjusted to this datum to ensure the correct execution of the model. Presented below are the model inputs, including the water level time series (Figure 21d) applied through observation points (Figure 21c), the elevation data (Figure 21a), and the active cell domain (Figure 21b).

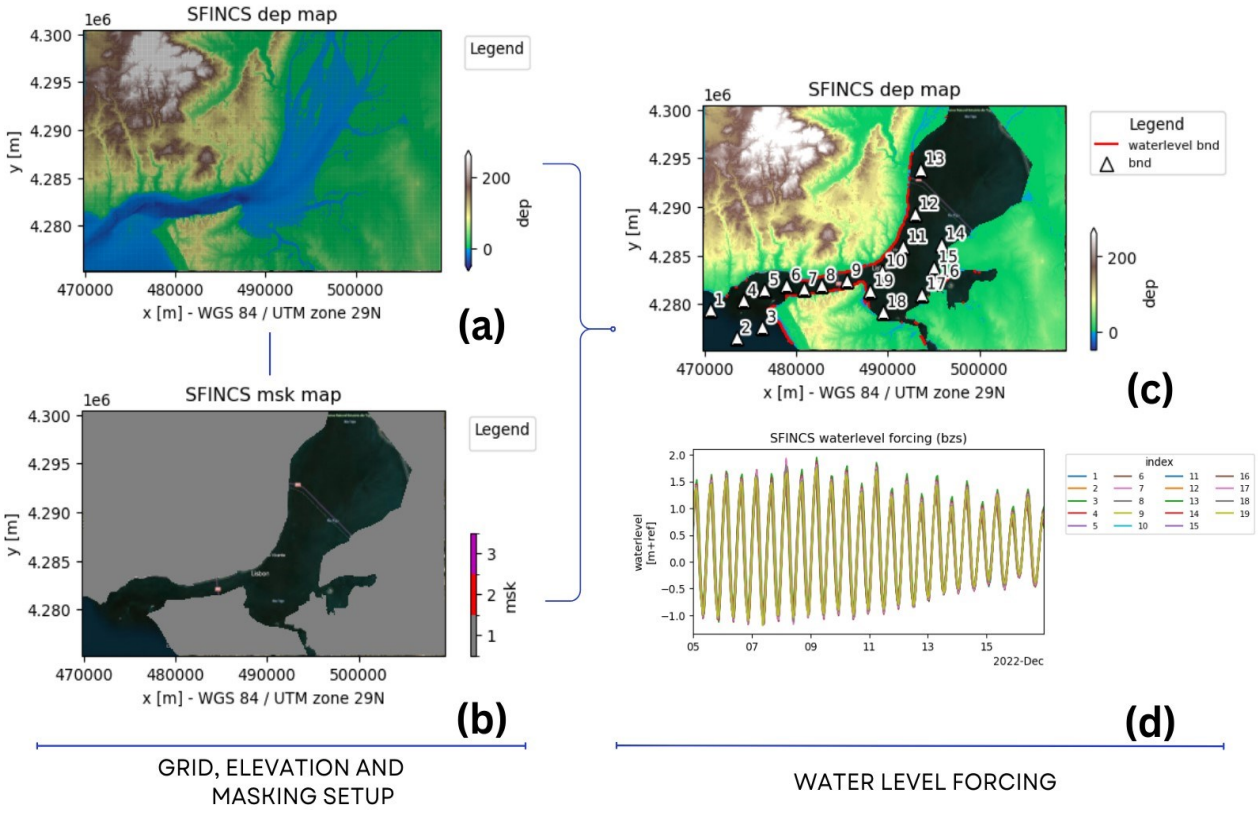

Figure 21. SFINCS initial Setup and water level forcing

Subsequently, a precipitation file in .prcp format was uploaded, as required by the numerical model, assigning a spatially uniform precipitation forcing based on the data obtained from the three rain gauge stations within the study area. Finally, a batch file (.bat) was generated, which was used to execute the model. The resulting files in .nc format were converted to raster (.tiff) format to be analyzed using GIS tools (QGIS). The procedure described above was replicated for both the validation scenario and the extreme condition scenarios, which are defined and explained later in this document.

4.6 Extreme Value and Joint Probability Analysis of Flood Drivers

An exploratory statistical analysis was conducted to examine the relationship between extreme precipitation and storm surge events in the study area. It is important to note that river discharge data were not included in the statistical analyses due to the artificially controlled nature of this

variable. The Multivariate Hazard Assessment Statistical Toolbox (MhAST), developed by Sadegh et al. (2018), was used for this purpose. This toolbox provides a variety of statistical methods to evaluate the dependencies between different hazards, including linear and nonlinear correlation measures. To isolate extreme events, the Peak Over Threshold (POT) method was applied to time series data on hourly precipitation and storm surge, using a threshold corresponding to the 98^{th} percentile. This ensured that only the most severe events were included in the dependence analysis. Three correlation measures were then computed: Pearson's correlation coefficient (for linear dependence), Spearman's rank correlation, and Kendall's tau (both nonparametric).

In parallel, an extreme value analysis (EVA) was performed in MATLAB to estimate the magnitude of extreme precipitation events. Using a 27-year dataset of hourly rainfall, the EVA aimed to identify the maximum hourly precipitation associated with a 100-year return period, representing more extreme conditions than the validation event. Three statistical distributions were tested: Gumbel, POT, and generalized extreme value (GEV). Their performance was evaluated using root mean square error (RMSE) and normalized RMSE as goodness-of-fit criteria.

To address the complex nature of flooding in the Tagus Estuary, a joint probability analysis was conducted to quantify the statistical dependence between storm surges and extreme precipitation. The MhAST copula-based framework was employed to estimate the joint and conditional return periods of these correlated variables. For the analysis, hourly storm surge data from the Copernicus Climate Change Service (2022) and precipitation data from Instituto Português do Mar e da Atmosfera (n.d.), were compiled. The marginal distribution of each variable was fitted individually using the most appropriate probability function based on goodness-of-fit tests. The dependence structure between storm surge and precipitation was modeled using copulas, which effectively capture nonlinear relationships.

Based on the fitted copula model, joint return periods were estimated for various combinations of storm surge and precipitation intensities. This analysis identified critical compound event scenarios. One such scenario, corresponding to a 100-year joint return period, was selected as a boundary condition for hydrodynamic flood simulations in SFINCS. This enabled an assessment of compound flooding under extreme conditions.

4.7 Scenario design and forcing conditions

Based on the results of the exploratory statistical and Joint Probability Analysis, the modeling scenarios were defined with the objective of analyzing pluvial, ocean, and compound forcings. In addition, different projections of Sea Level Rise (SLR) were incorporated, as shown in Figure 22, which show the conditions of the 11 scenarios defined.

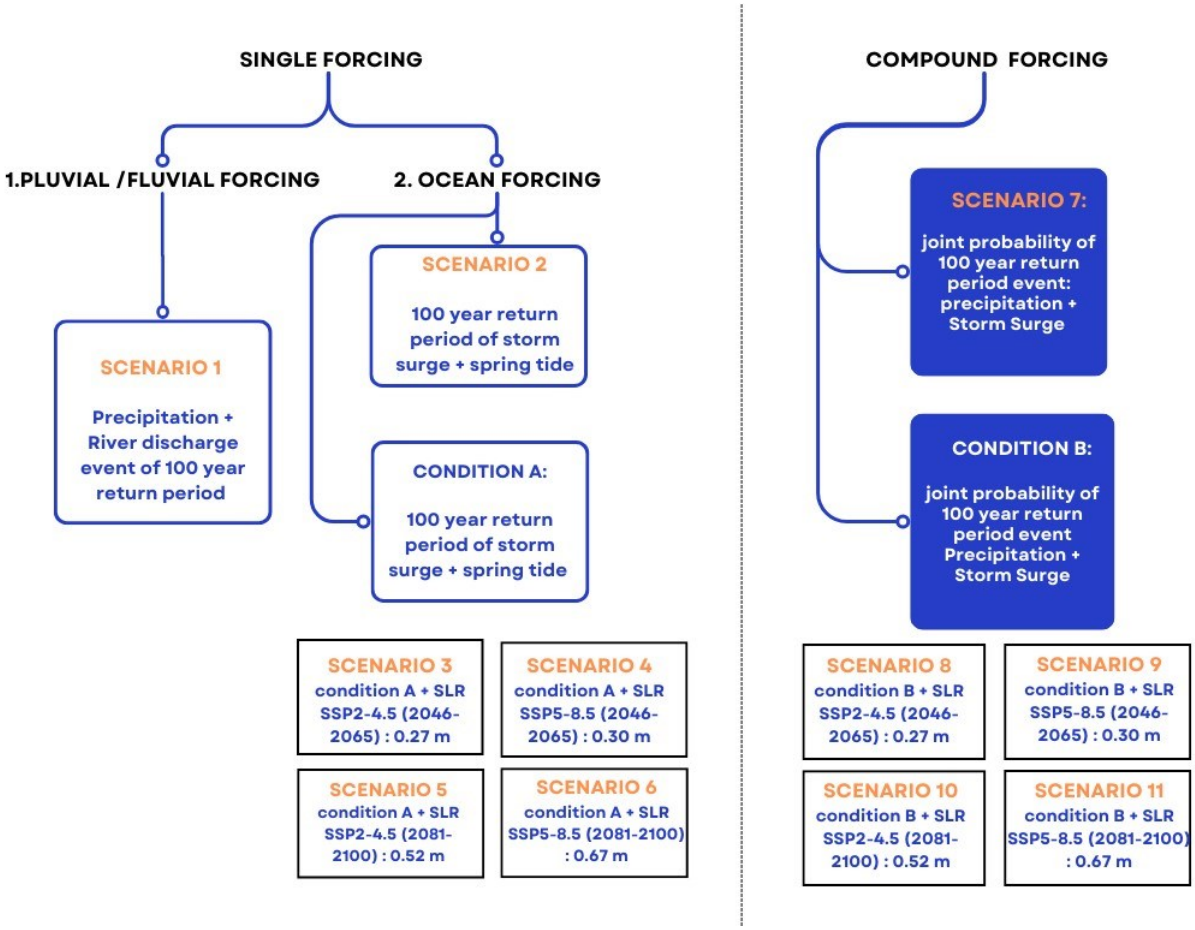

Figure 22. Schematic representation of scenario definitions used in the flood modeling study. Scenarios are grouped by forcing type: Single forcing, including pluvial/fluvial (Scenario 1), ocean forcing (Scenarios 2–6), and (Compound forcing, representing the joint occurrence of precipitation and storm surge (Scenarios 7–11). Sea level rise (SLR) projections are based on SSP2-4.5 and SSP5-8.5 for two future periods (2046–2065 and 2081–2100).

For each of the modelling scenarios developed in this study, a 15-day simulation length was defined. The pluvial/fluvial forcing boundary conditions were designed to replicate the storm pattern observed during the December 2022 flood event. This aimed to simulate realistic scenarios that could potentially occur in the study area. This involved representing the pre-conditioning phase with two intense precipitation peaks, followed by high river discharge values.

The storm pattern was then scaled to the extreme values obtained from the extreme value and joint probability analysis. For the single forcing scenario, normal total water level conditions were applied to focus the analysis specifically on the pluvial/fluvial forcings and their flood-generating capacity, as shown in Figures 23 (a) and 23 (b).

For the oceanic forcing scenarios (Scenarios 2–6), the simulations combined a 100-year storm surge return period of 0.58 m for the study area as described by Andrade et al. (2006), and a spring tide corresponding to a tidal cycle obtained from Antunes (n.d.). The storm surge was modelled as a triangle, with a 6-hour gradual increase to peak and a 6-hour decrease back to normal conditions. Figure 23 (c) shows the base shape of these oceanic storm conditions, corresponding to Scenario 2. Scenarios 3 to 6 used the same storm shape; the only difference was the respective increase in total water level based on each SLR projection. These scenarios excluded precipitation and used average river discharge values to isolate and analyse the flood potential of oceanic forcings alone.

For the compound forcing scenarios, the simulations combined pluvial/fluvial and oceanic forcings. In this case, the storm pattern was preserved, with values scaled based on the joint probability analysis for a compound event with a 100-year return period. Similarly, a triangular-shaped storm surge was applied, whose peak coincided with the spring tide and precipitation event, as illustrated in Figure 23 (d) and (e).

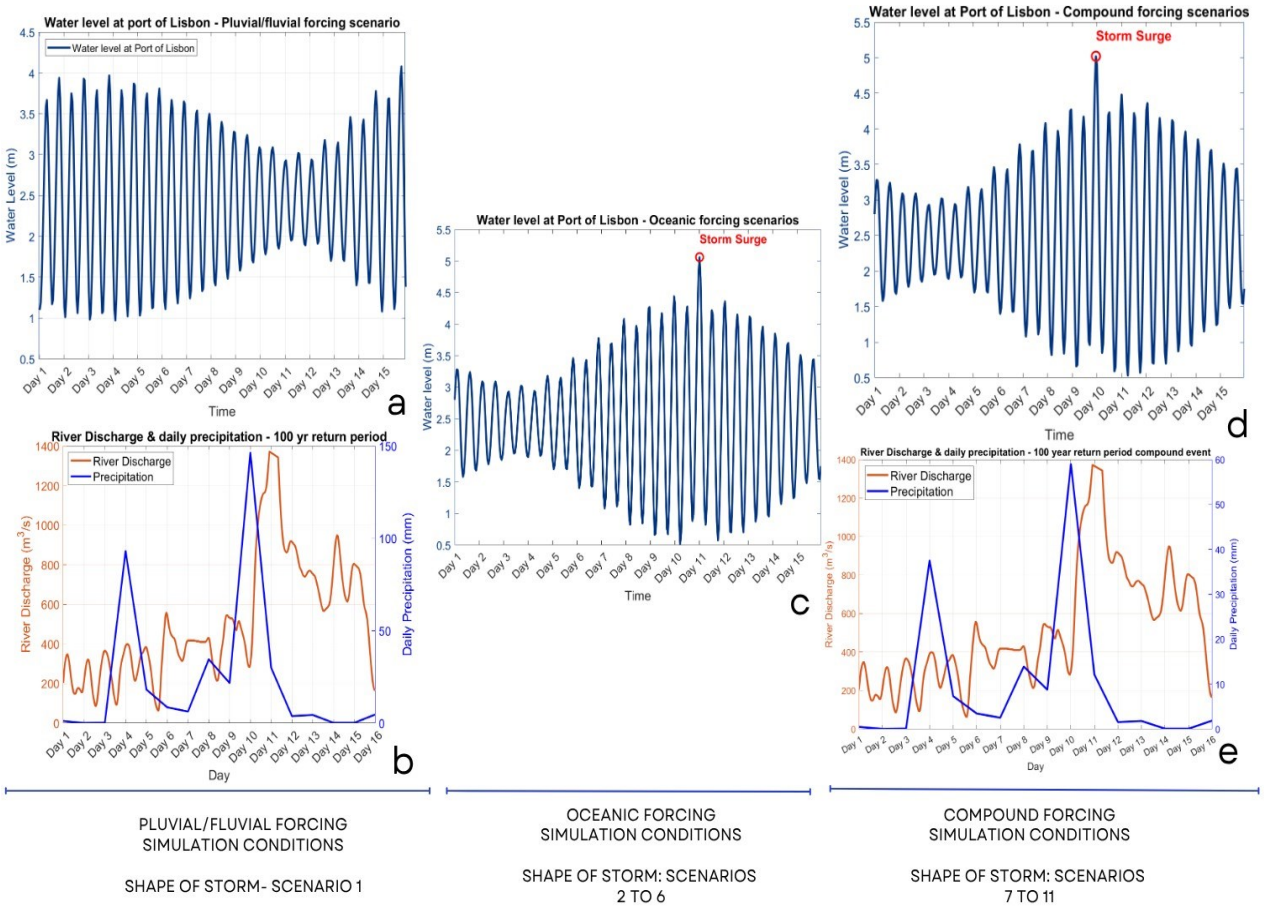

Figure 23. Boundary conditions used for each forcing type in the numerical simulations. (a) Water level at the Port of Lisbon under pluvial/fluvial forcing (Scenario 1); (b) River discharge and daily precipitation time series for a 100-year return period pluvial/fluvial event (Scenario 1); (c) Water level at the Port of Lisbon for oceanic forcing including storm surge and spring tide- 100 year return period event (Scenarios 2–6); (d) Water level under compound forcing with the superposition of storm surge and tide (Scenarios 7–11); (e) River discharge and daily precipitation for the 100-year return period compound event (Scenarios 7–11).

V. Results

5.1 Validation

This chapter compares flooded areas obtained from the numerical model simulations, a Sentinel-1 SAR analysis, and local footage of the flooded areas captured by video cameras from digital social media and news in order to assess the model performance regarding flooding extent and depth across the study area domain. The flood model, developed using the SFINCS tool, produced a maximum inundation map, representing the peak flood extent reached at any point over the entire simulation period during the storm event that took place in the study area from 7 to 13 December 2022. The results indicate widespread flooding along the northern margin of the estuary and in the eastern portion of the study area. Elsewhere, water flow is observed through various streams discharging into the estuary. Additionally, numerous small, flooded areas are present throughout the domain, the majority of which show inundation depths of less than 1 metre, as illustrated in Figure 24.

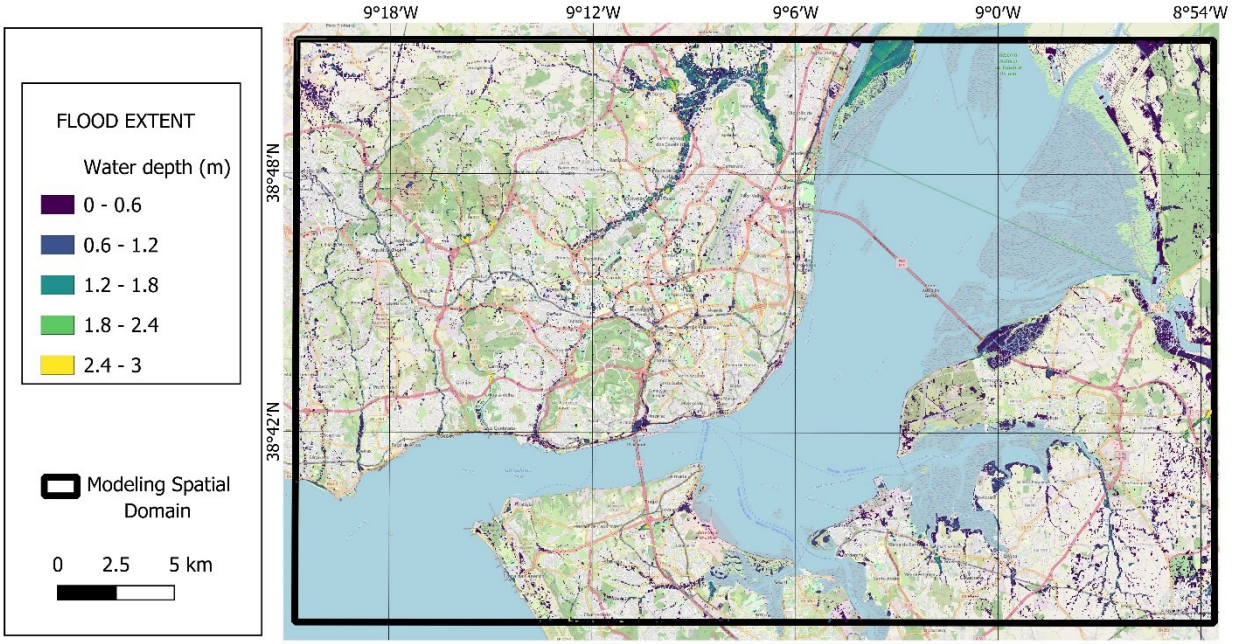

Figure 24. Simulated maximum flood extent during the December 2022 storm event using the SFINCS hydrodynamic model. Basemap source: OpenStreetMap (QGIS)

5.1.1 Satellite-based Flood detection of validation event

To assess the performance of the numerical model, the flood extent resulting from the December 2022 storm was also derived using SAR-based flood detection. Figure 25 presents a comparison between the SAR-derived flood map and the flood extent simulated by the numerical model, where blue and red indicates flood extent for each approach.

The figure focuses on two specific areas within the spatial domain, Loures (northwest) and Pancas (northeast), which showed the highest spatial agreement between the two datasets.

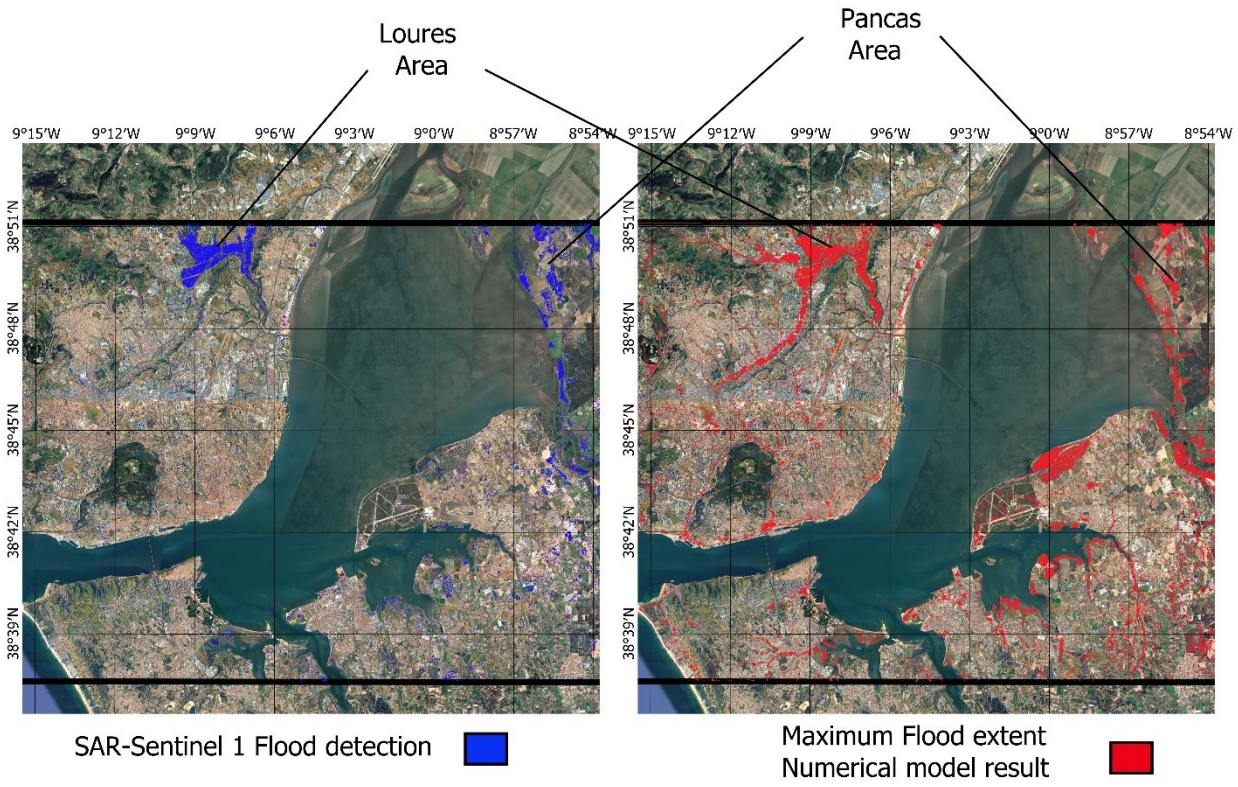

Figure 25. Comparison between SAR-based flood detection (Sentinel-1 imagery) and the simulated maximum flood extent from the SFINCS model for the December 2022 storm event. The left panel shows observed flood extents detected by SAR (blue), while the right panel presents the corresponding model results (red). Notable areas of interest include Loures and Pancas, where both datasets highlight significant inundation.

Different pixel-based comparison categories were calculated for the raster outputs of the numerical model and the SAR flood detection: TP, FP and FN. Next, the performance metrics of the numerical model were computed, including precision, recall and the F1 score. The results are presented in Table 2. For this analysis, it is important to note that the numerical model output representing the maximum flood extent was used and compared with the flood extent obtained from SAR-1 imagery.

Name	True Positives (TP)	False Positives (FP)	False Negatives (FN)	Precision	Recall	F1-Score
Overall Spatial Domain	339901	1827948	536644	0.1568	0.3878	0.2233
Loures area	171455	109920	30967	0.6093	0.847	0.7088
Pancas area	83107	169805	123957	0.3286	0.4014	0.3614

Table 2. Standard Performance metrics to compare SAR and SFINCS flood extent

It was observed that the Loures area showed the highest performance of the numerical model compared to the detection of flood extent from the analysis of SAR imagery, with an average performance of 72.17% based on the three indices. The Pancas area ranked second with an average performance of 36.47%, followed by an analysis of the entire spatial domain of the model which showed an average performance of 25.59%. This lower performance over the full domain is likely influenced by limitations in SAR flood detection, which can miss inundated areas due to the complex 3D geometry of the terrain, signal occlusion, and reflections from urban structures such as buildings. Therefore, the localised assessments in Loures and Pancas provide a more reliable basis for evaluating the numerical model's performance than the global comparison over the entire domain.

5.1.2 Qualitative assessment of flooding event with additional data resources

Based on visual evidence collected at specific locations along the northern margin of the estuary, the approximate flood depth in Algés was estimated to be between 20 and 40 cm, as inferred from photographs and visual references provided by emergency personnel. Similarly, in Alcântara, flood depth was estimated at 30–40 cm using the height of nearby vehicles as reference points at the time the images were taken. In Loures, photographic evidence indicates flood depths ranging from 20 to 40 cm. Although the exact date and time of the photographs could not be confirmed, it is certain that they were taken during the December 2022 flooding event (Expreso, 2022). Figure 26 presents all of this supporting flood evidence.

Figure 26. Locations of flooding footage collected during the December 2022 validation event. The map shows three georeferenced points (red circles) where flood evidence was documented via news reports and social media in the areas of Alges, Alcântara, and Loures.

The modelling results in terms of both maximum flood depth and extent are shown in Figure 27. GIS analysis showed that, throughout the entire simulation, the maximum flood depth in Alcântara, where the photograph was taken during the December 2022 storm, reached 0.67 m. In Loures, the maximum flood depth reached 1.5 m at this specific location, while in Algés, it reached 0.98 m. These maximum flood depths are higher than those observed in the corresponding photographs (see Figure 26). However, it is important to note that these values represent peak flooding during the entire storm, and the photographs were likely not taken at the moment of maximum inundation. Additionally, flood depths of approximately 20 to 40 cm were observed at these locations during other times in the simulation, which matches the flood conditions seen in the photographs. These findings support the argument that the model was capable of simulate the flooding conditions at these three locations during the storm.

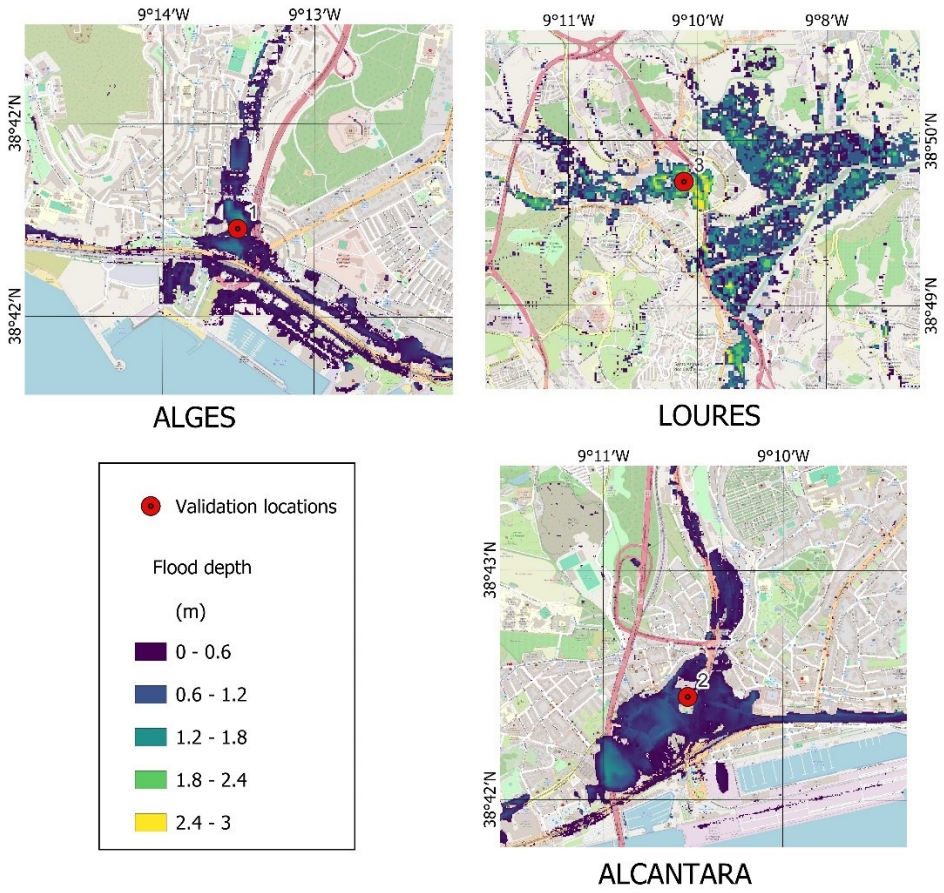

Figure 27. Simulated flood extent and depth at the three validation locations: Alges, Loures, and Alcântara. Each map shows water depth classifications overlaid on a basemap, with red markers indicating the positions where real-world flood observations were collected during the December 2022 event

5.2 Statistical Analysis of Flood Drivers

5.2.1 Extreme Value Analysis for Extreme Precipitation Event

Among the three statistical distributions applied, the generalized extreme value (GEV) distribution best fit the extreme precipitation regime. It yielded the lowest Root Mean Square Error (RMSE) (1.13) and normalized RMSE (0.0614), indicating the strongest agreement with the observed extreme values.

While RMSE is a useful quantitative measure of overall model accuracy, it is important to note that extreme value analysis focuses on accurately representing the upper tail of the distribution where extreme events occur. For this reason, visual inspection of the fitted distribution further supported the selection of the GEV model, as it confirmed that the GEV distribution best captured the observed extreme values compared to the other models tested. Applying the GEV model yielded an estimated maximum hourly precipitation of 46.01 mm for the 100-year return period.

Figure 28 illustrates this analysis and shows the fitted GEV curve (blue line), the confidence intervals (dashed lines), and the observed annual maximum precipitation values (black dots).

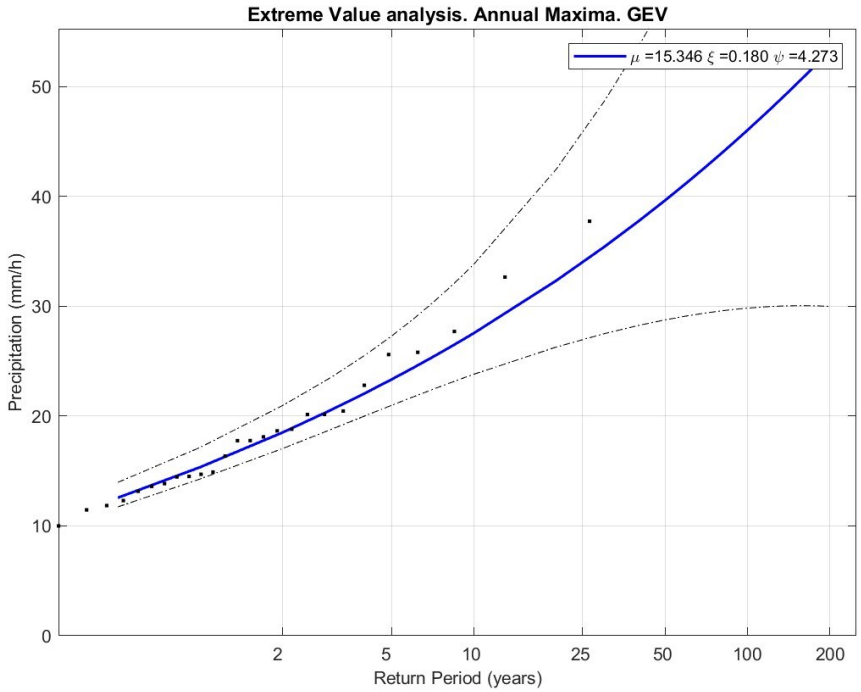

Figure 28. Extreme value analysis of annual maximum precipitation using the Generalized Extreme Value (GEV) distribution. The solid blue line represents the fitted GEV distribution, while the black dots indicate observed annual maxima. The dashed lines represent confidence intervals.

5.2.2 Joint Probability analysis for Compound Extreme Event Scenarios

Based on the exploratory statistical analysis for precipitation and storm surge (values above the 98th percentile) revealed that the resulting correlation coefficients were all close to zero: Pearson, 0.0671; Spearman, 0.0006; and Kendall, −0.0010. None were statistically significant ($p > 0.25$). These results indicate that there is no statistically significant dependence between the extreme values of the two variables in the available dataset.

The results obtained from the exploratory statistical analysis were confirmed based on the observational data for both variables. Most compound events involved either mild conditions in terms of both precipitation and storm surge or conditions in which one variable was extreme while the other remained low. Extreme compound events involving both hazards are absent in the 25-year record. Several events involving a storm surge exceeding 0.3 metres are evident, but

these generally coincide with low to moderate precipitation levels (less than 15 mm/h). This suggests that storm surges can occur independently. Furthermore, events with high precipitation rates, particularly those exceeding 15 mm/h, tend to occur around storm surge values near zero as shown in Figure 29.

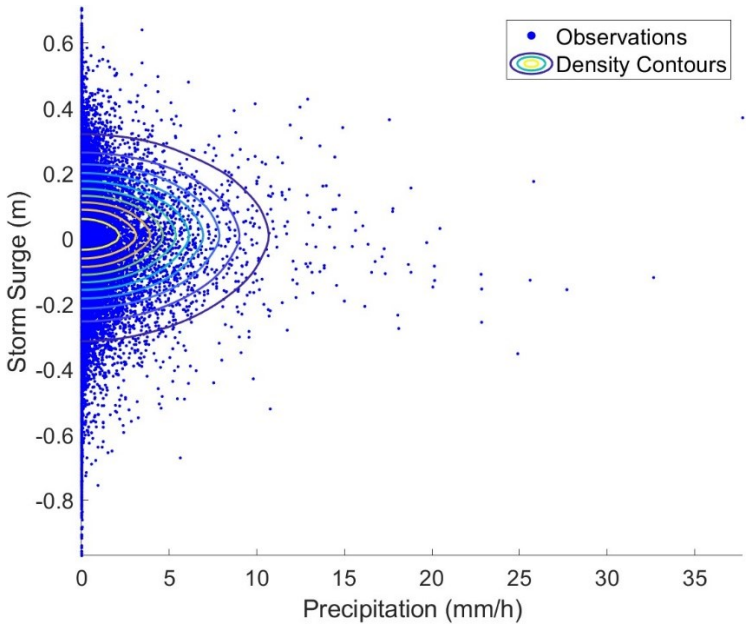

Figure 29. Joint scatter plot of observed storm surge and precipitation events over a 25-year period. The scatter plot shows individual paired observations, while the overlaid density contours highlight the concentration of data points.

Based on the lack of statistical dependence between variables the independence copula was applied. This copula assumes that the occurrence of one variable does not affect the probability of the other. In this case, the joint distribution is simply the product of the marginal distributions. Consequently, the return period curves derived from this copula do not exhibit any variation in likelihood, reflecting the constant and uniform nature of the assumed independence. The independence copula assigns an equal joint exceedance probability to all points along a given return period curve. This results in a joint probability plot where the curves are rendered in a single uniform colour, emphasising that no preferential joint behaviour exists between storm surge and precipitation extremes in the analysed dataset as shown in Figure 30. Based on this analysis, the joint exceedance probability contours were used to define compound flood scenarios corresponding to return periods of 100 years, under the scenario where both storm surge and precipitation thresholds are exceeded simultaneously.

The estimated values for a compound event with a 100-year return period are 0.6 metres of storm surge and 19.27 mm/h of maximum precipitation.

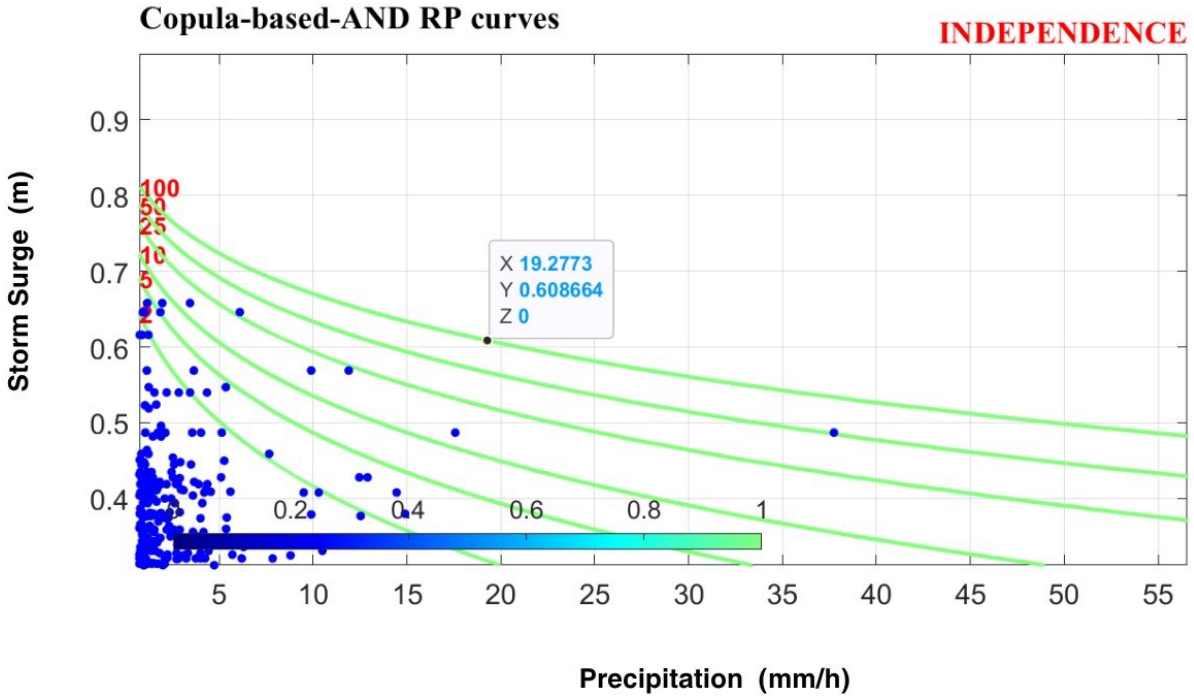

Figure 30. Joint return period (RP) curves for storm surge and precipitation based on the assumption of statistical independence, using a copula-based AND approach. The green curves represent return periods (in years), while the blue scatter points show observed paired events.

5.3 Flood Scenario Simulations

5.3.1 Pluvial/Fluvial- driven Extreme Event (Scenario 1)

The pluvial/fluvial-driven scenario indicates that, during a maximum precipitation, and a subsequent high river discharge, event with a return period of 100 years, the maximum flood extent is approximately 89.94 km², highlighting a high flood hazard. Extensive inundation occurs along the northern margin of the estuary, where many urban areas are located. In this part of the estuary, there are multiple flood zones adjacent to streams that discharge into the estuary. The deepest floodwaters occur near river channels and natural depressions. In areas such as Loures, which is located on the northern side of the estuary, high flood depths are observed along the stream crossing this area, with water depths exceeding 2.5 metres.

A large inundated area is also present on the northern edge of the southern estuarine margin, reaching maximum flood depths of around 1.5 metres. This area is directly influenced by the discharge of the Tagus river flowing into the estuary.

In the rest of the southern margin, inundation is also present, particularly in low-lying agricultural and peri-urban areas such as Pancas. Figure 31 provides a detailed description of this.

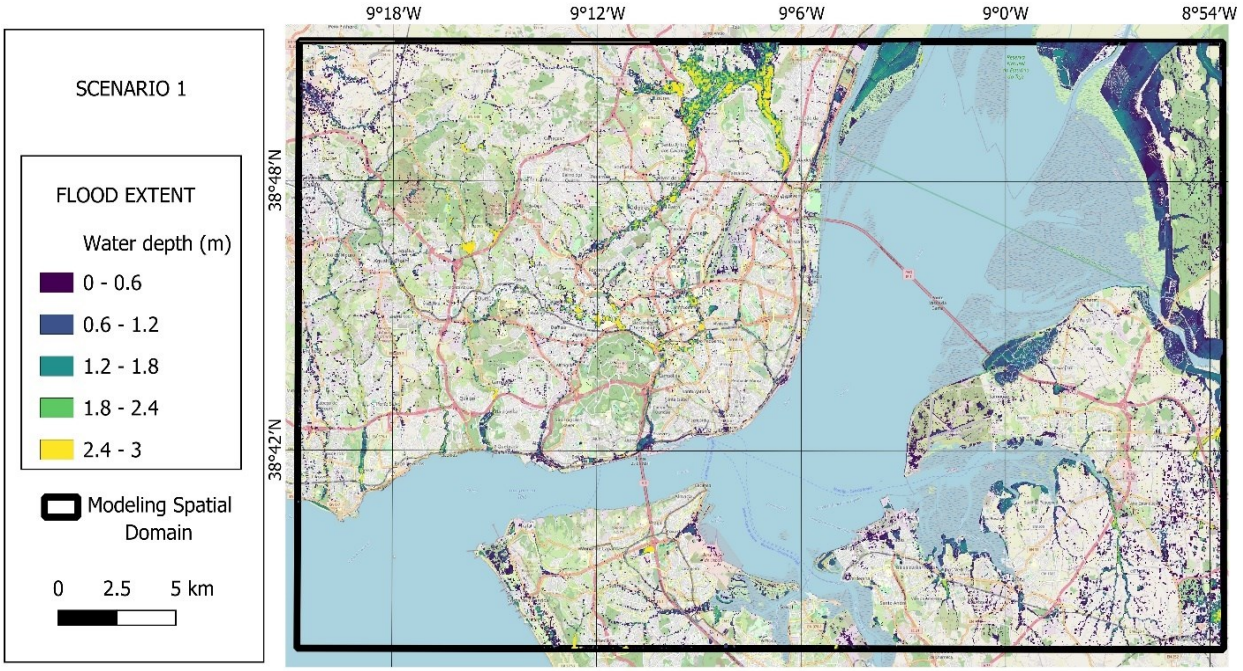

Figure 31. Simulated flood extent for Scenario 1: pluvial/fluvial forcing representing a 100-year return period event. The map shows maximum water depth across the model domain, with inundation depths classified into five ranges. Basemap source: OpenStreetMap (QGIS)

5.3.2 Extreme Oceanic-driven Extreme Events (Scenarios 2 - 6)

The oceanic-driven scenarios reveal the Tagus Estuary's clear sensitivity to rising sea levels during extreme storm events involving spring tides and storm surges. While present-day conditions (Scenario 2) limit flooding to certain coastal areas, mid-century projections (Scenarios 3 and 4) under SSP2-4.5 and SSP2-8.5 show measurable migration of flooding inland. By the end of the century (Scenarios 5 and 6), flooding spreads significantly further inland, particularly across the northern floodplains and the low-lying southern areas. Water depths also rise considerably, exceeding two metres in several locations as it is illustrated in Figure 32. Additionally, Figure 33 illustrates flood extent results and highlights the critical role of sea level rise in shaping future coastal flooding driven by oceanic forcings.

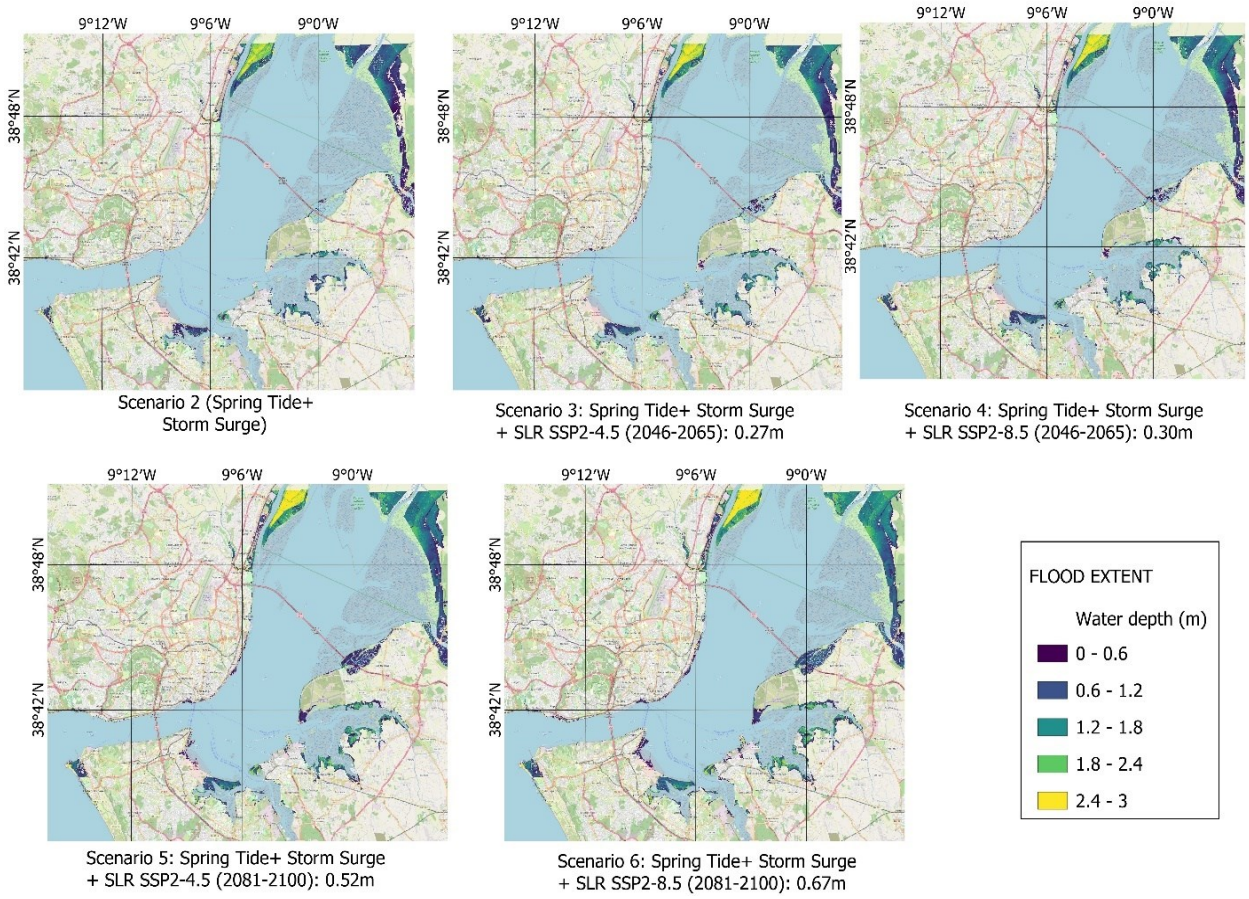

Figure 32. Simulated flood extent maps for coastal forcing scenarios (Scenarios 2 to 6). Scenario 2 represents the baseline condition with spring tide and storm surge. Scenarios 3 to 6 incorporate projected sea level rise (SLR) under SSP2-4.5 and SSP5-8.5 for two future time horizons: 2046–2065 and 2081–2100. Water depth is classified into five categories. Basemap source: OpenStreetMap (QGIS)

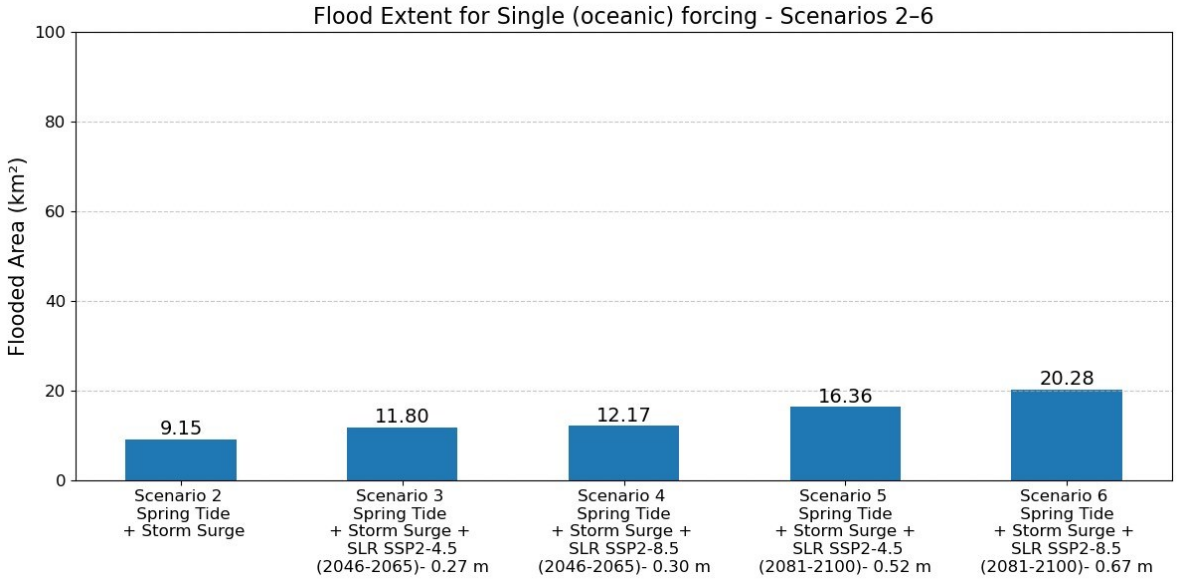

Figure 33. Total flooded area for oceanic forcing scenarios (Scenarios 2 to 6). The bar chart shows the increase in flood extent due to sea level rise (SLR) under SSP2-4.5 and SSP5-8.5 projections for mid-century (2046–2065) and end-century (2081–2100), relative to the baseline scenario (Scenario 2: spring tide + storm surge).

5.3.3 Compound events (Scenarios 7 – 11)

Compound flood scenarios (Scenarios 7–11), which combine fluvial and pluvial drivers with spring tides, storm surges and rising sea levels, show that the main flooded areas are located in low-lying zones. This reflects the dominant influence of oceanic forcings, i.e. high storm surge levels combined with moderate precipitation, in such compound events. Patches of inundation are observed along the northern margin of the estuary, particularly in areas previously identified as prone to flooding during extreme pluvial/fluvial events. Regions such as Loures exhibit these inundated patches adjacent to local streams. Along the northern edge of the southern estuarine margin, there is a gradual increase in flood depths across the different sea level rise projections, with maximum depths exceeding 2.5 metres. This behaviour is illustrated in Figure 34. Additionally, a consistent increase in maximum flood extent was observed with rising sea levels, identifying sea level rise as a key driver in the expansion of inundated areas. Figure 35 presents this trend.

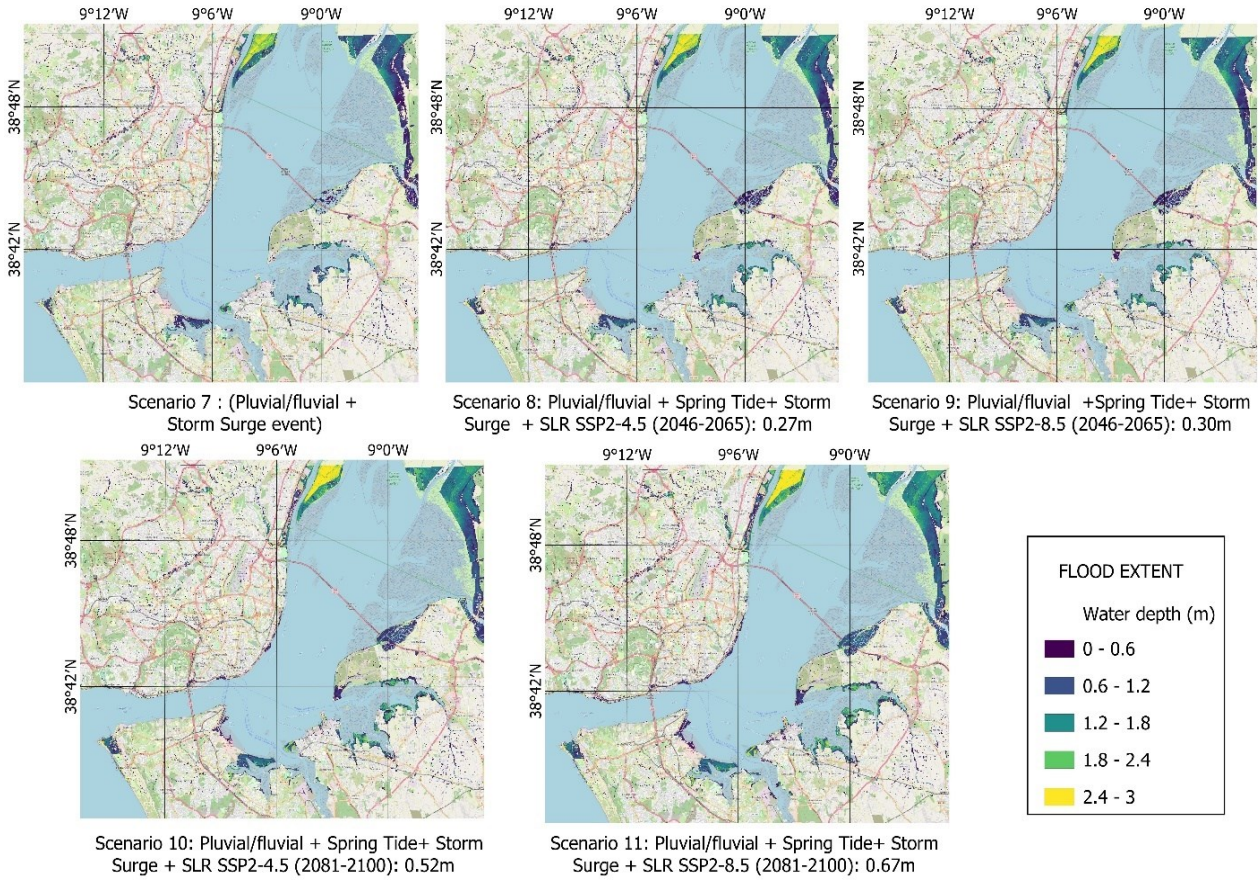

Figure 34. Simulated flood extent maps for compound forcing scenarios (Scenarios 7 to 11). Scenario 7 represents the baseline joint event combining pluvial/fluvial forcing and storm surge. Scenarios 8 to 11 incorporate sea level rise (SLR) projections under SSP2-4.5 and SSP5-8.5 for two future periods: 2046–2065 and 2081–2100. Water depths are classified into five categories. Basemap source: OpenStreetMap (QGIS)

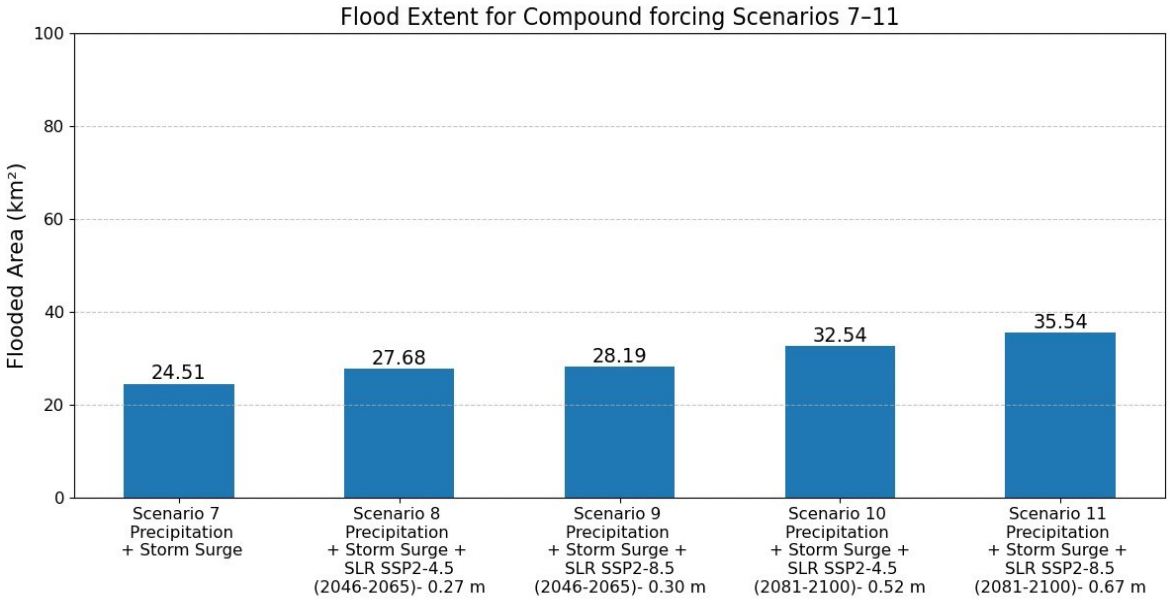

Figure 35. Total flooded area for compound forcing scenarios (Scenarios 7 to 11). Scenario 7 represents a baseline compound flood event combining precipitation and storm surge. Scenarios 8 to 11 incorporate projected sea level rise (SLR) under SSP2-4.5 and SSP5-8.5 for the mid-century (2046–2065) and end-century (2081–2100) timeframes.

Taking into account the influence of oceanic forcing within the spatial domain to a certain extent, a comparative analysis was conducted between pluvial/fluvial, oceanic and compound forcing for low-lying areas, which were identified as those located below 10 metres above sea level. GIS analysis confirmed that these areas are typically flooded during events driven by ocean forcing, as shown in Figure 36 in comparison with the previous flood maps.

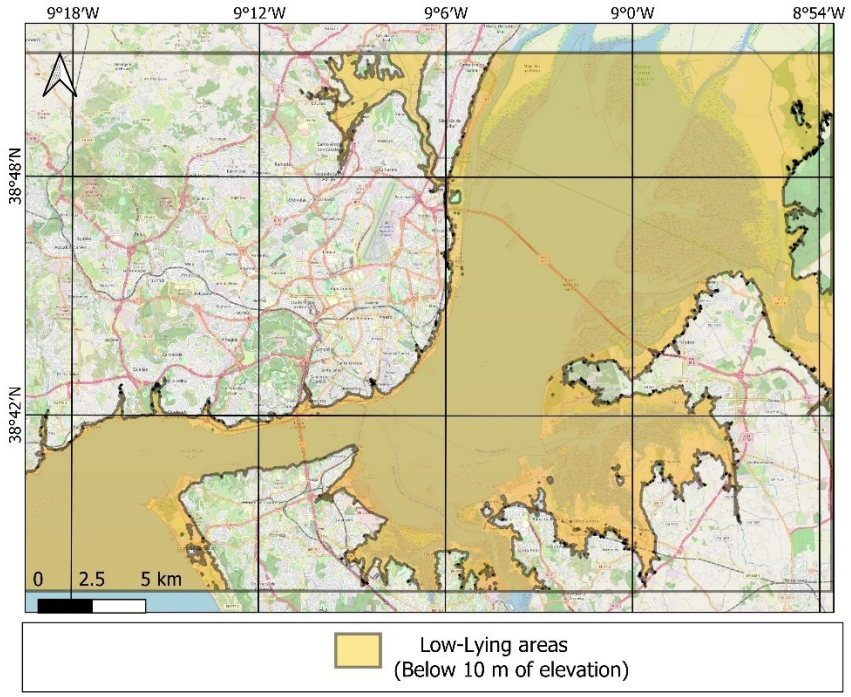

Figure 36. Low-lying areas in the Tagus Estuary region below 10 meters of elevation. Basemap source: OpenStreetMap (QGIS)

Overall, the analysis shows that the pluvial/fluvial forcing generates the greatest maximum flood extent of all the simulations performed. This highlights the significant influence of this triggering factor on flooding hazards in the estuary. Meanwhile, the flood extent generated by the compound forcing is almost half that of the pluvial/fluvial forcing. Figure 37 shows the maximum flood extents for each forcing.

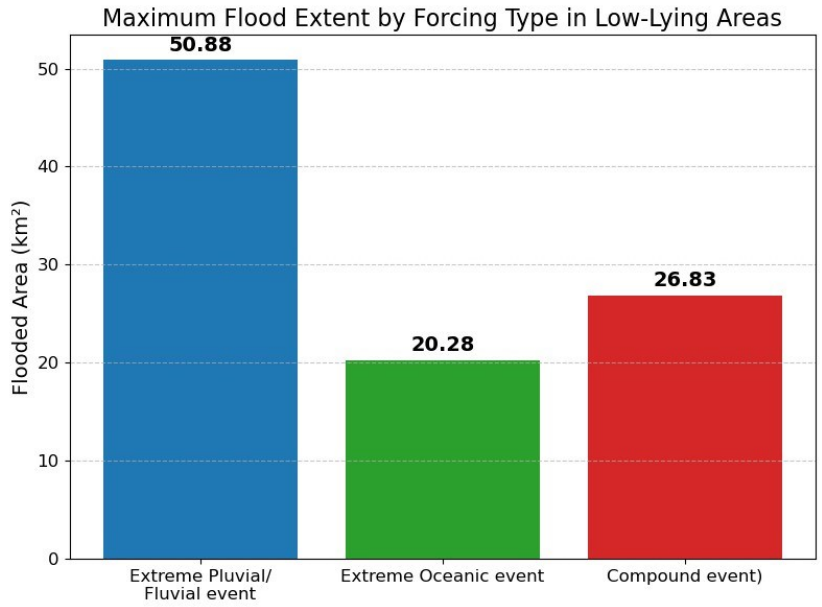

Figure 37. Maximum flooded area in low-lying zones (<10 m elevation) for different forcing types. The bar chart compares flood extent resulting from an extreme pluvial/fluvial event, an extreme oceanic event (storm surge + spring tide), and a compound event (pluvial/fluvial + oceanic forcing).

5.4 Spatial Distribution of Flooded areas by Land Cover Category

A GIS analysis was conducted to evaluate the intersection between flooded areas and various land cover types: artificial (urbanised), agricultural, and natural. The results confirmed that Scenario 1 (pluvial/fluvial forcing) produced the largest inundated area of all the modelled scenarios. A clear pattern emerged, with agricultural areas, primarily located along the southern margin of the estuary, experiencing the greatest flood extent. These were followed by natural areas, which were mainly covered by vegetation and also showed considerable flooding. Finally, urbanised areas also exhibited extensive flood coverage under the pluvial/fluvial scenario, with smaller but still significant flood extents under the oceanic and compound forcing scenarios. Overall, there was a progressive increase in flood extent from Scenario 2 to Scenario 11, which highlights the amplification effect of compound forcings compared to oceanic-only scenarios. In some cases, the increase in flood magnitude significantly exceeds that of scenarios with the same sea-level rise projection. Figure 38 illustrates this behaviour.

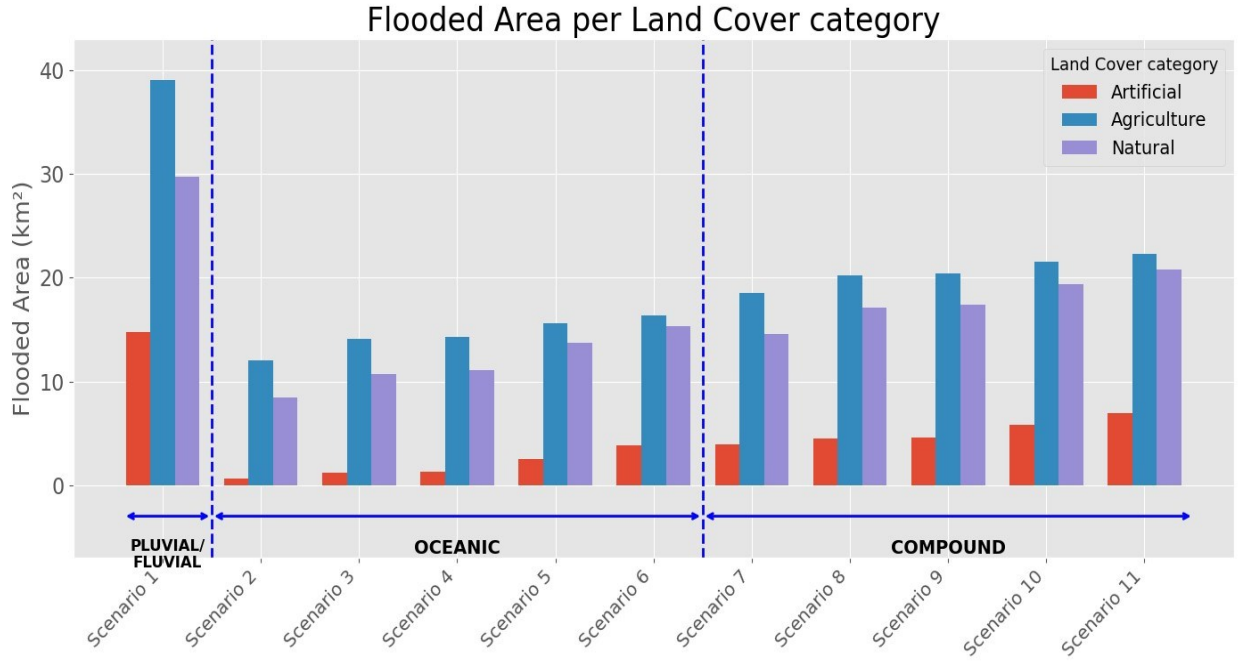

Figure 38. Flooded area per land cover category across all simulation scenarios. The bar chart presents the flooded area (in km²) for three land cover types—artificial surfaces, agricultural areas, and natural land—under pluvial/fluvial (Scenario 1), oceanic (Scenarios 2–6), and compound forcing scenarios (Scenarios 7–11).

VI. Discussion

This chapter presents the analysis of flood extents in the Tagus estuary under various scenarios, including individual (pluvial/fluvial or oceanic), compound (combined pluvial/fluvial and oceanic), and projected sea-level rise conditions. It discusses the model's applicability, the relative contributions of different flood drivers, the dynamics and impacts of compound flooding, the identification of flood-prone areas, and how these findings compare with previous assessments. Key limitations of the modeling approach are also addressed.

6.1 Performance and Limitations of the Numerical Modelling Framework

6.1.1 Model Accuracy in Simulating the December 2022 Storm

Overall, the modelling framework used in this study was capable of accurately simulating the conditions of the December 2022 storm in areas where there was observational data available for comparison, such as Loures, Alcântara and Algés. These locations experienced flooding during the event, and the model successfully reproduced the observed flood extents. The numerical model could also replicate the extent of flooding in the northern part of the estuary, especially in the Loures part. This area experienced the most extensive flooding in the Lisbon Metropolitan Area. This was confirmed using flood detection from Sentinel-1 SAR imagery.

However, in urban areas, the model showed less agreement with the extent of flooding derived from Sentinel-1 SAR data. This discrepancy is likely due to inherent limitations of SAR in dense urban environments, where strong signal reflections and layover effects from buildings distort the radar return. These phenomena can obscure the presence of water beneath and around built structures, leading to an underestimation of flood extent in SAR-based mapping (Mason et al., 2021). Such limitations are particularly evident along the densely developed northern margin of the estuary, including areas like Algés and Alcântara.

Although SAR-based flood detection did not identify these urban areas as flooded, photographic and video evidence confirms the presence of significant inundation, as illustrated in Figure 39. These a lternative data sources, including citizen-generated footage, provided valuable validation of both flood extent and depth in key locations such as Algés and Alcântara, complementing the limitations of remote sensing in dense urban settings.

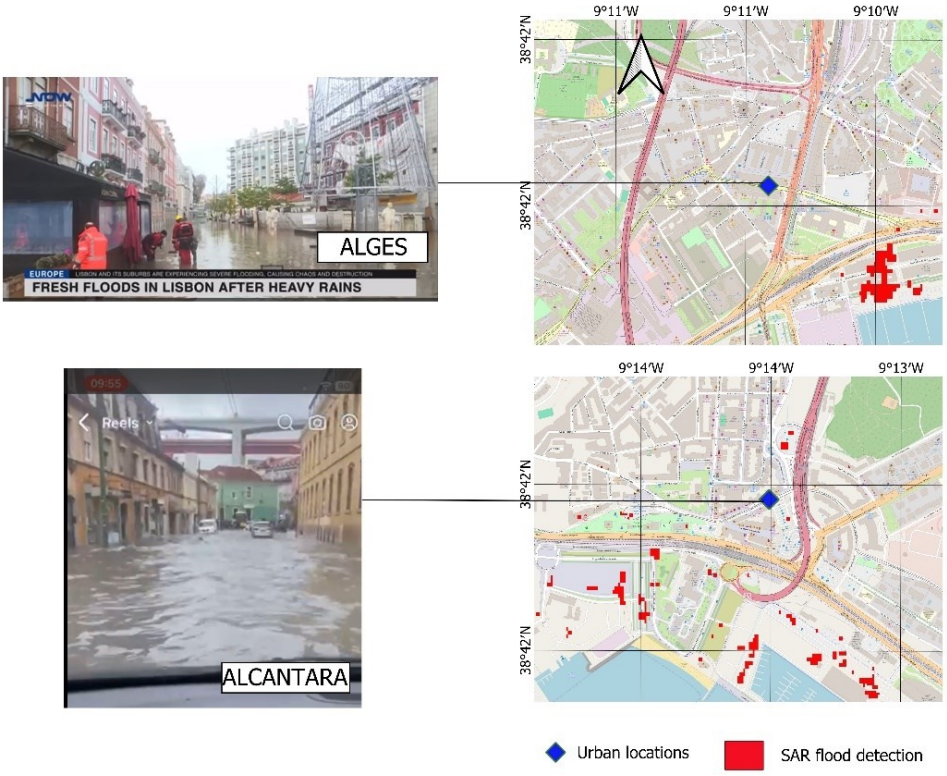

Figure 39. Comparison between SAR-based flood detection and observed urban flood locations in Alges and Alcântara. Photographic evidence from news and social media captures localized flooding during the December 2022 event. Corresponding SAR Sentinel-1 flood detection (red) is shown overlaid on OpenStreetMap basemaps, with urban reference points (blue diamonds) marking the reported observation sites.

6.1.2 Factors Contributing to Modelling Uncertainty

A key factor influencing the accuracy of the flood model is the quality and resolution of the topographic data used as input. The model's performance was affected by the integration of datasets with varying spatial resolutions. High-resolution LiDAR data (2 × 2 m) was employed for low-lying coastal areas where flood impacts are most critical, while inland and elevated zones relied on coarser ALOS AW3D30 data (25 × 25 m). This inconsistency may have affected the flood simulations in higher-elevation urban areas. Using a uniformly high-spatial resolution topographic dataset across the entire study area would likely produce more reliable results, particularly for inland regions. Despite the limitation of not having fully updated, high-resolution topographic data across the entire study area, the availability of detailed LiDAR data in the low-lying urban zones, where flood impacts are typically most severe, supports confidence in the accuracy of the modelled flood extents and depths in these sensitive areas (See Figures 7 and 8). In contrast, in higher elevation inland regions, the reliance on lower-resolution topographic data likely introduces greater uncertainty, particularly in simulating pluvial-driven flooding.

Another relevant factor that may contribute to modelling uncertainties, particularly in urban areas, is the role of drainage infrastructure in controlling surface water dynamics. As highlighted by Rilo et al. (2015), limitations in the urban drainage system can significantly influence the spatial and temporal behaviour of flooding in densely built-up areas of the estuary. In this study, the numerical model did not explicitly represent the drainage network, which may have led to under- or overestimation of flood extent in certain zones. Incorporating a comprehensive dataset, including detailed drainage network mapping, infrastructure characteristics, and system condition assessments, would likely improve the accuracy of simulated flood magnitudes, particularly under pluvial and compound forcing scenarios.

Furthermore, the precipitation dataset used in this study spans 27 years, while the storm surge dataset covers a 25-year period. Access to a longer dataset spanning more than 30 years would have enabled a more robust analysis of extreme rainfall and storm surge events and a more reliable joint probability assessment. This would have been particularly useful for estimating conditions associated with 100-year return period events.

6.1.3 Comparison with Existing Flood Studies

As demonstrated in the model validation chapter, the present study was able to accurately reproduce several flood-prone areas, providing confidence in the model's performance. To further support the robustness of the modelling framework, a comparative analysis was conducted between the flooding scenarios generated in this study and those from existing published work. In particular, the sea level rise (SLR) scenarios developed here were compared with the results of Antunes et al. (2019), who assessed inundation patterns under projected SLR and oceanic storm conditions for the same region. Their study simulated a 100-year return period event for 2050, incorporating spring tides, storm surges, and SLR projections—conditions closely aligned with those applied in Scenario 4 of this study. The side-by-side comparison of results (Figures 40(a) and 40(b)) reveals a high degree of spatial agreement, reinforcing the validity of the modelling outcomes. This alignment, together with comparisons to observational data from the 2022 event, strengthens the confidence that the present model reliably captures coastal flooding dynamics in the study area.

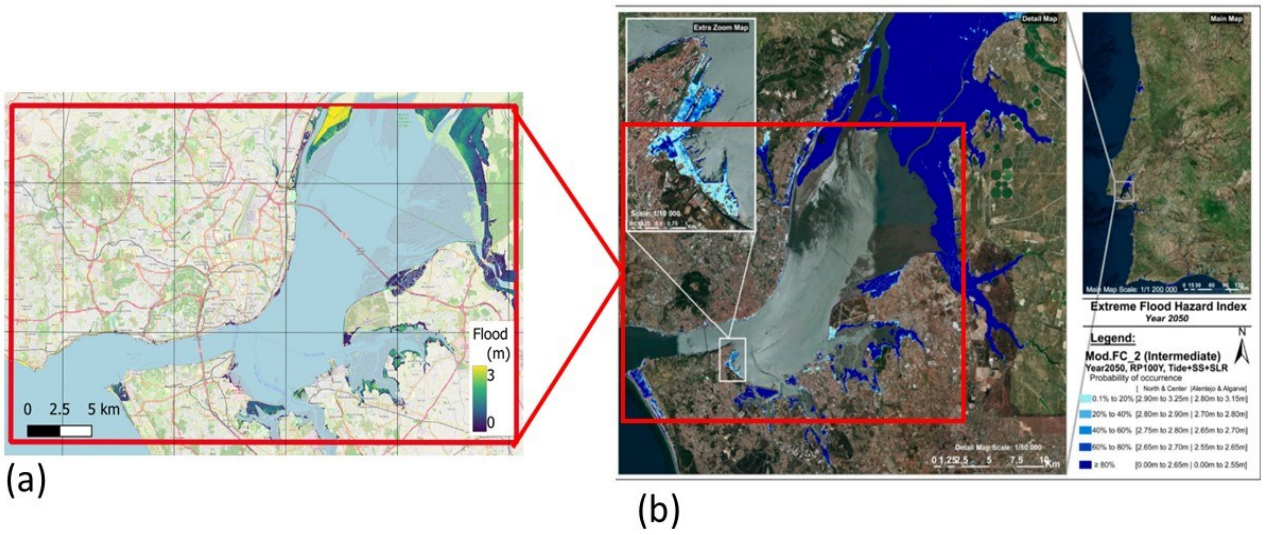

Figure 40. Comparison between modeled flood extent and projected flood hazard index for the Tagus Estuary. (a) Maximum flood extent simulated by the numerical model for Scenario 4 (spring tide + storm surge + SLR SSP2-8.5, 2046–2065); (b) Extreme Flood Hazard Index map for the year 2050, adapted from Antunes et al. (2019)

Additionally, a comparison was made between the numerical model results and a flood risk map developed by (Agência Portuguesa do Ambiente, 2019), which shows flood-prone areas in the Loures-Odivelas region. This comparison is presented in Figure 41 (a and b), where a visual similarity can be observed between the areas projected to be flooded for a 20-year return period and those that were actually inundated during the 2022 storm event.

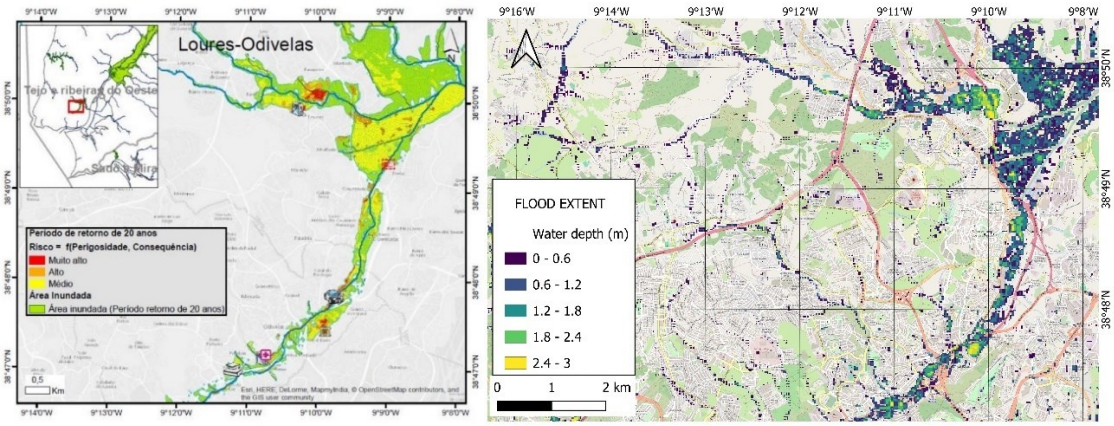

Figure 41. Comparison of official flood risk mapping with model simulation results for the Loures–Odivelas area. (a) Left: Flood risk map produced by Agência Portuguesa do Ambiente (2019), showing hazard levels (low, medium, high) based on a 20-year return period scenario. (b) Right: Flood extent simulated by the SFINCS model, with water depth classifications under December 2022 event.

6.2 Contribution of individual drivers to flooding

The numerical model results clearly indicate that the largest flood extent occurred under the extreme pluvial/fluvial event with a 100-year return period (Scenario 1), underscoring the dominant role of precipitation in driving flooding in the region. This finding aligns with Rilo et al. (2015), who analysed flood events in the Tagus Estuary between 1865 and 2013 and found that 96% were triggered by intense rainfall. These results confirm that precipitation is the primary driver of major flood events in the study area.

Furthermore, 74% of these flood events were followed by peak river discharges from the Tagus River (Rilo et al., 2015). These findings confirm that the joint occurrence of extreme precipitation and peak river discharges have the potential to generate large-magnitude flood events in the study area. In this scenario, extensive flooding was observed in the northern part of the estuary, near the Tagus River's mouth. This aligns with the conclusions of Vargas et al. (2008), who argued that river discharge significantly contributes to flooding in the upstream reaches of the estuary. This compound mechanism is critical because extreme precipitation can lead to surface flooding in areas with higher elevations, while increased river discharge and elevated water levels simultaneously contribute to flooding in lower-lying areas, especially in the most upstream regions. Such peak discharges may result from the release of high flow volumes from upstream dams during intense rainfall events, as occurred during the December 2022 storm.

Regarding oceanic forcings, as depicted in Scenarios 2–6, the simultaneous occurrence of a spring tide and a storm surge was found to trigger significant flooding, resulting in widespread inundation along the northern and, to a greater extent, southern margins of the estuary. According to Rilo et al. (2015), low atmospheric pressure systems and high tide levels were triggering factors in 39% and 33% of historical flood events in the region, respectively. Therefore, the results from these scenarios provide insight into the potential magnitude of floods that could occur under such conditions. It is also important to note that a gradual increase in flood magnitude was observed with rising sea levels, in line with the different sea level rise projections analysed in this study.

In relation to the above, Fortunato et al. (2017) used numerical modelling to recreate the storm that hit Portugal in 1941. The authors argue that the main causes of flooding in the Tagus estuary

margins during this event were the regional storm surge combined with swell-induced setup, which was further amplified by estuarine resonance. They estimated that, under similar conditions today, approximately 25 km² could be inundated, primarily in the upstream reaches of the estuary where there are extensive areas of agricultural land, such as Pancas, located in the northern part of the spatial domain of this study. These areas were also identified as being prone to flooding in the present study under coastal, pluvial and fluvial drivers.

6.3 Comparative Flood Dynamics of Pluvial and Oceanic Drivers in the Tagus Estuary

Flooding patterns in the Tagus Estuary are significantly influenced by the geomorphological characteristics of the region. Oceanic forcings, such as storm surges and elevated sea levels, primarily affect low-lying areas along the estuarine margins, particularly on the southern shore, where topography is low. Their inland penetration, however, is limited, making ocean-related flooding less dominant in elevated areas further from the coast. In contrast, pluvial/fluvial drivers, particularly under extreme precipitation events, produce more widespread flooding across the estuary. These drivers not only impact the low-lying zones but also generate substantial flood extents in inland urban areas, especially along the northern margin, where the terrain rises more abruptly. This highlights the dominant role of precipitation in triggering widespread flooding in the region.

Notably, several areas within the low-lying coastal fringe are affected by both types of forcings, leading to compound flooding scenarios. In this context, integrated flood risk management strategies that consider both upstream and downstream processes in a geomorphologically diverse estuarine landscape, are needed.

6.4 Compound effects on flood events

The results of this study clearly demonstrate that compound flooding scenarios, driven by the simultaneous occurrence of high storm surges, spring tides, and pluvial/fluvial events, generate significantly greater flood magnitudes than scenarios involving oceanic forcing alone. This interaction between multiple drivers amplifies flood impacts, resulting in more widespread inundation, particularly in vulnerable low-lying and urban areas. In several scenarios analysed, the presence of compound conditions led to an increase in flooded extent by up to almost four times compared to ocean-only events.

These findings highlight the critical importance of accounting for compound effects in flood risk assessments and climate adaptation planning, especially in estuarine regions like the Tagus.

Although those compound events are not frequent it is assumed that the role of precipitation plays a key role in flooding as it was found by Rolim et al. (2014) who applied the ADCIRC numerical model to analyse the extent of flooding caused by Tropical Cyclone Xynthia making landfall along the Portuguese coast in 2010, particularly in the Tagus Estuary. During this event, storm surge and precipitation occurred simultaneously, though not with extreme values, but rather moderate intensities. The model results led the authors to conclude that the sea level at the peak of the storm was not high enough to cause flooding in the urban areas of the estuary. Based on the results of this numerical model, the authors argue that the few floods reported in these areas were most likely due to rainfall, surface runoff and limited drainage capacity. This moderate-magnitude compound event confirms the need for hydrodynamic modelling to assess flood conditions resulting from such compound events, which go beyond those previously recorded.

The compound effect has been identified as a key factor amplifying flood magnitudes in the Tagus Estuary. In particular, Bevacqua et al. (2020) demonstrated that compound events, arising from the interaction between storm surge and precipitation, are likely to increase in severity under various sea level rise (SLR) scenarios across Europe. In this context, the present study highlights the role of SLR as a critical driver of future flood hazard in the region.

To better contextualize the results, a review of previous studies on SLR impacts in the Tagus Estuary was conducted. Antunes et al. (2019) modelled flooding associated with a 100-year return period event for the year 2050, combining projected SLR, spring tides, and storm surges. Their flood maps revealed extensive inundation along the southern estuarine margin, particularly in Montijo and Caparica, as well as in northern areas of the study area domain. These flood-prone zones closely match those identified in the SLR scenarios analysed in the present study, supporting the model's accuracy and alignment with published projections.

Urban drainage capacity is another critical factor influencing compound flood dynamics, particularly in the northern parts of the Lisbon Metropolitan Area. According to Rilo et al. (2015), approximately 70% of historical flood events in the region were linked to drainage system limitations. During intense storm events, an initial peak in rainfall can saturate soils and overwhelm existing infrastructure, leaving little time for recovery before subsequent peaks occur—potentially triggering widespread flooding, as seen in the 2022 event. Although the

present modelling framework does not explicitly simulate drainage infrastructure, its effects were indirectly incorporated via infiltration parameters applied to urban zones using the Curve Number method (Jaafar & Ahmad, 2019). Nonetheless, consistent with previous research, it is assumed that urban drainage constraints significantly aggravate flood magnitude in vulnerable areas.

6.5 Spatial variability and hot spots

Based on the flood extent analysis across all modelling scenarios, this section synthesizes the main findings to identify the most flood-prone areas within the Tagus estuary. The results demonstrate that precipitation is the dominant flooding driver, responsible for the widest flood extents, including inland and elevated zones, while oceanic drivers such as storm surges and spring tides tend to affect only the low-lying areas adjacent to the shoreline, as illustrated in Figure 42. This distinction is closely related to the geomorphology of the estuary, particularly the steep elevation of the northern margin, where terrain rises quickly above 10 m, limiting the inland penetration of oceanic floods.

Despite this, compound events that combine oceanic and pluvial/fluvial drivers consistently produced the greatest flood extents, especially in transitional areas where both processes can overlap. This reinforces the importance of considering multiple drivers and their interactions when identifying areas at highest flood risk.

Several locations emerge as flood hotspots based on their topography, hydrological characteristics, and consistent flood occurrence across scenarios:

- Loures (north margin): A low-lying area with multiple river channels prone to overflow during heavy rainfall. Confirmed as a high-risk zone in previous assessments (e.g., Agência Portuguesa do Ambiente (2019)).
- Alcântara and Algés: Urban districts that experienced extensive flooding during the December 2022 event. Also inundated under simulated pluvial/fluvial and compound scenarios.
- Seixal, Montijo, and Caparica (south margin): Characterized by broad low-lying coastal areas susceptible to inundation under pluvial/fluvial, oceanic and compound forcing.
- Pancas area (north margin): Although more elevated, this agricultural region is vulnerable under scenarios of increased precipitation and river discharge combined with elevated total water levels.

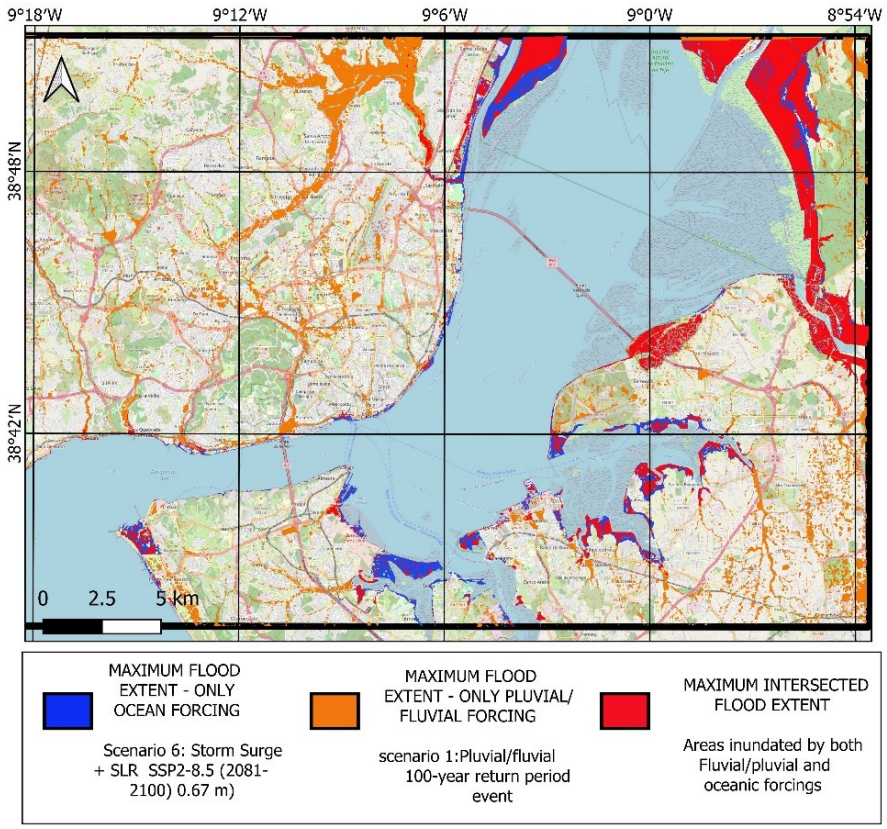

Figure 42. Spatial comparison of maximum flood extents caused by oceanic forcing, pluvial/fluvial forcing, and their intersection. The map illustrates the maximum flood extent due to: Oceanic forcing alone (blue), based on Scenario 6 (storm surge + SLR SSP5-8.5, 2081–2100), Pluvial/fluvial forcing alone (orange), based on Scenario 1 (100-year return period precipitation and river discharge), Overlapping areas inundated by both forcings (red), indicating regions most at risk from compound flood events.

This integrated overview supports the identification of key flood hazard zones in the Tagus estuary and provides an evidence-based foundation for prioritizing adaptation and mitigation strategies.

VII. Conclusions

This study demonstrated that compound flooding events, driven by the co-occurrence of extreme precipitation, river discharge, and oceanic drivers, significantly amplify flood magnitude in the Tagus Estuary when compared to events triggered solely by oceanic drivers. In simulations using identical sea level rise (SLR) projections, compound scenarios resulted in flood extents up to 3 to 4 times greater than those from ocean-only events in low-lying areas. These findings underscore the critical role of compound processes in shaping flood hazard, particularly in regions where conventional flood management has focused predominantly on oceanic drivers.

The modelling results also revealed that precipitation extremes and elevated river discharges are the primary drivers of large-scale flood events in the estuary. Extreme rainfall leads to widespread inundation across both the northern and southern margins of the estuary, while fluvial inputs have a more localized effect, especially near the Tagus River mouth on the northern margin. The interplay between pluvial, fluvial, and tidal/oceanic components results in increases in flood depth and extent, illustrating the importance of integrating multiple hazard sources in future flood risk assessments.

Analysis of the 25-year observational dataset showed that true compound events involving simultaneous extreme precipitation and extreme storm surge were rare, with most joint occurrences involving moderate-to-high precipitation coinciding with high storm surges. Nonetheless, their impact potential is disproportionately high.

Spatial variability in flood exposure was also evident. The southern margin, with its extensive low-lying terrain, showed greater susceptibility under both oceanic and compound scenarios, affecting areas such as Seixal, Montijo, and Caparica. Conversely, the northern margin, which rises steeply just a few meters inland, showed less sensitivity to oceanic drivers but remains highly exposed to pluvial events, with Loures, Alcântara, and Algés identified as critical hotspots. These findings highlight the need for location-specific flood management strategies:

- In southern areas, where storm surge and SLR impacts are dominant, options may include coastal protection infrastructure and nature-based solutions (e.g., salt marsh restoration).

- In urban areas along the northern margin, addressing urban drainage limitations is critical. Improvements in drainage system capacity could significantly reduce exposure during high-intensity rainfall events.

By expanding on earlier studies, this work provides an integrated, process-based understanding of flood dynamics in the Tagus Estuary, supported by multi-scenario modelling and alignment with historical flood observations and vulnerability assessments. The results provide actionable insights for flood risk governance, land-use planning, infrastructure protection, and climate adaptation, particularly for the Lisbon Metropolitan Area and adjacent low-lying agricultural regions.

Future research should prioritize:

- The explicit representation of urban drainage networks within compound flood models,
- The integration of socio-economic impact assessments, and
- The development of robust and adaptive strategies capable of responding to evolving climate and land-use conditions.

References

- Agência Portuguesa do Ambiente. (2019). *Avaliação preliminar dos riscos de inundações: Região Hidrográfica do Tejo e Ribeiras do Oeste – RH5A*. Departamento de Recursos Hídricos. https://apambiente.pt
- Agência Portuguesa do Ambiente. (n.d.). *Sistema Nacional de Informação de Recursos Hídricos (SNIRH)*. Retrieved March 10, 2025, from https://snirh.apambiente.pt/
- Andrade C, Pires HO, Silva P, Taborda R, Freitas MC (2006) Zonas Costeiras. In: Santos FD, Miranda P (eds) Alteracoes climaticas em Portugal. Cenarios, impactes e medidas de adaptacao. Projecto SIAMII, Gradiva, Lisboa, pp 169–208
- Antunes, C. (n.d.). *Hidrografia – Marés e Níveis da Água do Mar*. Faculdade de Ciências da Universidade de Lisboa. Retrieved March 11, 2025, from https://webpages.ciencias.ulisboa.pt/~cmantunes/hidrografia/hidromares.html
- Antunes, C., Rocha, C., & Catita, C. (2019). Coastal flood assessment due to sea level rise and extreme storm events: A case study of the Atlantic coast of Portugal's mainland. *Geosciences, 9*(5), 239. https://doi.org/10.3390/geosciences9050239
- Barbier, E. B., Hacker, S. D., Kennedy, C., Koch, E. W., Stier, A. C., & Silliman, B. R. (2011). The value of estuarine and coastal ecosystem services. *Ecological Monographs*, 81(2), 169–193. https://doi.org/10.1890/10-1510.1ResearchGate+2
- Bermudez, M., Farfán, J. F., Willems, P., & Cea, L. (2021). *Assessing the effects of climate change on compound flooding in coastal river areas. Water Resources Research, 57*(10), e2020WR029321. https://doi.org/10.1029/2020WR029321
- Bevacqua, E., Maraun, D., Hobæk Haff, I., Widmann, M., and Vrac, M.: Multivariate statistical modelling of compound events via pair-copula constructions: analysis of floods in Ravenna (Italy), Hydrol. Earth Syst. Sci., 21, 2701–2723, https://doi.org/10.5194/hess-21-2701-2017, 2017.
- Bevacqua, E., Maraun, D., Vousdoukas, M. I., Voukouvalas, E., Vrac, M., Mentaschi, L., and Widmann, M.: Higher probability of compound flooding from precipitation and storm surge in Europe under anthropogenic climate change, Science Advances, 5, eaaw5531, https://doi.org/10.1126/SCIADV.AAW5531, 2019.
- Bevacqua, E., Vousdoukas, M. I., Shepherd, T. G., & Vrac, M. (2020). Brief communication: The role of using precipitation or river discharge data when assessing

global coastal compound flooding. *Natural Hazards and Earth System Sciences, 20*, 1765–1782. https://doi.org/10.5194/nhess-20-1765-2020

- Blanton, B., McGee, J., Fleming, J., Kaiser, C., Kaiser, H., Lander, H., Luettich, R., Dresback, K., and Kolar, R.: Urgent Computing of Storm Surge for North Carolina's Coast, Procedia Comput. Sci., 9, 1677–1686, https://doi.org/10.1016/J.PROCS.2012.04.185, 2012.
- Booi, S., Mishi, S., & Andersen, O. (2022). Ecosystem Services: A systematic review of provisioning and cultural ecosystem services in Estuaries. *Sustainability*, *14*(12), 7252. https://doi.org/10.3390/su14127252
- CIIMAR – Interdisciplinary Centre of Marine and Environmental Research. (2025). *About CIIMAR*. https://www.fc.up.pt/pessoas/jagoncal/dems/index_en.html
- Coles, S. G., & Tawn, J. A. (1994). Statistical methods for multivariate extremes: An application to structural design. *Journal of the Royal Statistical Society: Series C (Applied Statistics), 43*(1), 1–31. https://doi.org/10.2307/2986112
- Copernicus Climate Change Service (2022): Global sea level change time series from 1950 to 2050 derived from reanalysis and high resolution CMIP6 climate projections. Copernicus Climate Change Service (C3S) Climate Data Store (CDS). DOI: 10.24381/cds.a6d42d60 (Accessed on 15-MAY-2025)
- De Pablo, H., Sobrinho, J., Garcia, M., Campuzano, F., Juliano, M., & Neves, R. (2019). Validation of the 3D-MOHID hydrodynamic model for the Tagus coastal area. *Water*, *11*(8), 1713. https://doi.org/10.3390/w11081713
- Dietrich, J. C., Bunya, S., Westerink, J. J., Ebersole, B. A., Smith, J. M., Atkinson, J. H., Jensen, R., Resio, D. T., Luettich, R. A., Dawson, C., Cardone, V. J., Cox, A. T., Powell, M. D., Westerink, H. J., and Roberts, H. J.: A High-Resolution Coupled Riverine Flow, Tide, Wind, Wind Wave, and Storm Surge Model for Southern Louisiana and Mississippi. Part II: Synoptic Description and Analysis of Hurricanes Katrina and Rita, Mon. Weather Rev., 138, 378–404, https://doi.org/10.1175/2009mwr2907.1, 2010.
- Direção-Geral do Território (2022). COS, *SMOS-CLMS – Solos, ocupação e uso do solo: Contributo nacional para o programa Copernicus Land Monitoring Services (CLMS)*. https://www.dgterritorio.gov.pt/cartografia/cartografia-tematica/SMOS-CLMS
- Direção-Geral do Território (n.d.). *Cartografia topográfica*. Retrieved March 14, 2025, from https://www.dgterritorio.gov.pt/cartografia/cartografia-topografica
- Dixon, M. J., & Tawn, J. A. (1994). *Extreme sea-levels at the UK A-class sites: Site-by-site analyses* (Proudman Oceanographic Laboratory Internal Document No. 65,

229 pp.). Proudman Oceanographic Laboratory. https://ntslf.org/sites/ntslf/files/pdf/other_reports/id65.pdf

- Eilander, D., Couasnon, A., Leijnse, T., Ikeuchi, H., Yamazaki, D., Muis, S., Dullaart, J., Haag, A., Winsemius, H. C., & Ward, P. J. (2023). *A globally applicable framework for compound flood hazard modeling. Natural Hazards and Earth System Sciences, 23*(2), 823–846. https://doi.org/10.5194/nhess-23-823-2023
- Emery, C. M., Larnier, K., Liquet, M., Hemptinne, J., Vincent, A., & Peña Luque, S. (2021). Extraction of roughness parameters from remotely-sensed products for hydrology applications. *Hydrology and Earth System Sciences Discussions*. https://doi.org/10.5194
- Expresso. (2022). Mau tempo provoca uma morte, mais de 100 deslocados e 10 desalojados. https://expresso.pt/sociedade/2022-12-08-Mau-tempo-provoca-uma-morte-mais-de-100-deslocados-e-10- desalojados.-Houve-47-resgatados-de-veiculos-0c87fd50
- Fakhri, F., & Gkanatsios, I. (2025). Quantitative evaluation of flood extent detection using Attention U-Net: Case studies from Eastern South Wales, Australia in March 2021 and July 2022. *Scientific Reports, 15*, Article 12377. https://doi.org/10.1038/s41598-025-92734-x
- Ferreira, T. M., Trigo, R. M., Gaspar, T. H., Pinto, J. G., & Ramos, A. M. (2025). The record-breaking precipitation event of December 2022 in Portugal. *Natural Hazards and Earth System Sciences, 25*(2), 609–623. https://doi.org/10.5194/nhess-25-609-2025
- Fortunato, A. B., Freire, P., Bertin, X., Rodrigues, M., Ferreira, J., & Liberato, M. L. R. (2017). A numerical study of the february 15, 1941 storm in the Tagus Estuary. Continental Shelf Research, 144, 50–64. https://doi.org/10.1016/j.csr.2017.06.023
- Ganguli, P., Paprotny, D., Hasan, M., Güntner, A., and Merz, B.: Projected Changes in Compound Flood Hazard From Riverine and Coastal Floods in Northwestern Europe, Earth's Future, 8, e2020EF001752, https://doi.org/10.1029/2020EF001752, 2020
- Green, J., Haigh, I. D., Quinn, N., Neal, J., Wahl, T., Wood, M., Eilander, D., de Ruiter, M., Ward, P., & Camus, P. (2025). Review article: A comprehensive review of compound flooding literature with a focus on coastal and estuarine regions. *Natural Hazards and Earth System Sciences*, *25*(2), 747–775. https://doi.org/10.5194/nhess-25-747-2025
- Guerreiro, M., Fortunato, A. B., Freire, P., Rilo, A., Taborda, R., Freitas, M. C., Andrade, C., Silva, T., Rodrigues, M., Bertin, X., & Azevedo, A. (2015). *Evolution of the hydrodynamics of the Tagus estuary (Portugal) in the 21st century*. Revista de Gestão Costeira Integrada, 15(1), 65–80. https://doi.org/10.5894/rgci515

- Harrison, L. M., Coulthard, T. J., Robins, P. E., & Lewis, M. J. (2021). Sensitivity of estuaries to compound flooding. *Estuaries and Coasts*, *45*(5), 1250–1269. https://doi.org/10.1007/s12237-021-00996-1
- Hawkes, P. J., & Svensson, C. (2003). *Joint probability: Dependence mapping and best practice* (Defra/Environment Agency R&D Technical Report FD2308/TR1). Department for Environment, Food and Rural Affairs / Environment Agency.
- Herdman, L., Erikson, L., and Barnard, P.: Storm Surge Propagation and Flooding in Small Tidal Rivers during Events of Mixed Coastal and Fluvial Influence, Journal of Marine Science and Engineering, 6, 158–158, https://doi.org/10.3390/JMSE6040158, 2018.
- Hewitt, K. and Burton, I., (1971). The hazardousness of a place: A regional geology of damaging events, University of Toronto, Department of Geography Research Publication, 5, pp 154-155.
- Ho, F. P., & Myers, V. A. (1975). *Joint probability method of tide frequency analysis applied to Apalachicola Bay and St. George Sound, Florida* (NOAA Technical Report NWS 18, 43 pp.). U.S. Department of Commerce, National Oceanic and Atmospheric Administration, National Weather Service. https://repository.library.noaa.gov/view/noaa/33908/noaa_33908_DS1.pdf
- Hoegh-Guldberg, O.; Beal, D.; Chaudhry, T.; Abdullat, A.; Etessy, P.; Smits, M. *Reviving the Ocean Economy: The Case for Action*; WWF International: Gland/Geneva, Switzerland, 2015; p. 60
- Instituto Hidrográfico. (2025). *Hidrográfico+* [Web portal]. Retrieved July 13, 2025, from https://geomar.hidrografico.pt/
- Instituto Português do Mar e da Atmosfera. (n.d.). *IPMA – Instituto Português do Mar e da Atmosfera*. Retrieved July 10, 2025, from https://www.ipma.pt/
- Jaafar, Hadi; Ahmad, Farah (2019). GCN250, global curve number datasets for hydrologic modeling and design. figshare. Dataset. https://doi.org/10.6084/m9.figshare.7756202.v1
- Jones, D. A. (1998). *Joint probability fluvial-tidal analyses: Structure functions and historical emulation*. Institute of Hydrology.
- Kerr, P. C., Westerink, J. J., Dietrich, J. C., Martyr, R. C., Tanaka, S., Resio, D. T., Smith, J. M., Westerink, H. J., Westerink, L. G., Wamsley, T., Ledden, M. v., and Jong, W. d.: Surge Generation Mechanisms in the Lower Mississippi River and Discharge

Dependency, J. Waterw. Port C., 139, 326-335, https://doi.org/10.1061/(ASCE)WW.1943-5460.0000185, 2013.

- Klerk, W. J., Winsemius, H. C., Van Verseveld, W. J., Bakker, A. M. R., and Diermanse, F. L. M.: The co-incidence of storm surges and extreme discharges within the Rhine-Meuse Delta, Environ. Res. Lett., 10, 035005, https://doi.org/10.1088/1748-9326/10/3/035005, 2015
- Kumbier, K., Carvalho, R. C., Vafeidis, A. T., and Woodroffe, C. D.: Investigating compound flooding in an estuary using hydrodynamic modelling: a case study from the Shoalhaven River, Australia, Nat. Hazards Earth Syst. Sci., 18, 463–477, https://doi.org/10.5194/nhess-18-463-2018, 2018.
- Kupfer, S., Vafeidis, A. T., & MacPherson, L. R. (2025). *Accounting for compound flooding can prevent maladaptation—A Baltic Sea case study. Earth's Future*. Advance online publication. https://doi.org/10.1029/2024EF005106
- Lee, C., Hwang, S., Do, K., and Son, S.: Increasing flood risk due to river runoff in the estuarine area during a storm landfall, Estuar. Coast. Shelf S., 221, 104–118, https://doi.org/10.1016/J.ECSS.2019.03.021, 2019
- Leijnse, T., van Ormondt, M., Nederhoff, K., & van Dongeren, A. (2021). Modeling compound flooding in coastal systems using a computationally efficient reduced-physics solver: Including fluvial, pluvial, tidal, wind- and wave-driven processes. *Coastal Engineering*, *163*, 103796. https://doi.org/10.1016/j.coastaleng.2020.103796
- Leonard, M., Westra, S., Phatak, A., Lambert, M., & Stafford-Smith, M. (2014). *A compound event framework for understanding extreme impacts. Wiley Interdisciplinary Reviews: Climate Change, 5*(1), 113–128. https://doi.org/10.1002/wcc.252
- Lian, J. J., Xu, K., and Ma, C.: Joint impact of rainfall and tidal level on flood risk in a coastal city with a complex river network: a case study of Fuzhou City, China, Hydrol. Earth Syst. Sci., 17, 679–689, https://doi.org/10.5194/hess-17-679-2013, 2013.
- Liang, J., & Liu, D. (2020). A local thresholding approach to flood water delineation using Sentinel-1 SAR imagery. *ISPRS Journal of Photogrammetry and Remote Sensing, 159*, 53–62. https://doi.org/10.1016/j.isprsjprs.2019.10.017
- Lin, N., Smith, J. A., Villarini, G., Marchok, T. P., and Baeck, M. L.: Modeling extreme rainfall, winds, and surge from Hurricane Isabel (2003), Weather Forecast., 25, 1342–1361, https://doi.org/10.1175/2010WAF2222349.1, 2010.

- Loganathan, G. V., Kuo, C. Y., & Yannaccone, J. (1987). Joint probability distribution of streamflows and tides in estuaries. *Hydrology Research, 18*(4-5), 237–246. https://doi.org/10.2166/nh.1987.0017
- Lopes, C. L., Sousa, M. C., Ribeiro, A., Pereira, H., Pinheiro, J. P., Vaz, L., & Dias, J. M. (2022). Evaluation of future estuarine floods in a sea level rise context. *Scientific Reports, 12*(1), Article 8083. https://doi.org/10.1038/s41598-022-12122-7
- Luisetti, T., Turner, R. K., Jickells, T., Andrews, J., Elliott, M., Schaafsma, M., Beaumont, N., Malcolm, S., Burdon, D., Adams, C., & Watts, W. (2014). Coastal zone ecosystem services: From science to values and decision making; a case study. *Science of The Total Environment*, 493, 682–693. https://doi.org/10.1016/j.scitotenv.2014.05.099
- Mantz, P. A., & Wakeling, H. L. (1979). Forecasting flood levels for joint events of rainfall and tidal surge flooding using extreme value statistics. *Proceedings of the Institution of Civil Engineers: Part 2 – Research and Theory, 67*(1), 31–50. https://doi.org/10.1680/iicep.1979.2315
- Martins, F., Leitão, P., Silva, A., & Neves, R. (2001). 3D modelling in the Sado estuary using a new generic vertical discretization approach. Oceanologica Acta, 24, 51–62. https://doi.org/10.1016/s0399-1784(01)00092-5
- Mashriqui, H. S., Halgren, J. S., and Reed, S. M.: 1D River Hydraulic Model for Operational Flood Forecasting in the Tidal Potomac: Evaluation for Freshwater, Tidal, and Wind-Driven Events, J. Hydraul. Eng., 140, 04014005, https://doi.org/10.1061/(ASCE)HY.1943-7900.0000862, 2014
- Mason, D. C., Bevington, J., Dance, S. L., Revilla-Romero, B., Smith, R., Vetra-Carvalho, S., & Cloke, H. L. (2021). *Improving urban flood mapping by merging synthetic aperture radar-derived flood footprints with flood hazard maps. Water, 13*(11), 1577. https://doi.org/10.3390/w13111577
- McInnes, K. L., Hubbert, G. D., & Short, A. D. (2002). A numerical modelling study of coastal flooding. *Meteorology and Atmospheric Physics, 80*(1), 217–233. https://doi.org/10.1007/s007030200027
- Mora, C., & Vieira, G. (2020). *Climate of Portugal*. In *Landscapes and Landforms of Portugal* (pp. 33–47). Springer.
- Muis, S., Verlaan, M., Winsemius, H. *et al.* A global reanalysis of storm surges and extreme sea levels. *Nat Commun* **7**, 11969 (2016). https://doi.org/10.1038/ncomms11969

- Muñoz, D. F., Abbaszadeh, P., Moftakhari, H., and Moradkhani, H.: Accounting for uncertainties in compound flood hazard assessment: The value of data assimilation, Coast. Eng., 171, 104057, https://doi.org/10.1016/j.coastaleng.2021.104057, 2022
- Nederhoff, K.; Crosby, S.C.; Van Arendonk, N.R.; Grossman, E.E.; Tehranirad, B.; Leijnse, T.; Klessens, W.; Barnard, P.L. Dynamic Modeling of Coastal Compound Flooding Hazards Due to Tides, Extratropical Storms, Waves, and Sea-Level Rise: A Case Study in the Salish Sea, Washington (USA). Water 2024, 16, 346. https://doi.org/10.3390/w16020346
- Olbert, A. I., Comer, J., Nash, S., & Hartnett, M. (2017). High-resolution multi-scale modelling of coastal flooding due to tides, storm surges and rivers inflows. A Cork City example. *Coastal Engineering*, *121*, 278–296. https://doi.org/10.1016/j.coastaleng.2016.12.006
- Oliveira, F. S. B. F. (2008). Análise da Vulnerabilidade de uma Praia Estuarina à Inundação: Aplicação à Restinga do Alfeite (Estuário do Tejo). Revista De Gestão Costeira Integrada.
- Orton, P. M., Conticello, F. R., Cioffi, F., Hall, T. M., Georgas, N., Lall, U., Blumberg, A. F., & MacManus, K. (2018). Flood hazard assessment from storm tides, rain and sea level rise for a tidal River Estuary. *Natural Hazards*, *102*(2), 729–757. https://doi.org/10.1007/s11069-018-3251-x
- Pan Hu, Qiang Zhang, Peijun Shi, Bo Chen, Jiayi Fang, Flood-induced mortality across the globe: Spatiotemporal pattern and influencing factors, Science of The Total Environment, Volume 643 (2018) Pages 171-182, ISSN 0048-9697, https://doi.org/10.1016/j.scitotenv.2018.06.197.(https://www.sciencedirect.com/science/article/pii/S0048969718322745)
- Papaioannou, G., Efstratiadis, A., Vasiliades, L., Loukas, A., Papalexiou, S. M., Koukouvinos, A., Tsoukalas, I., & Kossieris, P. (2018). An operational method for Flood Directive implementation in ungauged urban areas. *Hydrology, 5*(2), Article 24. https://doi.org/10.3390/hydrology5020024
- Petroliagkis, T. I., Voukouvalas, E., Disperati, J., Bidlot, J., and European Commission. Joint Research Center: Joint Probabilities of Storm Surge, Significant Wave Height and River Discharge Components of Coastal Flooding Events. Utilising statistical dependence methodologies & techniques, Publications Office of the European Union, ISBN 978-92-79-57666-9, https://doi.org/10.2788/951583, 2016.

- Portela, L. (1996). Modelação matemática de processos hidrodi-nâmicos e da qualidade da água no estuário do Tejo [Instituto Superior Técnico]. http://repositorio.lnec.pt:8080/xmlui/hand-le/123456789/8737
- Prandle, D., & Wolf, J. (1978). The interaction of surge and tide in the North Sea and River Thames. *Geophysical Journal International, 55*(1), 203–216. https://doi.org/10.1111/j.1365-246X.1978.tb04758.x
- Ribeiro, A. F., Sousa, M., Picado, A., Ribeiro, A. S., Dias, J. M., & Vaz, N. (2022). Circulation and transport processes during an extreme freshwater discharge event at the Tagus Estuary. Journal of Marine Science and Engineering, 10(10), 1410. https://doi.org/10.3390/jmse10101410
- Rilo, A., Freire, P., Santos, P., Tavares, A., & Sá, L. (2015). Historical flood events in the tagus estuary: Contribution to risk assessment and management tools. *Safety and Reliability of Complex Engineered Systems*, 4281–4286. https://doi.org/10.1201/b19094-561
- Rilo, A., Tavares, A. M., dos Santos Freire, P. M., & Zêzere, J. L. (2022). Dealing with multisource information for estuarine flood risk appraisal in two Western European coastal areas. *International Journal of Disaster Risk Science*, *13*(2), 199–213. https://doi.org/10.1007/s13753-022-00403-8
- Rolim, J., Araújo, M. A. V. C., & Trigo-Teixeira, A. (2014). Simulation of a storm surge event in the Tagus Estuary. In *Proceedings of the 3rd IAHR Europe Congress* (Porto, 2014). International Association for Hydro-Environment Engineering and Research. https://www.iahr.org/library/infor?pid=10636
- Rossiter, J. R. (1961). Interaction between tide and surge in the Thames. *Geophysical Journal International, 6*(1), 29–53. https://doi.org/10.1111/j.1365-246X.1961.tb02960.x
- Rusu, L., Bernardino, M., & Guedes Soares, C. (2011). *Modelling the influence of currents on wave propagation at the entrance of the Tagus estuary*. Ocean Engineering, 38(10), 1174–1183. https://doi.org/10.1016/j.oceaneng.2011.05.016
- Sadegh, M., E. Ragno, and A. AghaKouchak (2018), Multivariate Copula Analysis Toolbox (MvCAT): Describing dependence and underlying uncertainty using a Bayesian framework, Water Resour. Res., 53, 5166–5183, doi:10.1002/ 2016WR020242
- Santos, P. P., Pereira, S., Zêzere, J. L., Reis, E., Oliveira, S. C., Garcia, R. A. C., & Ferreira, T. M. (2024). *Understanding flood risk in urban environments: Spatial analysis*

of building vulnerability and hazard areas in the Lisbon metropolitan area. *Natural Hazards*. Advance online publication. https://doi.org/10.1007/s11069-024-06731-w

- Santos, V.M., I.D. Haigh, and T. Wahl. 2017. Spatial and Temporal Clustering Analysis of Extreme Wave Events Around the Uk Coastline. *Journal of Marine Science and Engineering* 5: 19. https://doi.org/10.3390/jmse5030028.
- Seneviratne, S., Nicholls, N., Easterling, D., Goodess, C., Kanae, S., Kossin, J., & Zwiers, F. W. (2012). Changes in climate extremes and their impacts on the natural physical environment.
- Stamey, B. H., Wang, H. F., & Koterba, M. (2007). Predicting the next storm surge flood. *Sea Technology, 48*(8), 10–15.
- Sun, H., Zhang, X., Ruan, X., Jiang, H., & Shou, W. (2024). Mapping compound flooding risks for urban resilience in Coastal Zones: A comprehensive methodological review. *Remote Sensing*, *16*(2), 350. https://doi.org/10.3390/rs16020350
- Svensson, C., & Jones, D. A. (2002). Dependence between extreme sea surge, river flow and precipitation in eastern Britain. *International Journal of Climatology*, 22(10), 1149–1168. https://doi.org/10.1002/joc.794
- Tavares, A. O., dos Santos, P. P., Freire, P., Fortunato, A. B., Rilo, A., & Sá, L. (2015). Flooding hazard in the Tagus estuarine area: The challenge of scale in vulnerability assessments. *Environmental Science & Policy, 51*, 238–255. https://doi.org/10.1016/j.envsci.2015.04.010
- Tawn, J. A. (1992). Estimating probabilities of extreme sea-levels. *Journal of the Royal Statistical Society: Series C (Applied Statistics), 41*(1), 77–93. https://doi.org/10.2307/2347619
- Trigo, R. M., & DaCamara, C. C. (2000). *Circulation weather types and their influence on the precipitation regime in Portugal. International Journal of Climatology, 20*(13), 1559–1581. Available at: https://idlcc.fc.ul.pt/pdf/LWT.pdf
- Tromble, E., Kolar, R., Dresback, K., Hong, Y., Vieux, B., Luettich, R., Gourley, J., Kelleher, K., and Van Cooten, S.: Aspects of Coupled Hydrologic-Hydrodynamic Modeling for Coastal Flood Inundation, Proceedings of the International Conference on Estuarine and Coastal Modeling, 388, 724–743, https://doi.org/10.1061/41121(388)42, 2010
- Vargas, C., Oliveira, F., Oliveira, A., & Charneca, N. (2008). Vulnerability Analysis of an Estuarine Beach to Inundation: Application to Alfeite Spit (Tagus Estuary). Revista Da Gestão Costeira Integrada, 8(1):25-43.

- Vaz, N., Mateus, M., Pinto, L., Neves, R., & Dias, J. M. (2020). The Tagus Estuary as a numerical modeling test bed: A review. *Geosciences, 10*(1), 4. https://doi.org/10.3390/geosciences10010004
- Ward, P. J., Couasnon, A., Eilander, D., Haigh, I. D., Hendry, A., Muis, S., Veldkamp, T. I. E., Winsemius, H. C., & Wahl, T. (2018). Dependence between high sea-level and high river discharge increases flood hazard in global deltas and estuaries. *Environmental Research Letters, 13*(8), Article 084012. https://doi.org/10.1088/1748-9326/aad400
- White, C. J. (2007). *The use of joint probability analysis to predict flood frequency in estuaries and tidal rivers* (Doctoral thesis, University of Southampton, Faculty of Engineering, Science and Mathematics, School of Civil Engineering and the Environment). University of Southampton. https://eprints.soton.ac.uk/63847/
- Wu, W., Westra, S., and Leonard, M.: Estimating the probability of compound floods in estuarine regions, Hydrol. Earth Syst. Sci., 25, 2821–2841, https://doi.org/10.5194/hess-25-2821-2021, 2021.
- Yommy, A. S., Liu, R., & Wu, S. (2015). SAR image despeckling using the Refined Lee Filter (RLF). *2015 7th International Conference on Intelligent Human-Machine Systems and Cybernetics (IHMSC)*, Vol. 2, 236–239. https://doi.org/10.1109/IHMSC.2015.236
- Zhao, J., Xiong, Z., & Zhu, X. X. (2024). UrbanSARFloods: Sentinel-1 SLC-based benchmark dataset for urban and open-area flood mapping. In Proceedings of the IEEE/CVF Conference on Computer Vision and Pattern Recognition Workshops (CVPRW) (pp. 419–429). https://doi.org/10.48550/arXiv.2406.04111
- Zscheischler, J., Martius, O., Westra, S., Bevacqua, E., Raymond, C., Horton, R., van den Hurk, B., AghaKouchak, A., Jézéquel, A., Mahecha, M., Maraun, D., Ramos, A., Ridder, N., Thiery, W., & Vignotto, E. (2020). *A Typology of Compound Weather and Climate Events*. https://doi.org/10.5194/egusphere-egu2020-8572
- Zscheischler, J., Westra, S., van den Hurk, B.J.J.M. *et al.* Future climate risk from compound events. *Nature Clim Change* **8**, 469–477 (2018). https://doi.org/10.1038/s41558-018-0156-3